Study of the nature and roles of peroxy radicals in the atmosphere towards the understanding of oxidant formation using laser-flash photolysis and LIF detection technique

KOJI MIYAZAKI

Dissertation submitted to Tokyo Metropolitan University and University of Lille1 in partial fulfillment of the requirements for the degree of

DOCTOR OF PHILOSOPHY
IN
“Engineering”
and
“Sciences de la Matière, du Rayonnement et de l'Environnement”

Academic Advisor: Prof. Yoshizumi Kajii / Dr. Christa Fittschen
Tokyo Metropolitan University / University of Lille1
Tokyo, Japan / Lille, France

March, 2012

Date of the defense	**6. Feb. 2012**
Director of Thesis	**Prof. Yoshizumi Kajii** **Dr. Christa Fittschen**
Jury Reporters	**Dr. John C. Wenger** **Dr. Yugo Kanaya**
Jury Members	**Associate Prof. Shungo Kato** **Associate Prof. Jun Matsumoto** **Prof. Keitaro Yoshihara** **Prof. Jean-Francois Pauwels**

Abstract

Peroxy radicals RO_2 (with R = H or CxHy) play a major role in the photo-oxidation cycles of the troposphere. They are produced mainly via the atmospheric oxidation of hydrocarbons and carbon monoxide by OH radicals and subsequent reactions with O_2. They can further react with NO to recycle OH radicals. This oxidation of NO through reaction with peroxy radicals is an important source of tropospheric ozone. To understand the mechanism of this tropospheric ozone generation, precise and accurate measurements of ambient peroxy radical concentrations are essential. And not only atmospheric concentration measurements, but also atmospheric kinetics studies such as lifetime measurements of peroxy radicals are necessary. Recent publications show big differences between measured peroxy radical concentrations and those calculated with chemical models. These could be caused by missing reaction pathways and uncertainties in the reaction yields and rate cefficients. To investigate these missing reactions and the uncertainties in known peroxy radical reactions via ambient measurements, two recently developed instruments have been applied.

One is a technique for the selective measurement of atmospheric peroxy radical concentrations of HO_2 and RO_2 using the PERCA (PEroxy Radicals Chemical Amplification) technique. The experimental technique consists of the following: Ambient HO_2 and RO_2 radicals are amplified and converted to NO_2 with addition of high concentrations of NO (5 ppm) and CO (10 %). The NO_2 generated is measured by the LIF (Laser Induced-Fluorescence) technique at 532 nm. HO_2 radicals are selectively removed by using a glass denuder so that we could successfully determine concentration of RO_2 separately from HO_2.

The other one is a technique for total HO_2 loss rate measurement in the atmosphere by using the laser-flash photolysis and LIF detection of HO_2. The experimental technique consists of the following: OH radicals are generated using 266 nm laser photolysis of O_3 and subsequent reaction with H_2O. Excess CO is added to the reaction tube to convert all of OH radicals to HO_2 radicals. HO_2 radicals react with ambient reactive species such as NO_X. HO_2 loss is measured using LIF at 308 nm coupled with chemical conversion with NO. This new method provides accurate determination of total HO_2 loss rate in atmosphere.

As a result, significant amounts of HO_2 missing sink have been observed through ambient observations by using these instruments. The possible candidate species for these missing sinks were discussed.

Contents:

Chapter 1.

Introduction

In section 1-1, the roles of peroxy radicals in troposphere are described. Next in section 1-2, recent understandings of the peroxy radical reaction mechanism in the troposphere are described. In section 1-3, previous methods to measure the ambient peroxy radicals are described. At the last section 1-4, the objectives and scope of this study are described.

1-1. The roles of peroxy radicals in the troposphere

Peroxy radicals RO_2 (with R = H or CxHy) play an important role in the photo-oxidation cycles of the troposphere (Sadanaga et al., 2003, Monks, 2005). They are produced mainly via the atmospheric oxidation of volatile organic compounds (VOCs) and carbon monoxide by OH radicals and subsequent reactions with O_2. They can further react with NO to recycle OH radicals. This oxidation of NO via reaction with peroxy radicals is an important source of tropospheric ozone.

Ozone production through OH oxidation of CO.

$$CO + OH \rightarrow CO_2 + H \quad \text{(R1-1)}$$
$$H + O_2 + M \rightarrow HO_2 + M \quad \text{(R1-2)}$$
$$HO_2 + NO \rightarrow OH + NO_2 \quad \text{(R1-3)}$$
$$NO_2 + h\nu\ (< 424\ \text{nm}) \rightarrow NO + O(^3P) \quad \text{(R1-4)}$$
$$O(^3P) + O_2 + M \rightarrow O_3 + M \quad \text{(R1-5)}$$
$$\text{(net)} \quad CO + 2O_2 + h\nu \rightarrow CO_2 + O_3 \quad \text{(R1-6)}$$

Ozone production through OH oxidation of VOCs.

$$VOCs + OH + O_2 \rightarrow RO_2 \quad \text{(R1-7)}$$
$$RO_2 + NO \rightarrow RO + NO_2 \quad \text{(R1-8)}$$
$$RO + O_2 \rightarrow HO_2 + \text{calbonyl} \quad \text{(R1-9)}$$
$$HO_2 + NO \rightarrow OH + NO_2 \quad \text{(R1-3)}$$

$2(NO_2 + h\nu\,(< 424\ nm) \rightarrow NO + O(^3P))$ (R1-4)

$O(^3P) + O_2 + M \rightarrow O_3 + M$ (R1-5)

(net) $VOCs + 4O_2 + h\nu \rightarrow calbonyl + 2O_3$ (R1-10)

In addition to ozone production, peroxy radicals play an important role as intermediates in the production of SOA (Secondary Organic Aerosol).

These secondary products, ozone and SOA, are major constituents of photochemical oxidants that are detrimental to human health and contribute to climate change. Recent reports show the concentration of tropospheric ozone has significantly increased in recent years (Akimoto, 2003). To understand the mechanism of tropospheric ozone increase and SOA formation, precise and accurate measurement of atmospheric peroxy radicals is essential.

1-2. The loss and production process of peroxy radicals in the troposphere

The roles of peroxy radicals in troposphere are described briefly in the section 1-1. Peroxy radicals, including hydroperoxy radicals (HO_2) and organic peroxy radicals, are important tropospheric photochemical species having a critical role in tropospheric ozone and SOA formation. In this section, the loss and production process of peroxy radicals are described in more detail especially focused on the polluted and semi polluted air. A schematic diagram for the reaction path ways mentioned in this section is summarized in Figure.1-1.

1-2-1. The loss and production process of hydroperoxy radicals in the troposphere

HO_2 radicals in troposphere are produced mainly via four pathways, (1) OH reaction with CO and some VOCs, (2) RO_2 reaction with NO, (3) ozone reaction with alkenes and (4) the photolysis of OVOCs (Oxygenated VOCs).

From OH reaction with CO, HCHO, CH_3OH and SO_2, HO_2 radicals can be produced in the atmosphere as described below [Atkinson et al., 2004; 2006].

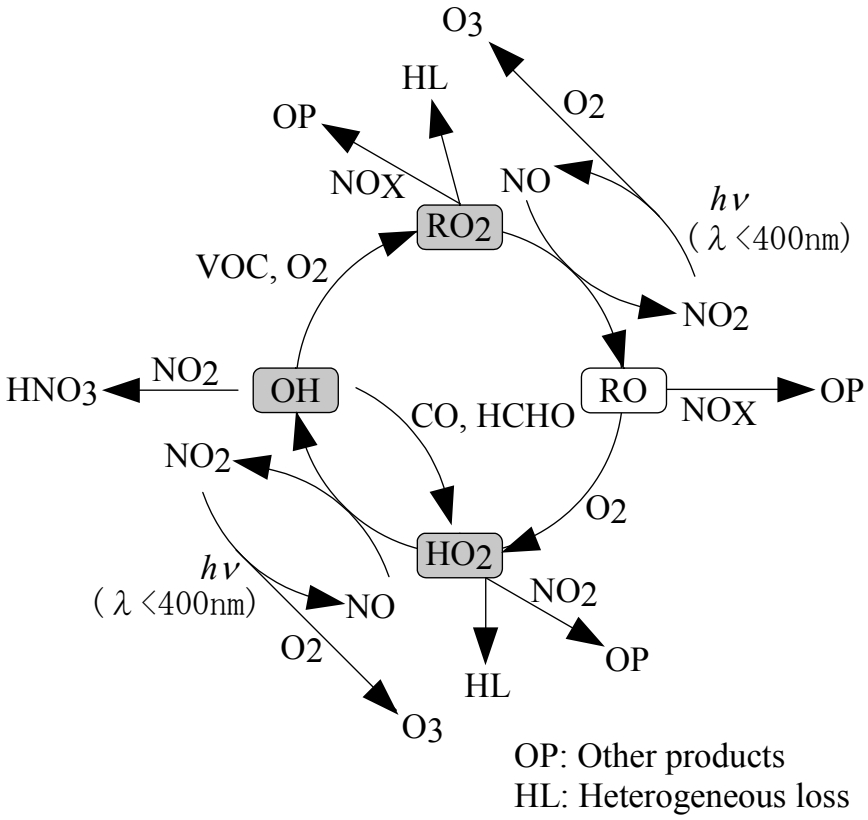

Figure.1-1 Schematic diagram of ambient reactions of peroxy radicals in relation to VOC oxidation

$CO + OH \rightarrow CO_2 + H$ (R1-1)

$H + O_2 + M \rightarrow HO_2 + M$ (R1-2)

$OH + HCHO \rightarrow H_2O + HCO$ (R1-11)

$HCO + O_2 \rightarrow HO_2 + CO$ (R1-12)

$OH + CH_3OH \rightarrow H_2O + CH_2OH$ (0.85) (R1-13)

$\rightarrow H_2O + CH_3O$ (0.15)

$CH_2OH + O_2 \rightarrow HCHO + HO_2$ (R1-14)

$CH_3O + O_2 \rightarrow HCHO + HO_2$ (R1-15)

$OH + SO_2 + M \rightarrow HSO_3 + M$ (R1-16)

$HSO_3 + O_2 \rightarrow HO_2 + SO_3$ (R1-17)

The production of HO_2 from RO_2 plus NO reaction is generally described by (R1-8)

and (R1-9).

The photolysis of OVOCs such as HCHO and CH_3CHO can produce HO_2 radicals. Although the quantum yield for HO_2 radical production depends on the photolysis wavelength, HCHO can be production of HO_2 radicals as below.

$$HCHO + h\nu (< 338\ nm) \rightarrow HCO + H \quad (R1\text{-}18)$$
$$H + O_2 + M \rightarrow HO_2 + M \quad (R1\text{-}2)$$
$$HCO + O_2 \rightarrow HO_2 + CO \quad (R1\text{-}12)$$

HO_2 radicals can be lost via its reaction with NO, with NO_2 and with aerosol.

$$HO_2 + NO \rightarrow OH + NO_2 \quad (R1\text{-}3)$$
$$HO_2 + NO_2 + M \leftrightarrow HO_2NO_2 + M \quad (R1\text{-}19)$$
$$HO_2 + aerosol \rightarrow products \quad (R1\text{-}20)$$

Peroxonitric acid (PNA, HO_2NO_2) has the role of HO_2 radicals' reservoir. It can be thermally dissociated to produce HO_2 radicals as (R1-19). HO_2 radical uptake onto aerosol is also an important HO_2 loss process (Thornton et al., 2008). It is reported that aerosol uptake coefficient of HO_2 radicals depends on humidity, temperature and the aerosol composition (Taketani et al., 2008). In the clean atmosphere, the self reaction of HO_2 radicals is one of the dominant radical loss processes. This self reaction is known to be accelerated by H_2O adduct to HO_2 radicals as below [Aloisio and Francisco, 1998; Kanno et al., 2005; Sander et al., 2006].

$$HO_2 + HO_2 \rightarrow H_2O_2 + O_2 \quad (R1\text{-}21)$$
$$HO_2 + H_2O \leftrightarrow HO_2 \cdot H_2O \quad (R1\text{-}22)$$
$$HO_2 \cdot H_2O + HO_2 \rightarrow Products \quad (R1\text{-}23)$$

1-2-2. The loss and production process of organic peroxy radicals in the troposphere

RO_2 radicals in the troposphere are produced mainly via four pathways, (1) OH reaction with VOCs, (2) the photolysis of OVOCs, (3) ozone reaction with alkenes, (4) NO_3 reaction with VOCs and (5) thermal dissociation of organic nitrates [Atkinson et al.,

2004; 2006].

The variety of VOC in atmosphere amounts to about a few hundreds [Lewis et al., 2000], and also the variety of RO_2 radicals generated from the OH reaction with VOCs can have also the same. The initiation involves a hydrogen atom abstraction from saturated hydrocarbon and OH adduct to unsaturated hydrocarbon forming the organic radicals. The organic radicals react with O_2 to produce RO_2 radicals described as (R1-7).

The photolysis of OVOCs such as CH_3CHO and $(CH_3)_2CO$ can produce RO_2 radicals. $(CH_3)_2CO$ can be photolyzed to produce RO_2 radicals as below.

$$(CH_3)_2CO + h\nu \rightarrow CH_3CO + CH_3 \quad (\lambda < 338\ nm) \quad \text{(R1-24)}$$
$$\rightarrow 2CH_3 + CO \quad (\lambda < 299\ nm)$$

The reaction of O_3 with alkenes has a complex reaction pathway. Recent studies provided reaction rate coefficients and product yields in the gas phase reaction of O_3 with some kinds of alkenes [e.g. Wegener et al.,2007, Johnson and Marston, 2008, Malkin et al., 2010]. General features of the mechanism of the reaction are described in Figure.1-2. The initiation involves the concerted [3+2] cycloaddition of ozone to the double bond of the alkene forming the primary ozonide. The primary ozonide then rapidly decomposes to give a pair of Criegee Intermediates (C.I.) and carbonyl compounds. The C.I. may then be collisionally stabilized or decompose finally to produce some products (RO_2, HO_2, OH etc).

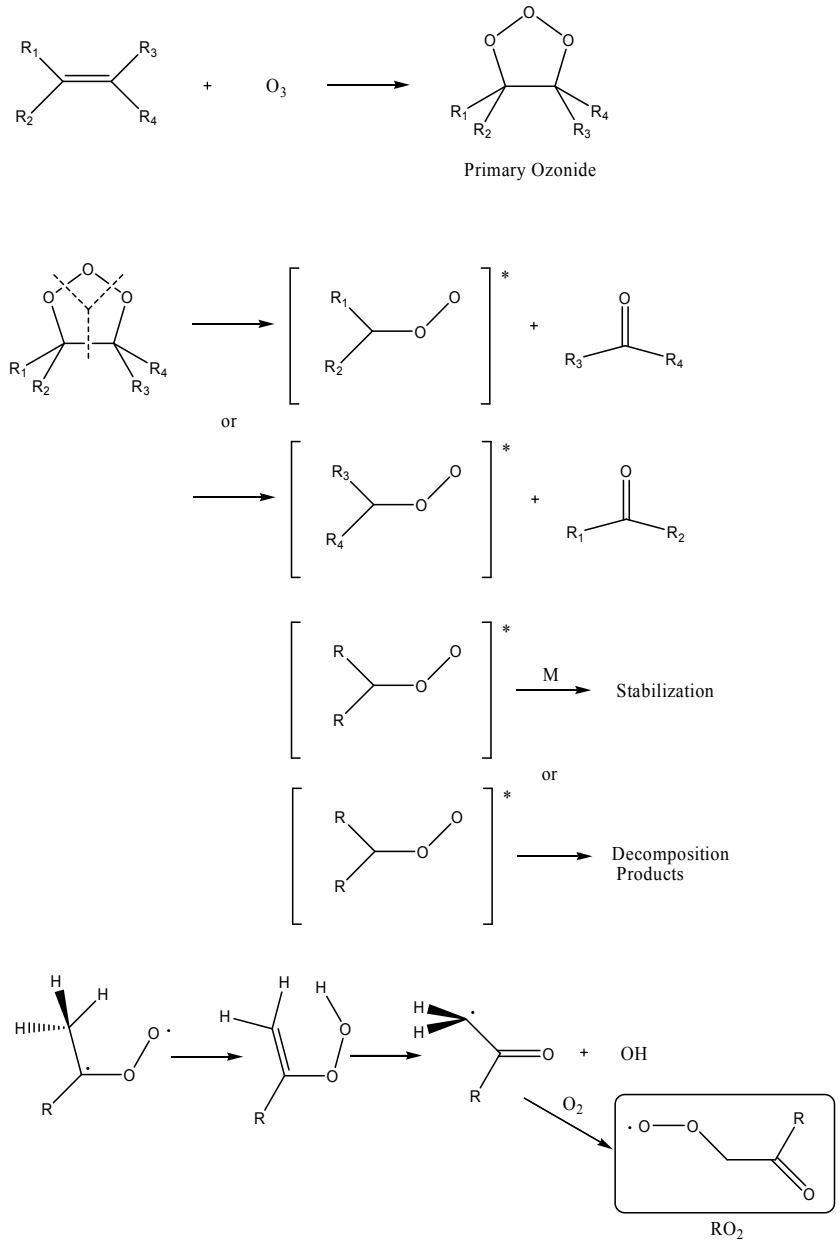

Figure.1-2 Schematic diagram of O_3-alkene reaction

Initial reactions of NO_3 involve a hydrogen atom abstraction from saturated hydrocarbon and NO_3 adduct to unsaturated hydrocarbon in much the same fashion as OH oxidation. NO_3 radicals abstract a hydrogen atom forming nitric acid; HNO_3 and organic radicals which produce RO_2 radicals through the reaction with O_2 as below.

$$NO_3 + RH \rightarrow HNO_3 + R \quad \text{(R1-25)}$$

$$R + O_2 + M \rightarrow RO_2 + M \quad \text{(R1-26)}$$

NO_3 addition to the double bond leads to two reaction pathways, one is to generate RO_2 radicals and the other one is to generate epoxide and NO_2 generally, described in Figure.1-3 [Skov et al., 1994].

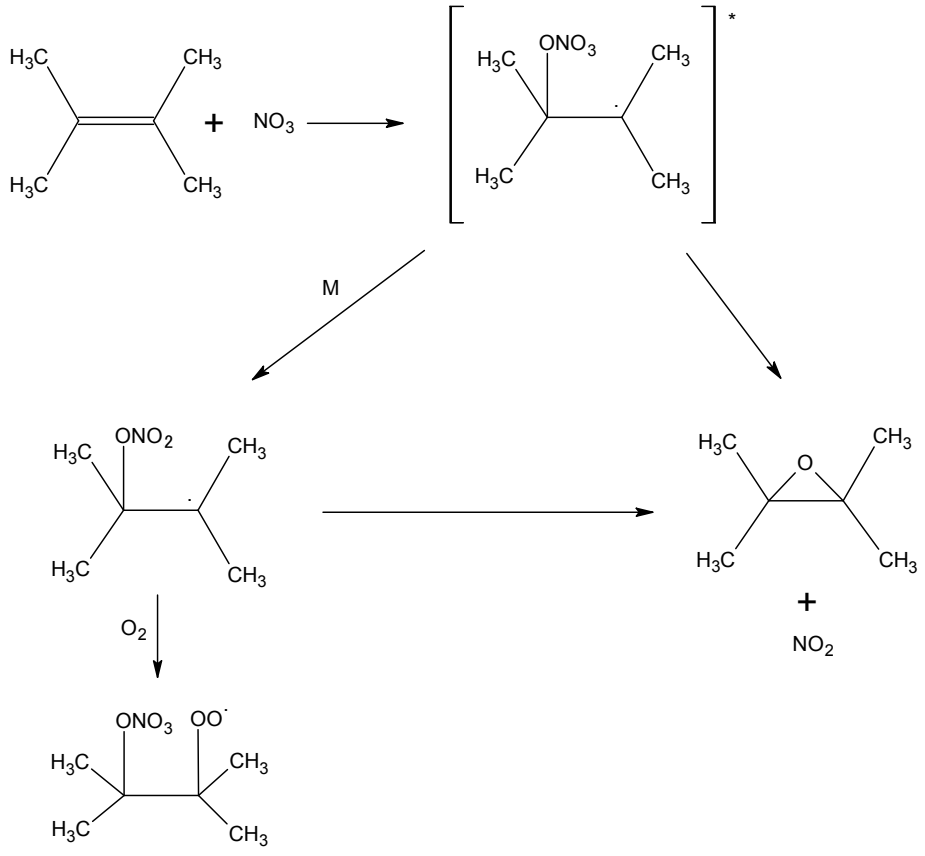

Figure.1-3 Schematic diagram of NO_3-alkene reaction

Thermal dissociation of organic nitrates, such as peroxyacetyl nitrates; PAN is one of the important RO_2 production process [Farmer et al., 2011]. OH radicals react with acetaldehyde to produce acetylperoxy radicals, forming PAN via the subsequent reaction with NO_2 as below. Organic nitrates are temporary reservoirs that release NO_X and organic peroxy radicals.

$$CH_3CHO + OH + O_2 \rightarrow CH_3C(O)O_2 + H_2O \quad \text{(R1-27)}$$
$$CH_3C(O)O_2 + NO_2 + M \rightarrow CH_3C(O)O_2NO_2 + M \quad \text{(R1-28)}$$
$$CH_3C(O)O_2NO_2 + \text{heat} \rightarrow CH_3C(O)O_2 + NO_2 \quad \text{(R1-29)}$$

RO_2 radicals can be lost via its reaction with NO and NO_2.

RO_2 reaction with NO leads to two reaction pathways, one is to generate RO radicals and NO_2, and the other one is to generate organic nitrates as below.

$$RO_2 + NO \rightarrow RO + NO_2 \quad \text{(R1-8)}$$
$$RO_2 + NO + M \rightarrow RONO_2 + M \quad \text{(R1-30)}$$

Because RO radicals can regenerate HO_2 radicals via the reaction with O_2 as (R1-9), the branching ratio between (R1-8) and (R1-30) becomes important, which is known to depend on the carbon number of RO_2 radical, temperature and pressure [Carter and Atkinson., 1989].

RO_2 radicals' reaction with NO_3 radicals is an important loss pathway in night time. In the clean atmosphere, RO_2 radicals' reaction with HO_2 radicals and RO_2 radicals itself are two of the dominant radical loss processes as below.

$$RO_2 + NO_3 \rightarrow RO + NO_2 + O_2 \quad \text{(R1-31)}$$
$$RO_2 + HO_2 \rightarrow ROOH + O_2 \quad \text{(R1-32)}$$
$$RO_2 + RO_2 \rightarrow ROOR + O_2 \quad \text{(R1-33)}$$

Recent experimental and theoretical work has, however, suggested that the reactions of HO_2 with some substituted RO_2 radicals do not exclusively terminate radical chemistry Thornton et al. [2002]. Hasson et al. [2004] reported a significant yield of OH radicals by the HO_2 reaction with acetylperoxy radicals [Hasson et al., 2004, Dillon and Crowley., 2008] as below. The other two reactions, (R1-34) and (R1-35) are well known radical termination pathway.

$$HO_2 + CH_3C(O)O_2 \rightarrow CH_3C(O)O_2H + O_2 \quad \text{(R1-34)}$$
$$\rightarrow CH_3C(O)OH + O_3 \quad \text{(R1-35)}$$
$$\rightarrow OH + CH_3C(O)O + O_2 \quad \text{(R1-36)}$$

1-3. Methods to measure the ambient peroxy radicals

Four kinds of the detecting techniques for tropospheric peroxy radicals are presented in this section. Except for MIESR (as described in Section.1-3-1.) technique, the other peroxy radical measurement technique employ chemical conversion method described as following. This is because the absence of absorption bands suitable for detection by optical methods.

1-3-1. Matrix Isolation and Electron Spin Resonance

Matrix Isolation and Electron Spin Resonance, MIESR technique is still the only direct method for atmospheric detection of HO_2 radicals with high selectivity [Mihelcic et al., 1978, 1985, 1990, 1993]. Sample air is introduced into a low-pressure region to trap the radicals in D_2O matrix at a temperature of 77 K, and collected samples are transferred to laboratory for analysis. Other species can also be analyzed simultaneously from ESR spectrum, for example NO_3, NO_2, $CH_3C(O)O_2$ and the sum of peroxy radicals [Mihelcic et al., 1990]. In spite of advantages of direct detection and multi-species observations, the sampling time is long (30 min) and the number of measurements is limited.

1-3-2. Peroxy radicals Chemical Amplification

Peroxy radical chemical amplification, PERCA originated by Cantrell and Stedman [1982] is a method of measuring the total concentration of peroxy radicals, i.e. the sum of HO_2 and RO_2. In this method, peroxy radicals are converted to relatively high concentrations of NO_2 via a chain reaction by the addition of high concentrations of NO and CO in a reaction tube. The NO_2 product is then quantified by the appropriate measurement technique, e.g. luminol chemiluminescence [Cantrell and Stedman 1982], laser-induced fluorescence [Sadanaga et al., 2004] and cavity ring-down [Liu et al., 2009] spectroscopy. In order to obtain absolute concentrations, the chain length of the

amplification and the response of the NO_2 detector have to be determined in calibration experiments. And its details are described further in Chapter.4.

1-3-3. Laser-induced fluorescence coupled with chemical conversion by NO

HO_2 radicals can be measured selectively by laser-induced fluorescence (LIF) OH detection coupled with chemical conversion method by the reaction with NO [Hard et al.,1995; Mather et al., 1997; Kanaya et al.,2001]. Sample air is introduced into a low-pressure fluorescence detection cell, and where pure NO is added for HO_2 conversion. In this system, ambient RO_2 radicals can not be converted to OH in the fluorescence cell in multistep as (R1-8), (R1-9) and (R1-3) because conversion reaction time is short and the oxygen number density is small due to the expansion of ambient air. Some kind of RO_2 radicals generated from the OH reaction with saturated hydrocarbon C_1-C_4 (hydrogen atom abstraction) was tested to be confirmed that interferences can be negligible [Kanaya et al., 2001, Ren et al., 2004]. Recently, however, Fuchs et al., [2011] reported that RO_2 radicals generated from OH reaction with alkene and aromatic precursors including isoprene (mainly OH-addition) are detected as HO_2 with the relatively high sensitivity larger than 80 % with respect to that for HO_2. They proposed a solution that by reducing the NO concentration and/or the transport time between NO addition and OH detection, interference from these RO_2 radicals can be reduced to values below 20% relative to the HO_2 detection sensitivity. And its technical details are described further in Chapter.3.

LIF OH detection technique has also expanded its capacity to RO_2 measurement [Fuchs et al., 2008]. In this system, RO_2 radicals are converted and reserved as HO_X ($OH + HO_2$) by adding CO and NO to pressure reduced flow reactor (25 hPa) and its reaction scheme is described as (R1-8, 9, 3, 1 and 2).

$$RO_2 + NO \rightarrow RO + NO_2 \quad \text{(R1-8)}$$
$$RO + O_2 \rightarrow HO_2 + \text{calbonyl} \quad \text{(R1-9)}$$
$$HO_2 + NO \rightarrow OH + NO_2 \quad \text{(R1-3)}$$
$$CO + OH \rightarrow CO_2 + H \quad \text{(R1-1)}$$
$$H + O_2 + M \rightarrow HO_2 + M \quad \text{(R1-2)}$$

Then HO_X radicals are measured by LIF OH detection coupled with chemical conversion by the reaction with NO.

1-3-4. Peroxy radicals Chemical Ionization Mass Spectrometry

Peroxy radicals Chemical Ionization Mass Spectrometry, called RO_XMAS or PerCIMS originated by Reiner et al [1997] is a method of measuring the total concentration of peroxy radicals, i.e. the sum of HO_2 and RO_2. In this method, peroxy radicals are converted to relatively high concentrations of H_2SO_4 via a chain reaction by the addition of high concentrations of NO and SO_2 in a reaction tube. This technique differs from PERCA in that OH is recycled back to HO_2 via the reaction with SO_2 as below.

$$RO_2 + NO \rightarrow RO + NO_2 \quad \text{(R1-8)}$$
$$RO + O_2 \rightarrow HO_2 + \text{calbonyl} \quad \text{(R1-9)}$$

$$HO_2 + NO \rightarrow OH + NO_2 \quad \text{(R1-3)}$$
$$OH + SO_2 + M \rightarrow HSO_3 + M \quad \text{(R1-16)}$$
$$HSO_3 + O_2 \rightarrow HO_2 + SO_3 \quad \text{(R1-17)}$$
$$SO_3 + H_2O + M \rightarrow H_2SO_4 + M \quad \text{(R1-37)}$$

The H_2SO_4 product is then quantified by chemical ionization mass spectrometry (CIMS). A distinct advantage of this technique is much smaller instrumental background signal because ambient H_2SO_4 concentration is very low relative to amplified H_2SO_4 product.

This technique has also expanded to selective measurement of peroxy radical concentrations of HO_2 and RO_2. There are two kind of separating method between HO_2 and RO_2, but the idea comes from the same principle that radical loss reaction

$$RO + NO + M \rightarrow RONO + M \quad \text{(R1-38)}$$

is made to compete with the HO_2 recycle reaction (R1-9). Hanke et al., [2002] achieved the separation by diluting atmospheric air in either N_2 or O_2 buffer in which O_2 mixing ratio has changed from 2 % up to 70 %. And Edwards et al., [2003] has achieved the

separation by increasing the NO mixing ratio from the order of 10 ppm up to 1000 ppm or more. These competing methods are so called chemical modulation method.

Recent instrumental development of PerCIMS coupled with oxygen dilution modulation method by Hornbrook et al., [2011] has succeeded in efficient removal of RO_2 radicals generated from the OH reaction with methane (hydrogen atom abstraction) with the removal efficiency larger than 80%. Whereas RO_2 radicals generated from OH reaction with alkene and aromatic precursors including isoprene (mainly OH-addition) can not be removed so much with the efficiency lower than 20%. This can be caused by the same reason as interferences by LIF HO_2 detection that RO radicals' reaction of (R1-38) and (R1-9) can compete with the RO reaction pathways of decomposition or isomerization easily to produce HO_2 radicals.

1-4. The concept of OH and HO_2 reactivity measurement

So far in Chapter 1, recent understandings of ambient peroxy radical reactions and its measurement techniques are reviewed. Peroxy radicals play the important role in the photo oxidation cycle of the troposphere producing ozone and SOA. As described above, peroxy radicals have the difficulty to evaluate its complicated ambient reaction mechanism; this can be caused mainly by the diversity of organic peroxy radicals and lack of direct detection of peroxy radicals. So up to now, a number of step by step laboratory experiments have been build up to describe the ambient peroxy radicals' reactions. However, bottom up study like this does not always ensure the whole picture of atmospheric chemistry, especially in troposphere where a huge kind of chemical species exist.

Recent strategy to investigate ambient OH reaction mechanism has been successfully explored by adopting the total OH loss rate measurement to ambient measurement [e.g. Kovacs et al., 2001, Sadanaga et al., 2004].

Kovacs et al.,[2001] successfully implemented ambient OH reactivity measurement by using a moveable injector for OH addition and LIF detection technique. This technique is based on the decay of OH concentrations when mixed with ambient air in a flow tube. Approximately 500 ppt of OH and HO_2 in approximately a 1:1 ratio, produced by photolysis of water vapor by a mercury lamp, is released in to a 5 cm diameter, glass flow tube by a moveable injector. Ambient air flows into the flow tube

and the relative OH concentration is measured downstream by LIF. As the total flow rate and reaction distance are known, the reaction time between the injected OH and the ambient air is known for any injector tube position. Plotting OH concentration versus reaction time yields decay profiles that are fit by single exponentials to extract the first order rate coefficient. On the other hand, Sadanaga et al., [2004] successfully implemented ambient OH reactivity measurement by using laser-flash photolysis and LIF detection technique. Briefly, ambient air is pumped through the photolysis cell, and OH radicals are generated by 266 nm photolysis of ambient O_3 in the presence of ambient water vapor. Generated OH radicals react with ambient reactive species, and its time profiles are monitored by time resolved laser-induced fluorescence (LIF) OH detection technique.

The advantage of this total OH loss rate measurement is that it is not possible to measure every compound with which OH reacts. This technique can investigate exclusively ambient loss rate for OH radicals. The total OH loss rate measured was compared with total OH loss rate calculated by summing the concentrations of the individually measured OH sinks (e.g. NO_X, VOCs, etc) with their respective reaction rate coefficient with OH, resulted in that there exist missing sinks[e.g. Kovacs et al., 2003, Sadanaga et al., 2004]. Resulting, only OH production rate can be derived by combining total loss rate measurement and concentration measurement assuming OH radicals concentration is a steady state with a balance between production and loss, and hence

$$\frac{d[OH]}{dt} = P(OH) - L(OH) = P(OH) - [OH]\sum_i k_{i+OH}[i] \quad (1.1)$$

$$\text{Assuming} \quad P(OH) = L(OH) \quad (1.2)$$

$$\therefore P(OH) = [OH] \times \sum_i k_{i+OH}[i] \quad (1.3)$$

where [i] is the concentration of a given and/or missing sink.

1-5. Objectives of this study

In this study, to get better understandings of nature and roles of peroxy radicals, ambient kinetic measurement such as applied to OH radicals has been adopted to peroxy radicals study. Specifically, a technique for total HO_2 loss rate measurement has been

developed. Two instruments for OH reactivity measurement based on a laser-induced pump and probe technique have been used in each experiment. One is owned by Dr. Christa Fittschen laboratory, University of Lille1, which is used for the experiments described in Chapter.2 titled as “Characterization of the instrument for the OH reactivity measurement”. The other one is owned by Prof. Yoshizumi Kajii laboratory, Tokyo Metropolitan University, which is used for the experiments described in Chapter.3 titled as “Development of a technique for total HO_2 reactivity measurement”. The constructions and characters of each instrument are specified in each chapter. Also in Chanpter.3, ambient total HO_2 reactivity observation conducted at Hachioji campus of Tokyo Metropolitan University is depicted and the possible candidates for observed missing HO_2 reactivity are discussed.

As for peroxy radical concentration measurement, a recently developed technique for the selective measurement of atmospheric peroxy radical concentrations of HO_2 and RO_2 using a denuding method is described in detail in Chapter.4. PERCA technique which is thought to be able to measure total peroxy radicals concentration (HO_2+RO_2) has been explored for the selective measurement of atmospheric peroxy radical concentrations. These techniques have been evaluated through the atmospheric measurement.

In Chapter.5 as conclusion, in addition to the summary of this study, the future applications of these instruments are mentioned.

Chapter 2.
Characterization of an instrument for the OH reactivity measurement

The characterization of the instrument for the OH reactivity measurement will be discussed in this chapter. Sadanaga et al., [e.g. 2004], who firstly applied a laser pump and probe OH loss rate measurement technique to ambient measurement, reported that OH signals in zero air show two distinct decay components (Figure 2-1). They suggested that the slower decay reflects the true OH reactivity, OH diffusion, and/or turbulence in the flow tube. On the other hand, the faster decay rate is suggested to be dilution of OH due to heat expansion process by the laser shot as a possible cause. Parker et al., [2011], however, reported that OH decay signal in zero air obtained by the instrument at University of Lille1 consists of only single exponential slow decay. The occurrence factor for two decay components was investigated by changing some physical factors. This characterization should be important procedure to determine the upper and lower detection limit for OH loss rate measurement.

Additions to this, OH recycle effects caused by HO_2 reaction with NO in the photolysis cell were investigated. CO and CH_4 are tested both which can re-produce OH radicals under NO-rich condition. These effects can be the interference to OH reactivity measurement. The influence of the additional OH production via the HO_2 reaction with NO is evaluated by experiments and chemical model simulations.

2-1. Experimental

2-1-1. Instrumental description of OH reactivity measurement

A recently developed OH reactivity measurement system at University of Lille1 [Parker et al., 2011, Amedro et al., 2012] was used for the experiments described in this chapter, which comprised of three main components- a photolysis laser, a reaction cell, and the LIF OH detection. A schematic diagram of the instrument is shown in Figure 2-2.

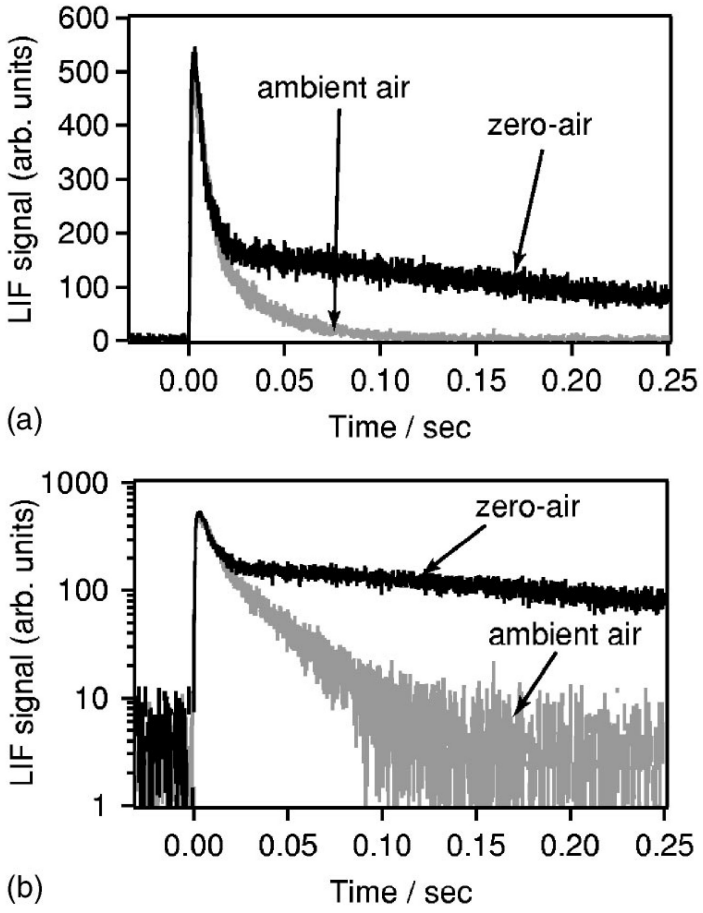

Figure.2-1 OH decay profiles (adapted from Sadanaga et al., 2004)

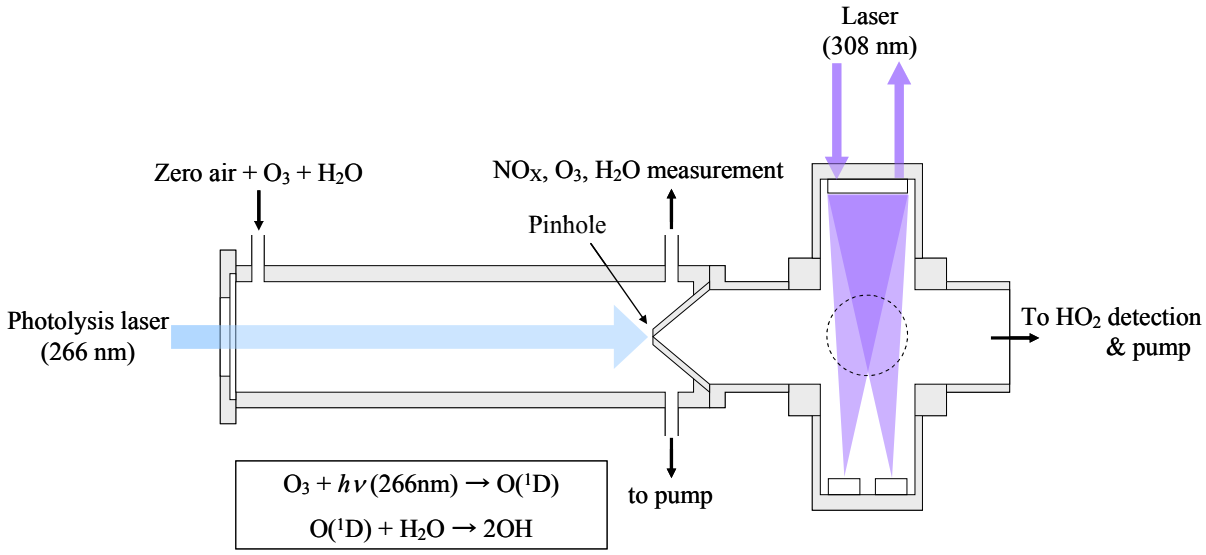

Figure.2-2 Schematic diagram of the instrument for OH reactivity measurement:

The photolysis laser is a Quantel Brillant YAG laser operating at 1 Hz with a pulse energy of ~ 4 mJ at 266 nm after frequency quadrupling. The beam is expanded before entering the reaction cell, and in this work normally had a diameter of 25 mm. An iris diaphragm is mounted in front of the reaction cell to reduce the beam size entering the reaction cell.

The reaction cell is a stainless steel cylinder 48 cm long with an internal diameter of 5 cm. One end is closed by a Suprasil quartz window (CVI Melles Griot) allowing the photolysis laser beam to enter, the other end is designed in such a way as to adapt onto the sampling cone of the LIF cell, sealed with an o-ring. Gas is introduced via a Swagelok fitting at the quartz window end, at the other end four further Swagelok fittings are mounted equally spaced around the cylinder: these fittings allow a pump to be attached along with additional sampling instruments (O_3, NO_X, H_2O) as well as pressure/temperature monitoring. The flow within the cell was ~18 SLPM (Standard Litters per Minute), of which ~9 SLPM is drawn into the LIF cell with 1 mm pinhole and ~3 SLPM with 0.4 mm pinhole, respectively. The excess gas flow passes by additional analyzers for O_3, NO_X and H_2O measurements.

The hydroxyl radicals are detected with the newly developed University of Lille Fluorescence Assay by Gas Expansion (UL-FAGE) instrument. As can be seen in Figure 2-2, two White type multipass cells (approximately 30 passes alignment) similar to those used at Pennsylvania State University [Faloona et al., 2004] mounted in series in order to detect OH and HO_2 simultaneously. The first cell is for OH detection, the second one is for HO_X (OH + HO_2) detection by injecting NO to convert the HO_2 to OH which is subsequently detected by LIF. But only the first OH detection cell was used in this study. The pressure inside both fluorescence detection cells is reduced to ca. 1.5 Torr using a pinhole (1 mm or 0.4 mm id) and a dry vacuum pump (Edwards GX6/100L) in order to minimize the collisional quenching of the excited OH molecules by air (FAGE technique). The A-X(0,0) $Q_1(3)$ line of OH (corresponding to λ = 308.1541 nm [Dorn et al., 1995]) was excited by use of a tunable frequency-doubled dye laser (Sirah Laser PrecisionScan PRSC-24-HPR) pumped by the frequency doubled output of a Nd:YVO_4 laser (Spectra Physics Navigator II YHP40-532QW) with a repetition rate of 5 kHz. The laser energy is split between the OH cell (2 mW), the HO_2 cell (1 mW) and the wavelength reference cell (0.3 mW) using CVI Melles Griot beam splitters, the OH and HO_2 beams being coupled to two 10 m OZ Optics fibres of 200 µm diameter via collimators (Melles Griot) for transport to the detection cells. The fluorescence is collected and focused through two optical lenses and passes through an interference filter (Barr Associates) onto a gated CPM (Channel Photon Multiplier,

Perkin-Elmer MP-1982). The output signal from the CPM is counted between 400 and 1200 ns after the laser excitation using a photon counting board (National Instruments PCI-6602).

The synchronization of both pump and probe laser is achieved with two delay generators (DG535, Stanford research Systems) and the PC counting card via LabView (v2011, National Instruments). Data are normally accumulated for 5 – 10 minutes (i.e. 300 – 600 photolysis shots).

2-1-2. Gas preparation and data analysis

O_3 was produced with an ozone generator (Ansyco SYCOS KT-GPTM) and mixed with variable flows of humid air (generated by passing a fraction of the bath gas through a water bubbler) and CH_4 (or CO) (both Air Liquide, N55 and 1% in N_2 for CH_4 and CO, respectively). In the OH recycle experiment, NO (Air Liquide, 5 ppm in N_2) was added to the sample and its concentration was measured by a commercial NO_X analyzer (Thermo, 42i TL). All experiments were carried out at 295 K and 760 Torr of air. The different gases were introduced to the reactor using calibrated mass flow controllers (Bronkhorst F-201 and Brooks 5800S). Pressure within the photolysis cell was kept constant and monitored with a 0 – 3 bar pressure transmitter (Keller PAA-41). Typical concentrations of O_3 and water vapor inside the photolysis cell are 30 ppbv and 5000 ppmv which are monitored by an O_3 analyzer (Thermo Scientific model 49i) and a dew point hygrometer (Michell Instruments S8000), respectively. A large excess of CH_4 (or CO) over the radical concentration (~3×10^8 molecules cm^{-3}, typically) has been used, allowing pseudo-first order conditions. As a consequence, radical decay kinetics follows Equations. (2-1 and 2-2):

$$\frac{d[OH]}{dt} = -\left(k_{CH_4+OH}[CH_4] + k_{NO+OH}[NO] + k_{wall}\right)\times[OH] \quad (2\text{-}1)$$

$$\frac{d[OH]}{dt} = -\left(k_{CO+OH}[CO] + k_{NO+OH}[NO] + k_{wall}\right)\times[OH] \quad (2\text{-}2)$$

with k_i being the second-order rate coefficient for OH reaction with corresponding species and k_{wall} the wall losses. The decay rate was analyzed by fitting to the following equation.

$$S = a + b \cdot \exp(-k't) \qquad (2\text{-}3)$$

where S is the LIF signal normalized by energy of each 308 nm shot, a and b are parameters according to the background signal and the initial OH concentrations, respectively.

2-2. Results and discussion

– OH decay profile variation against physical factors –

Some physical factors were changed to investigate which factor was more influential to the slower decay component. Pinhole size (i.e. to change the flow rate introduced to LIF cell), total flow rate inside the photolysis cell, laser energy and the beam size were changed in this study. OH sensitivity can be reduced due to inlet wall loss reaction for OH when using smaller pinhole. But, inlet wall loss was not observed effectively.

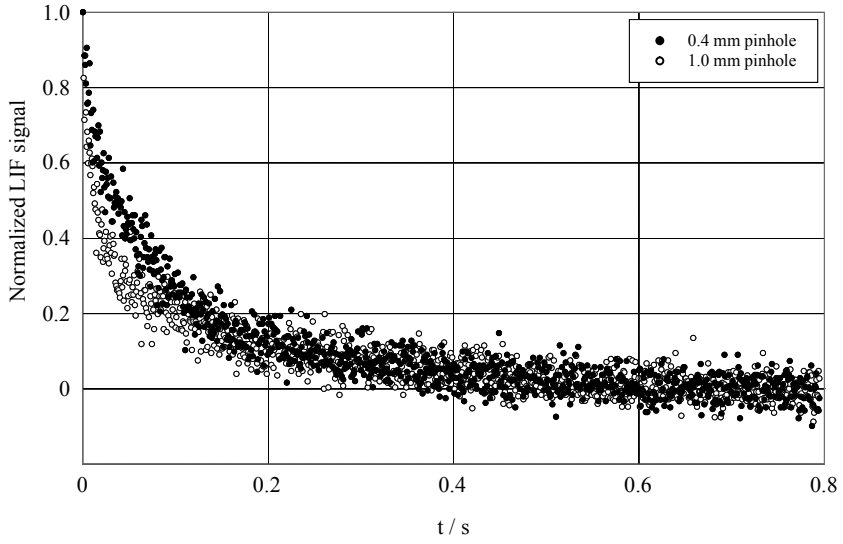

Figure.2-3 The normalized OH decay profile in zero air obtained with 1 mm and 0.4 mm pinhole. OH signals are divided by its signals at the time of laser flash photolysis. Total flow rate:18 SLPM, Laser energy:4 mJ, Beam size:25 mm dia, Photolysis laser repetition rate: 1 Hz. Background signal in LIF detection is subtracted from its raw data.

Figure.2-3 shows the normalized OH decay profile in zero air obtained with 1 mm and 0.4 mm pinhole. Both two OH decays do not show one phase exponential in this condition. The decay with 1 mm pinhole has faster OH signal decrease in initial step than that with 0.4 mm. To investigate how influential the faster OH decay component is to the slower OH decay component, these two OH decays are analyzed by changing the starting point of analysis range using the fitting equation (2-3) (Figure.2-4). The end point of analysis range is fixed to be 0.8 sec. Both analyzed OH decay rate are decreasing with the starting point increasing as shown in Figure.2-5. The analyzed OH decay rate with 0.4 mm is decreasing gradually from the starting point of 0 to 0.1 sec. On the other hand, the analyzed OH decay rate with 1 mm fall steeply with increasing the starting point, then it is decreasing slowly. This indicates that both the faster decay components for 1 mm and 0.4 mm affect the determination of slower decay component and the faster decay component for 1 mm is faster than that for 0.4 mm.

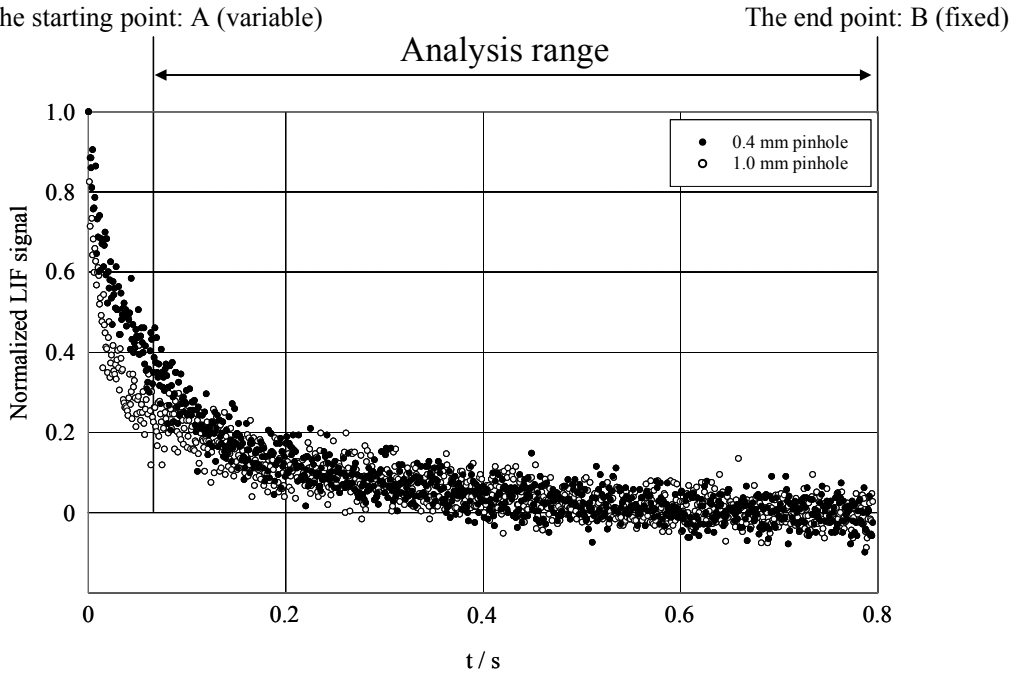

Figure.2-4 Schematic diagram of analysis range, indicating the starting point and the end point.

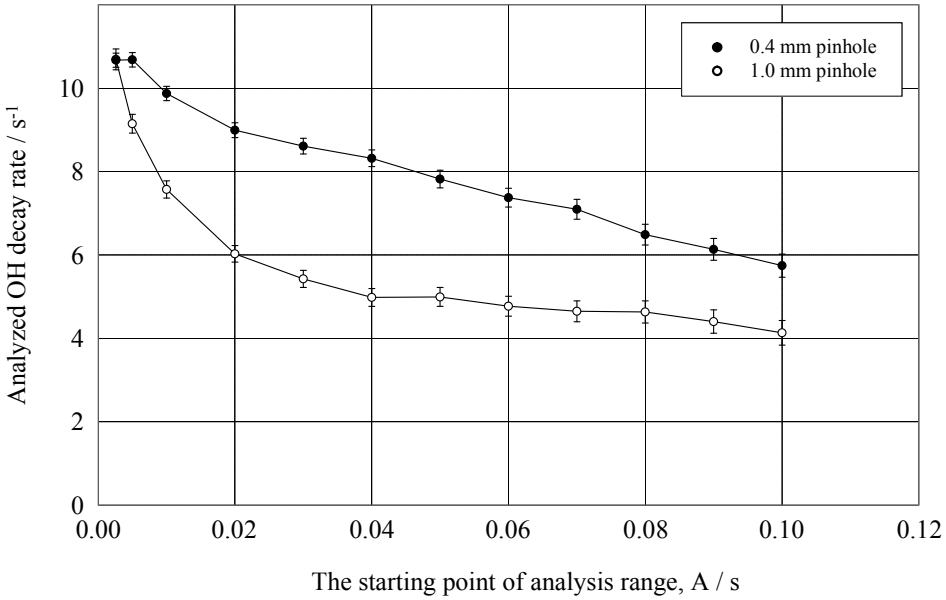

Figure.2-5 Plot of analyzed OH decay rate as a function of analysis starting point with 0.4 mm pinhole (closed circle) and 1.0 mm pinhole (open circle).

Next, fixing the pinhole size of 0.4 mm, the observed OH decay in zero air changed by other factors, flow rate, laser energy and beam size in zero air have been analyzed in the same manner as shown in Figure.2-6, 2-7 and 2-9, respectively. The normalized OH decay profiles obtained with each beam size are shown in Figure.2-8. With higher flow rate condition (18 SLPM), the analyzed OH decay rate is gradually decreasing from the starting point of 0 to 0.1 sec, whereas with lower flow rate condition (9.5 SLPM) approaching to the constant value of 7 s^{-1} at around the starting point of 0.05 sec. Not much difference of the OH decay rates against each laser energy has found as shown in Figure.2-7. A large dependency was observed in changing the beam size; the faster decay component can be faster with decreasing the beam size (Figure.2-9). But the slower decay component approach to the same constant value of around 7 s^{-1} with all beam size. This can be also confirmed visually apparent as shown in Figure.2-8. It should be noted that the beam size has been changed using an iris diaphragm, that is, the total laser energy entering to the photolysis cell is different in each laser beam size. Because there is no dependency against the laser energy as shown in Figure.2-7, the behavior of analyzed OH decay rate in Figure.2-9 is considered to be caused mainly by the beam size.

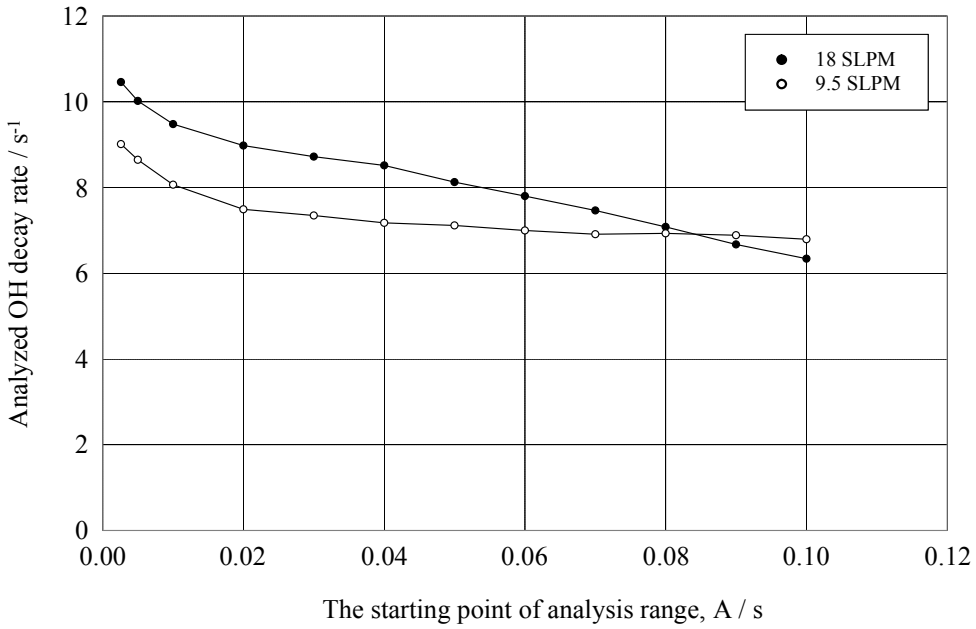

Figure.2-6 Plot of analyzed OH decay rate as a function of analysis starting point with the flow rate of 18 SLPM (closed circle) and 9.5 SLPM (open circle). Pinhole size:0.4 mm

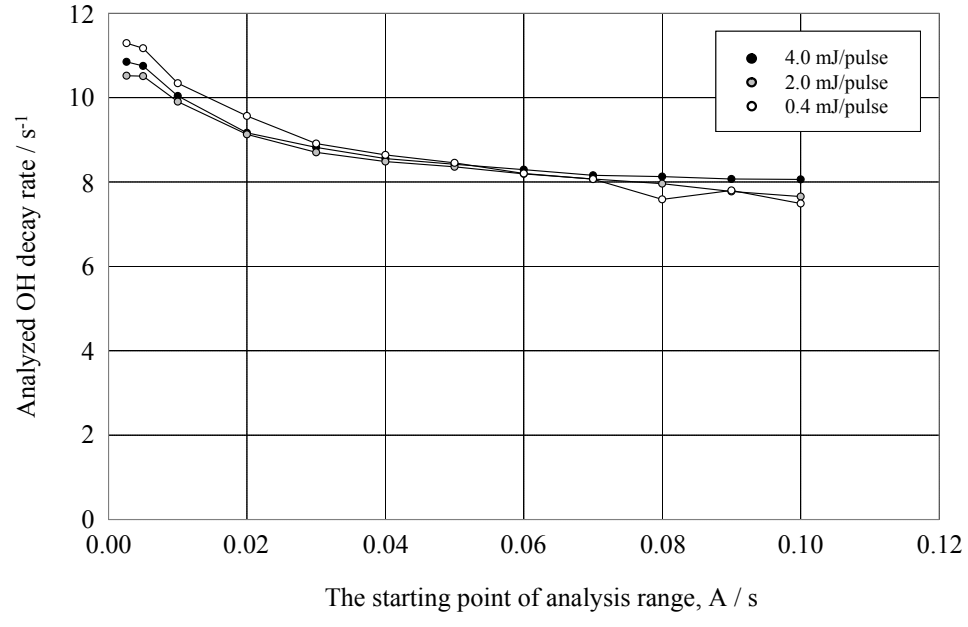

Figure.2-7 Plot of analyzed OH decay rate as a function of analysis starting point with 4 mJ/pulse (closed circle), 2 mJ/pulse (gray circle) and 0.4 mJ/pulse (open circle). Pinhole size:0.4 mm

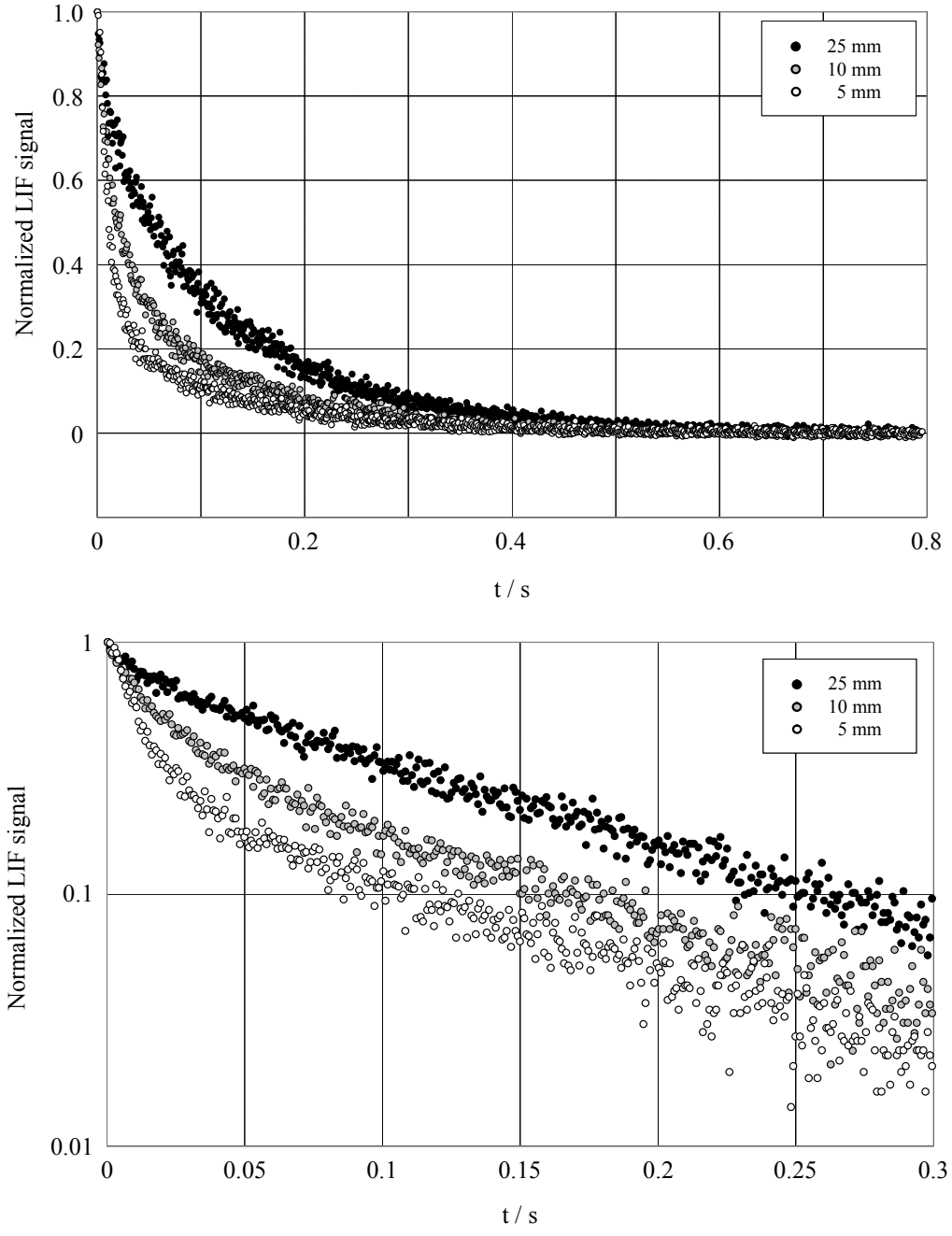

Figure.2-8 The OH decay profiles with each beam size, 25 mm (closed circle), 10 mm (gray circle) and 5 mm (open circle). Pinhole size:0.4 mm. Upper shows linear scale plot and lower shows log scale plot.

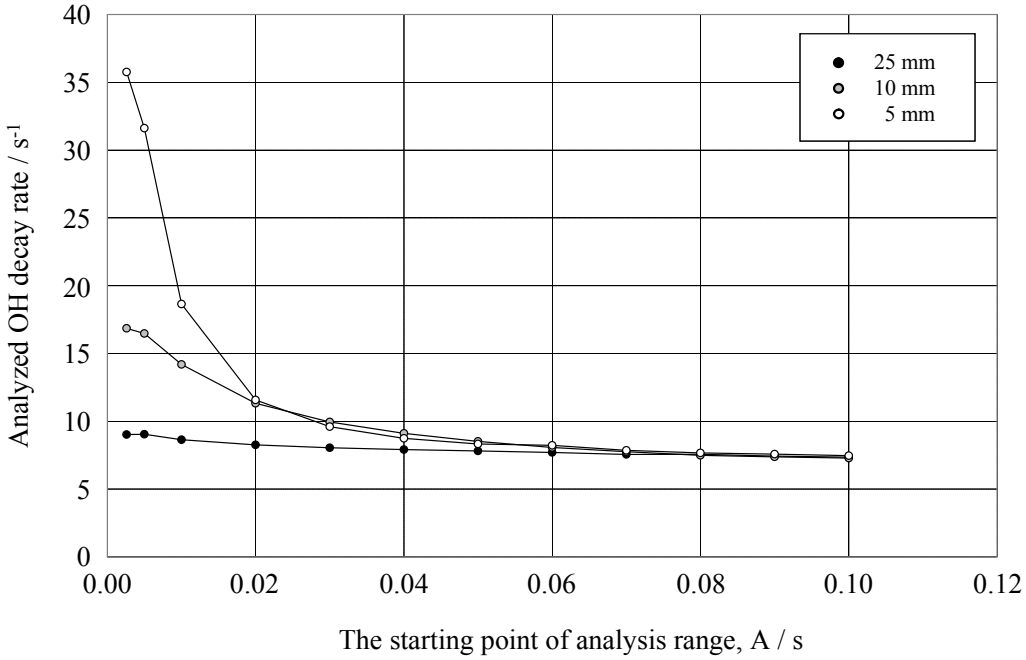

Figure.2-9 Plot of analyzed OH decay rate as a function of analysis starting point with beam size of 25 mm (closed circle), 10 mm (gray circle) and 5 mm (open circle). Pinhole size:0.4 mm

The same experiments as above with the pinhole size of 1 mm are conducted and resulted in Figure.2-10, 2-11 and 2-13, which represent the analyzed OH decay rate in which flow rate, laser energy and beam size, respectively are changed. The normalized OH decay profiles obtained with each beam size are shown in Figure.2-12. Almost the same behaviors have been found as the experiments conducted with 0.4 mm pinhole. The faster decay component in higher flow rate condition (18 SLPM) is faster than that in lower flow rate (9.5 SLPM).

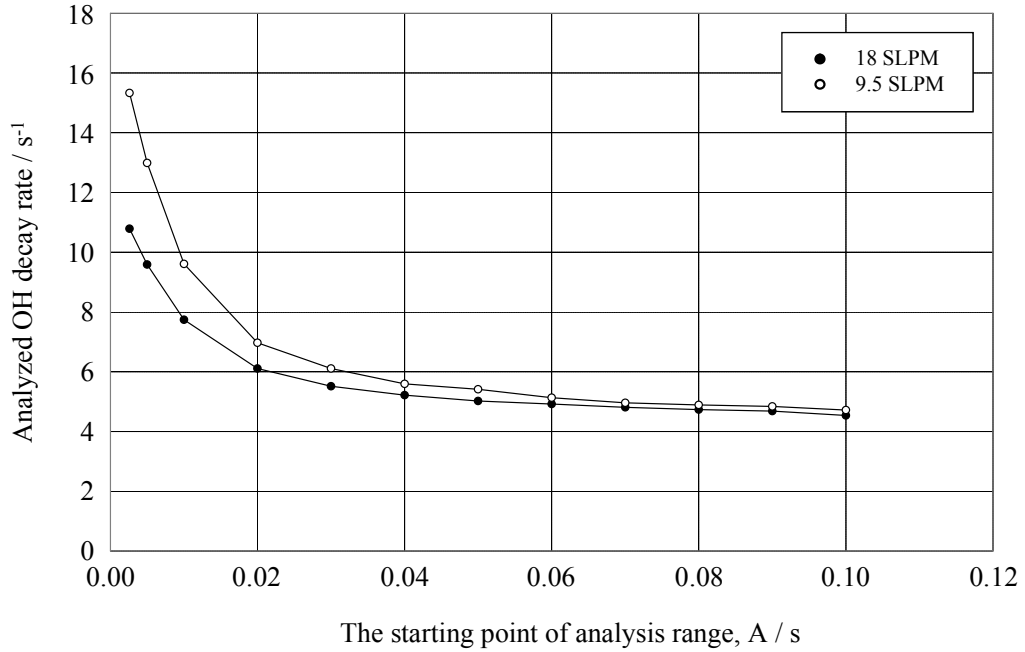

Figure.2-10 Plot of analyzed OH decay rate as a function of analysis starting point with the flow rate of 18 SLPM (closed circle) and 9.5 SLPM (open circle). Pinhole size:1.0 mm

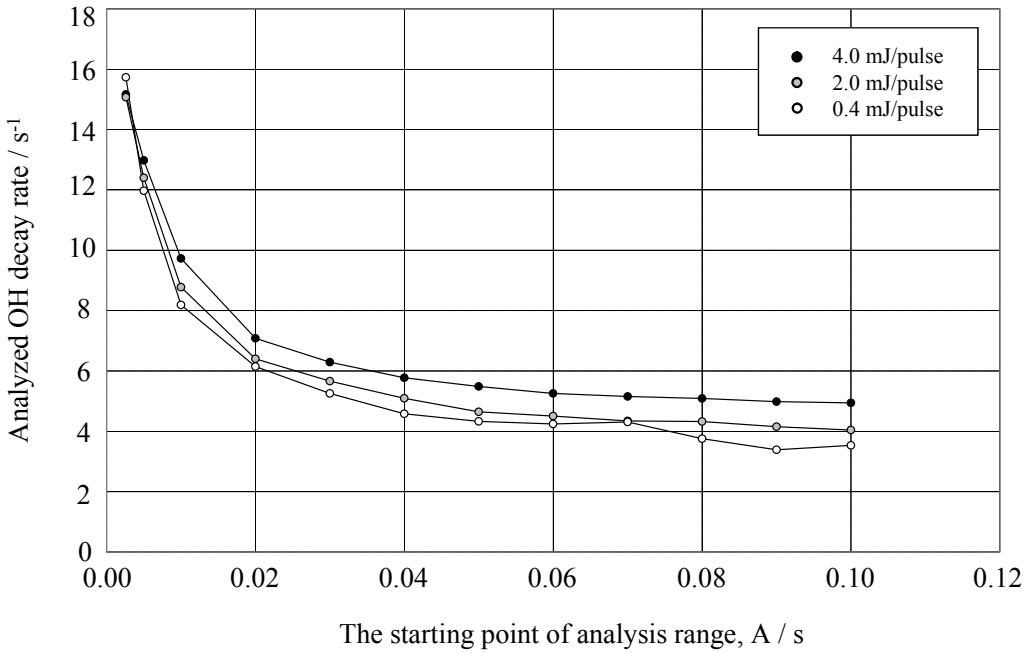

Figure.2-11 Plot of analyzed OH decay rate as a function of analysis starting point with 4 mJ/pulse (closed circle), 2 mJ/pulse (gray circle) and 0.4 mJ/pulse (open circle). Pinhole size:1.0 mm

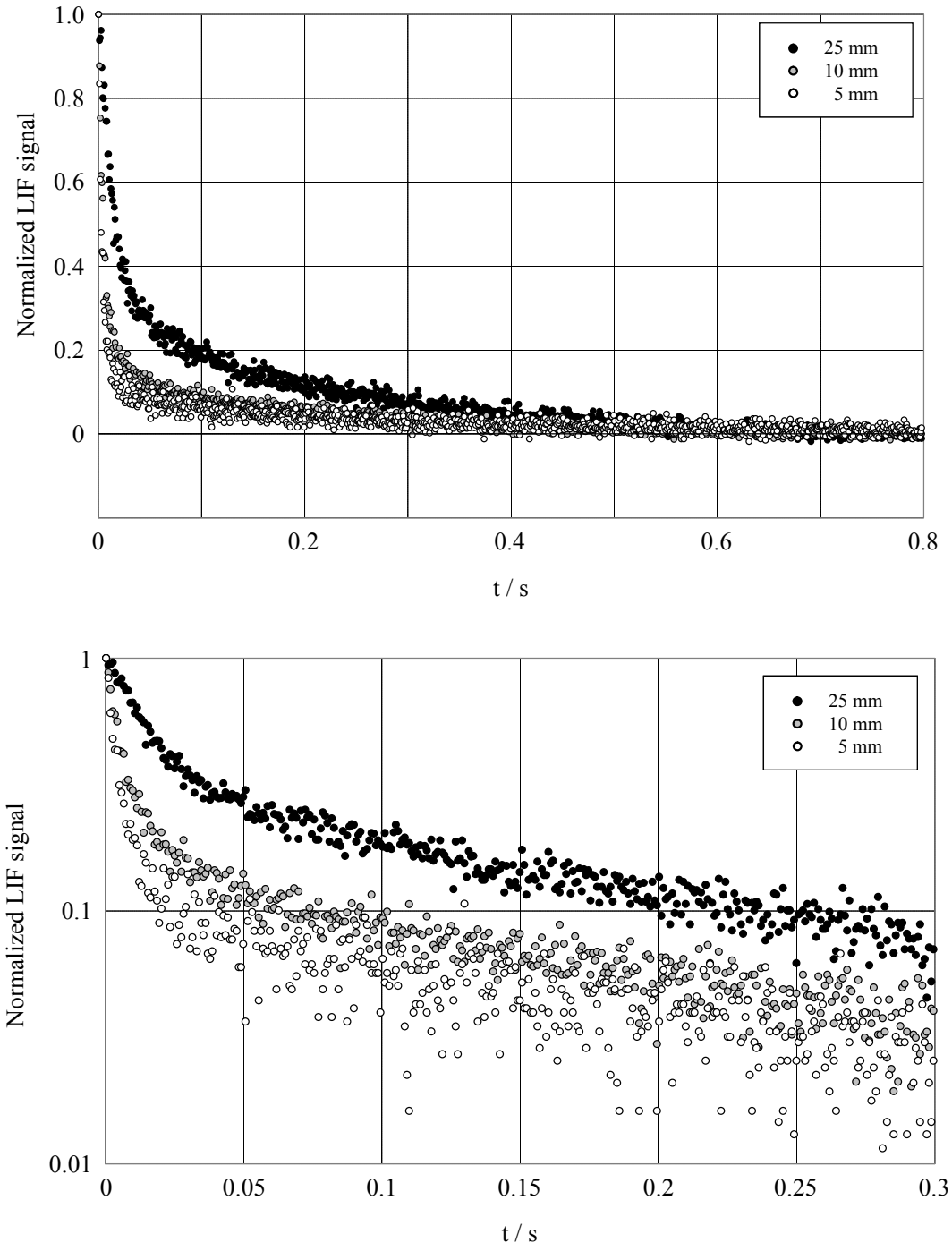

Figure.2-12 The OH decay profiles with each beam size, 25 mm (closed circle), 10 mm (gray circle) and 5 mm (open circle). Pinhole size:1.0 mm. Upper shows linear scale plot and lower shows log scale plot.

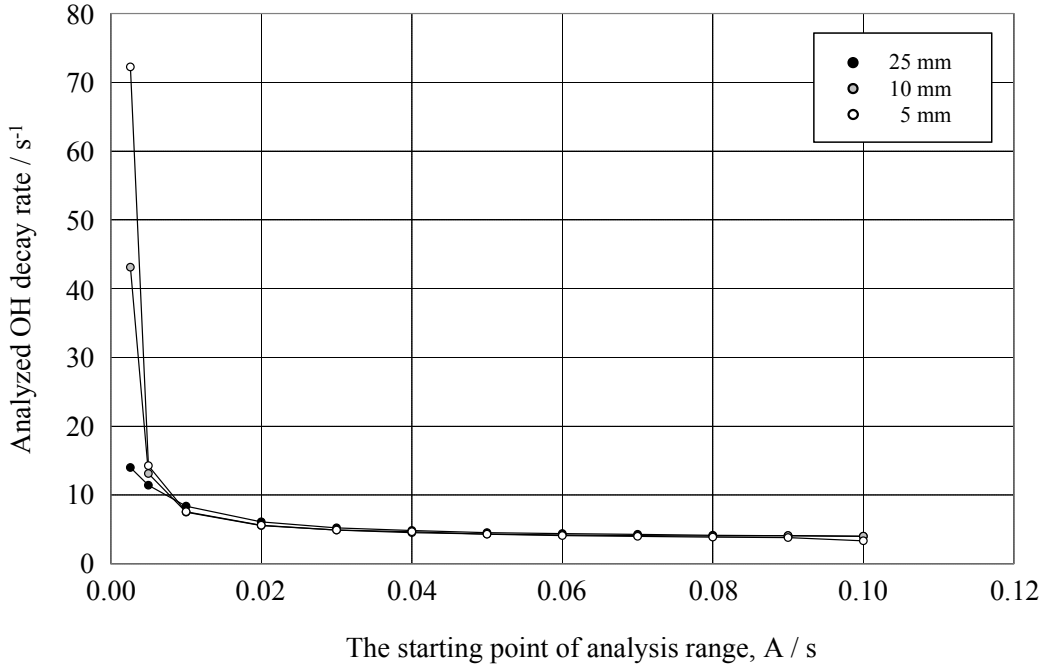

Figure.2-13 Plot of analyzed OH decay rate as a function of analysis starting point with beam size of 25 mm (closed circle), 10 mm (gray circle) and 5 mm (open circle). Pinhole size:1.0 mm

From these experiments and results, a question arises that which configuration is better for the OH reactivity measurement, configuration 1 in which the fast decay component can achieved to be slower with the condition of 0.4 mm pinhole, higher flow rate in the photolysis cell and/or larger beam size or configuration 2 in which the fast decay component achieved to be faster with the condition of 1 mm pinhole, lower flow rate in the photolysis cell and/or smaller beam size. Both two configurations are tested by measuring OH reactivity of the samples consist of zero air and various CH_4 concentration. CH_4 concentrations are changed from 0 to 7.9×10^{16} molecules cm^{-3}, comparable 0 to 500 s^{-1} of OH reactivity. Figure.2-14 and 2-15 show the measured OH decay profiles of each sample. They are analyzed in the same manner as changing the starting point from 0 to 0.05 sec using the fitting equation (2-3). In this experiment, only one factor, pinhole size is changed to achieve the configuration 1 and 2 for easy comparison to maintain the gas concentrations condition including for CO, CH_4 and water vaper as the same for each experiment. Results are shown in Figure.2-16 (pinhole size 0.4 mm) and 2-17 (pinhole size 1 mm). Ratios of OH decay rate indicate the analyzed OH decay rate divided by the calculated OH decay rate using CH_4 concentration and rate coefficient for OH reaction with CH_4. The value 0 of OH decay

rate ratios means the analysis can not be done properly because the LIF signal already decreased to zero at that analysis starting point. The analyzed OH decay rates are subtracted by the corresponding OH decay rate for zero air in each starting point. Configuration 1 (Figure.2-16) shows ratios of OH decay rate are relatively scattered at around the starting point from 0 to 0.005 sec.

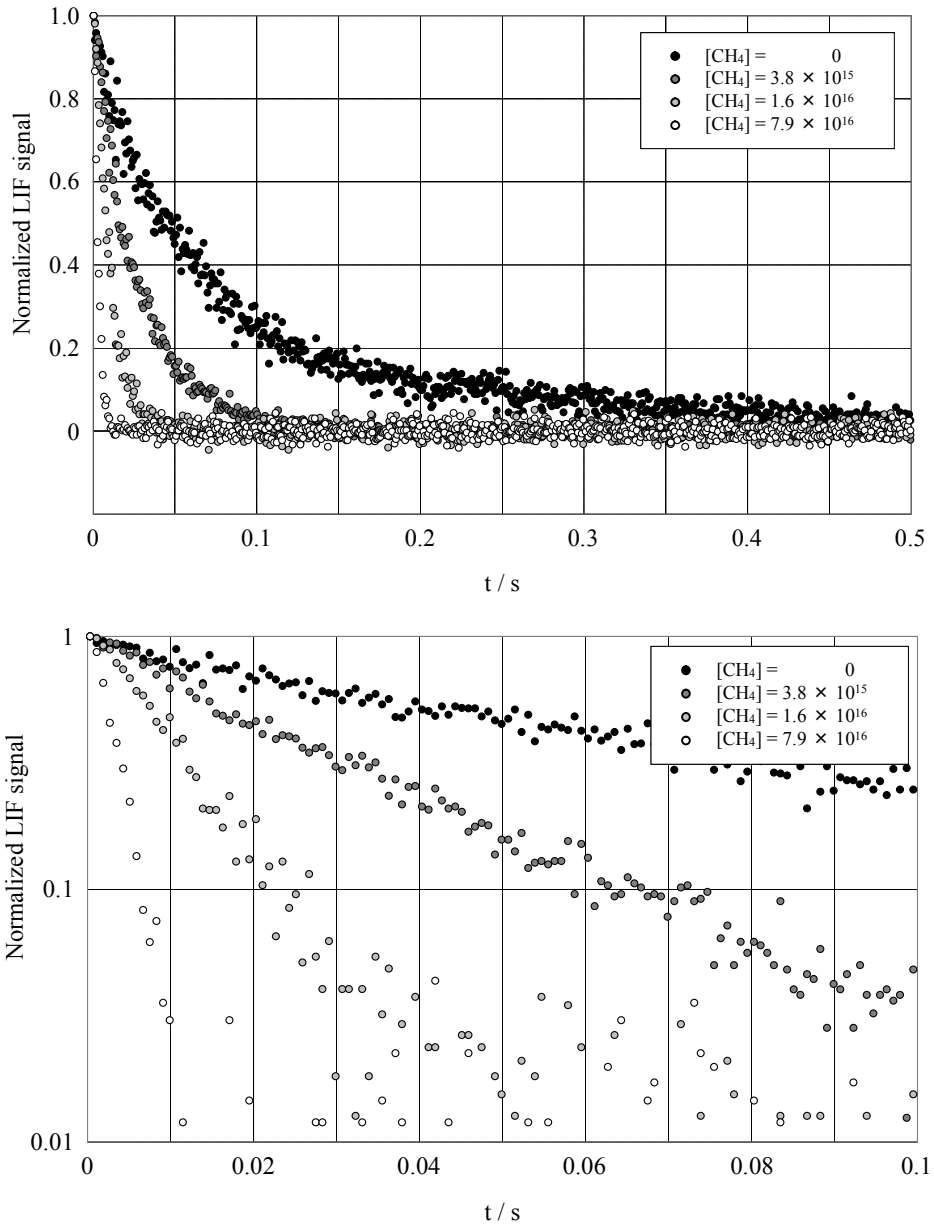

Figure.2-14 The OH decay profiles in several CH_4 concentrations (molecules cm^{-3}). Flow rare:18 SLPM, Pinhole size:0.4 mm, The beam dia.:25 mm. Upper shows linear scale plot and lower shows log scale plot.

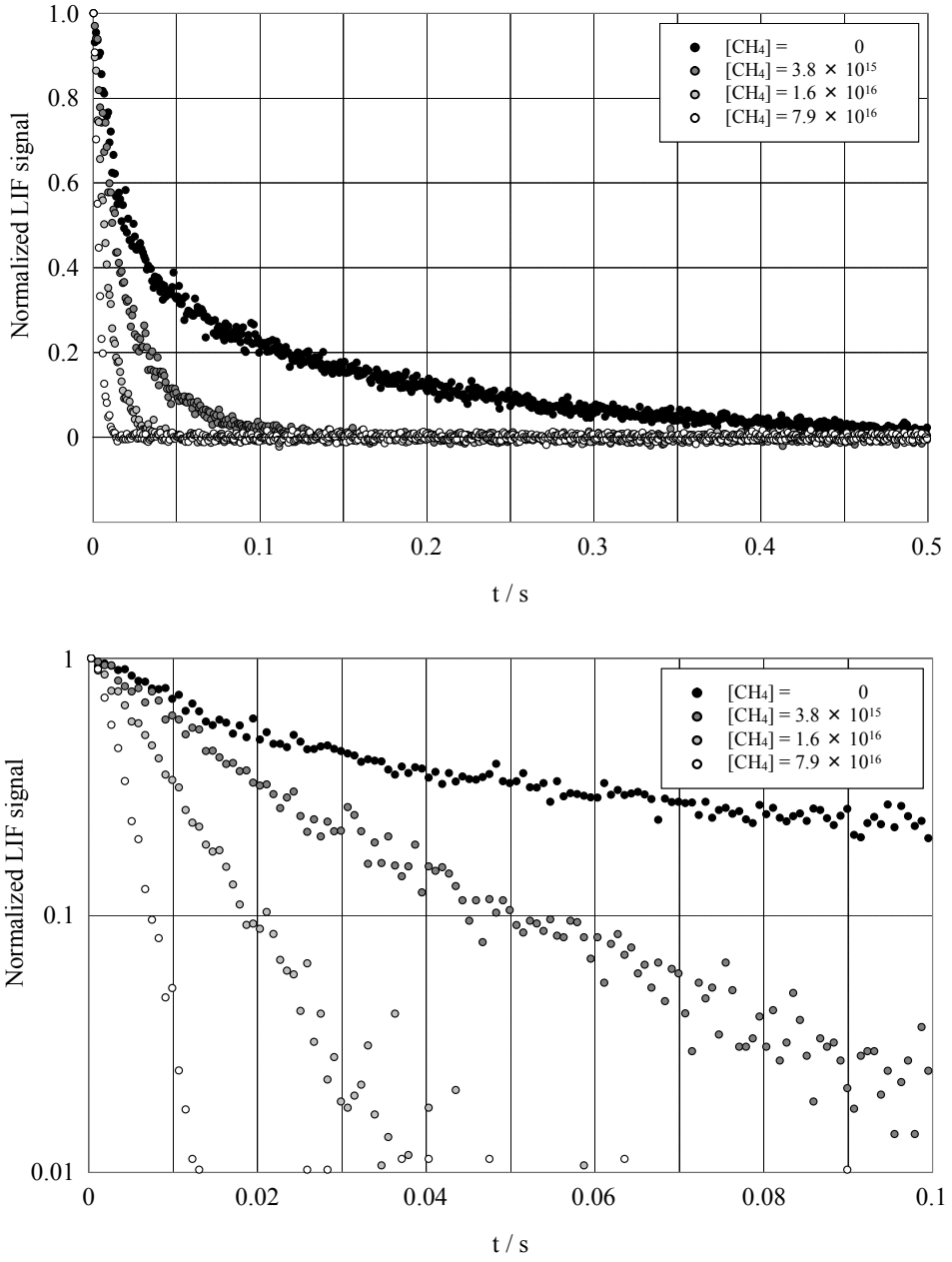

Figure.2-15 The OH decay profiles in several CH_4 concentrations (molecules cm^{-3}). Flow rare:18 SLPM, Pinhole size:1.0 mm, The beam dia.:25 mm. Upper shows linear scale plot and lower shows log scale plot.

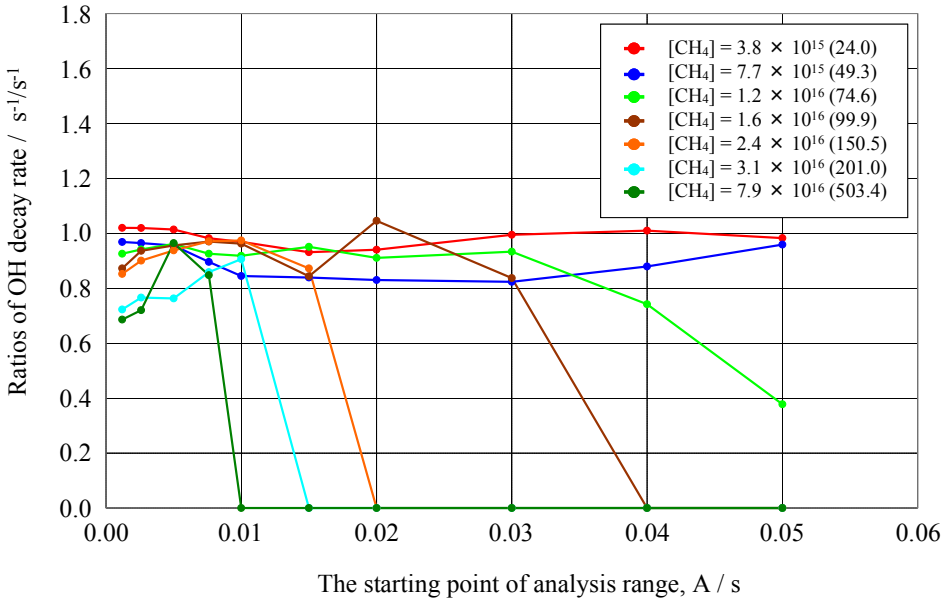

Figure.2-16 Plot of the ratios of OH decay rate as a function of analysis starting point in several CH_4 concentration (molecules cm^{-3}). The observed OH decay rates were divided by the calculated OH decay rate using CH_4 concentration and rate coefficient for OH reaction with CH_4. Pinhole size:0.4 mm

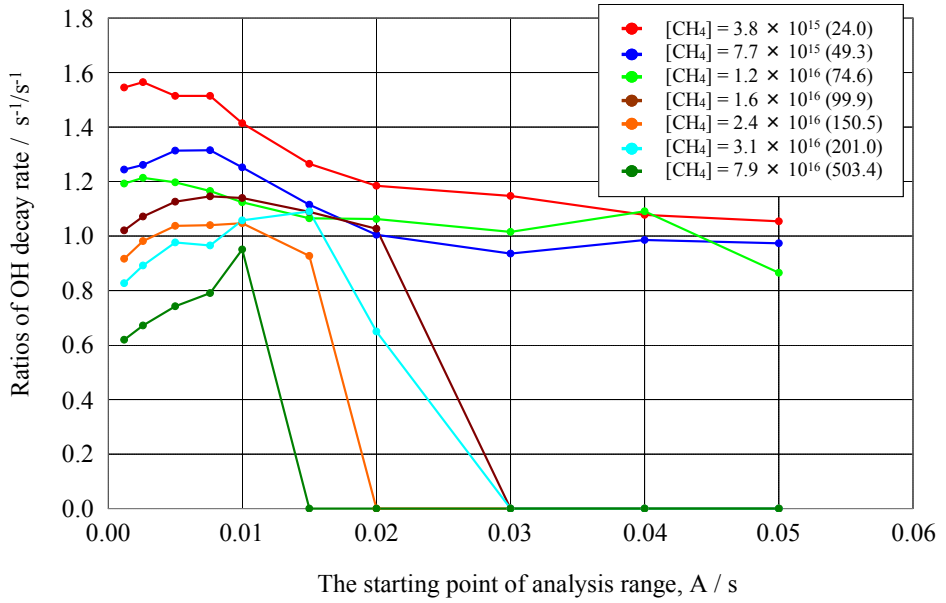

Figure.2-17 Plot of the ratios of OH decay rate as a function of analysis starting point in several CH_4 concentrations (molecules cm^{-3}). The observed OH decay rates were divided by the calculated OH decay rate using CH_4 concentration and rate coefficient for OH reaction with CH_4. Pinhole size:1.0 mm

But, it seems possible to measure the OH decay rate up to 500 s^{-1} within ± 10 % precision using the starting point of 0.0075 sec. On the other hand, configuration 2 (Figure.2-17) shows ratios of OH decay rate that are largely scattered around the starting point from 0 to 0.03 sec and converging within ± 10 % precision at the starting point of over 0.04 sec. The OH decay rate can be measured up to around 70 s^{-1} within ±10 % precision using a starting point of 0.05 sec.

Both configuration 1 and 2 in this study experience the influence of the fast decay component to the slow decay component. The results show that the fast decay component in configuration 1 and 2 should be removed by changing the analysis starting point in OH reactivity measurement. The fast decay component in configuration 1 is slow enough to affect all around analyzed range but can be neglected at the analysis starting point over 0.0075 sec. One of the big differences between two configurations is that the upper limit of OH reactivity measurement with configuration 1 is much higher than that with configuration 2. The influence of the fast decay component can be changed mainly by the pinhole size (i.e. flow rate introduced to LIF cell), flow rate inside the photolysis cell and photolysis laser beam size. This means the fast decay component can be reflected by physical process, particularly generated OH diffusion and turbulence at around the LIF inlet. The air around the center part of the photolysis cell was sucked into LIF cell. The other air was exhausted through the pump. Soon after the photolysis shot with bigger diameter of laser beam, OH radical exist widely in the photolysis cell and OH diffusion can be slower. On the other hand, with smaller diameter of laser beam, OH radical can be diffused faster to the outside from the center part of the photolysis cell and the fast decay component can be faster. To minimize that effect, configuration 1 which is achieved by smaller pinhole, higher flow rate in the photolysis cell and/or larger beam size is preferred. In that case, inner diameter of photolysis cell could affect the fast decay component. Additionally, these experiments have suggested that the regression analysis range should be considered carefully in each instrumental configuration.

2-3. Results and discussion – OH recycle effect –

The configuration 1 described in section 2-1-2 was used for the experiment in this section. CH_4 and CO concentrations were changed from 0 to 6.5×10^{16} molecules cm^{-3} and 2.6×10^{14} molecules cm^{-3}, respectively which was corresponding to about 45 s^{-1} of OH reactivity for both CH_4 and CO. NO concentration was changed from 0 to 7.2×10^{11} molecules cm^{-3}, comparable to 5.3 s^{-1} of OH reactivity. The tested NO range corresponds to the concentrations plausible in the real atmosphere. Observed OH decay profile was compared with that obtained by chemical simulation in which the reactions and their respective rate coefficients are summarized in Table.2-1. The differential equations derived from these reactions are solved by methods for the approximation of solutions of ordinary differential equations (BDF method) written in LabVIEW. Initial OH concentration is set to be 2.4×10^{8} molecules cm^{-3}, which is calculated from the photolysis laser energy and concentration of ozone and water vapor. The kinetic data for $O(^1D)$ reactions with N_2, O_2 and H_2O were referred from Sander et al., (2006). Two of the results for CO and CH_4 are shown in Figure.2-18 and 2-19, respectively. These results indicate observed OH decay profiles are well reproducible that obtained by chemical model.

Table.2-1 Reaction mechanism with their respective rate coefficients used in chemical model

Reaction		Rate coefficient
$OH + CO \rightarrow H + CO_2$	k_1	1.40×10^{-13}
$OH + NO \rightarrow HONO$	k_2	7.41×10^{-12}
$OH + NO_2 \rightarrow HNO_3$	k_3	1.06×10^{-11}
$OH \rightarrow$ wall loss	k_4	7.11 (measured)
$HO_2 + NO \rightarrow OH + NO_2$	k_5	8.10×10^{-12}
$HO_2 + NO_2 \rightarrow HO_2NO_2$	k_6	1.14×10^{-12}
$HO_2 \rightarrow$ wall loss	k_7	0.5 (measured)
$H + O_2 \rightarrow HO_2$	k_8	9.58×10^{-13}
$CH_4 + OH \rightarrow CH_3 + H_2O$	k_9	6.34×10^{-15}
$CH_3 + O_2 \rightarrow CH_3O_2$	k_{10}	8.10×10^{-13}
$CH_3O_2 + NO \rightarrow CH_3O + NO_2$	k_{11}	7.66×10^{-12}
$CH_3O_2 + NO_2 \rightarrow CH_3O_2NO_2$	k_{12}	3.82×10^{-12}
$CH_3O + NO \rightarrow CH_3ONO$	k_{13}	2.89×10^{-11}
$CH_3O + NO_2 \rightarrow CH_3ONO_2$	k_{14}	1.69×10^{-11}
$CH_3O + O_2 \rightarrow HO_2 + HCHO$	k_{15}	1.90×10^{-15}
$HO_2 + HO_2 \rightarrow H_2O_2 + O_2$	k_{16}	1.48×10^{-12}
$HO_2 + CH_3O_2 \rightarrow CH_3OOH + O_2$	k_{17}	5.08×10^{-12}
$CH_3O_2 \rightarrow$ wall loss	k_{18}	0.5 (assumed)

298 K, 760 Torr (Sander et al., 2006)

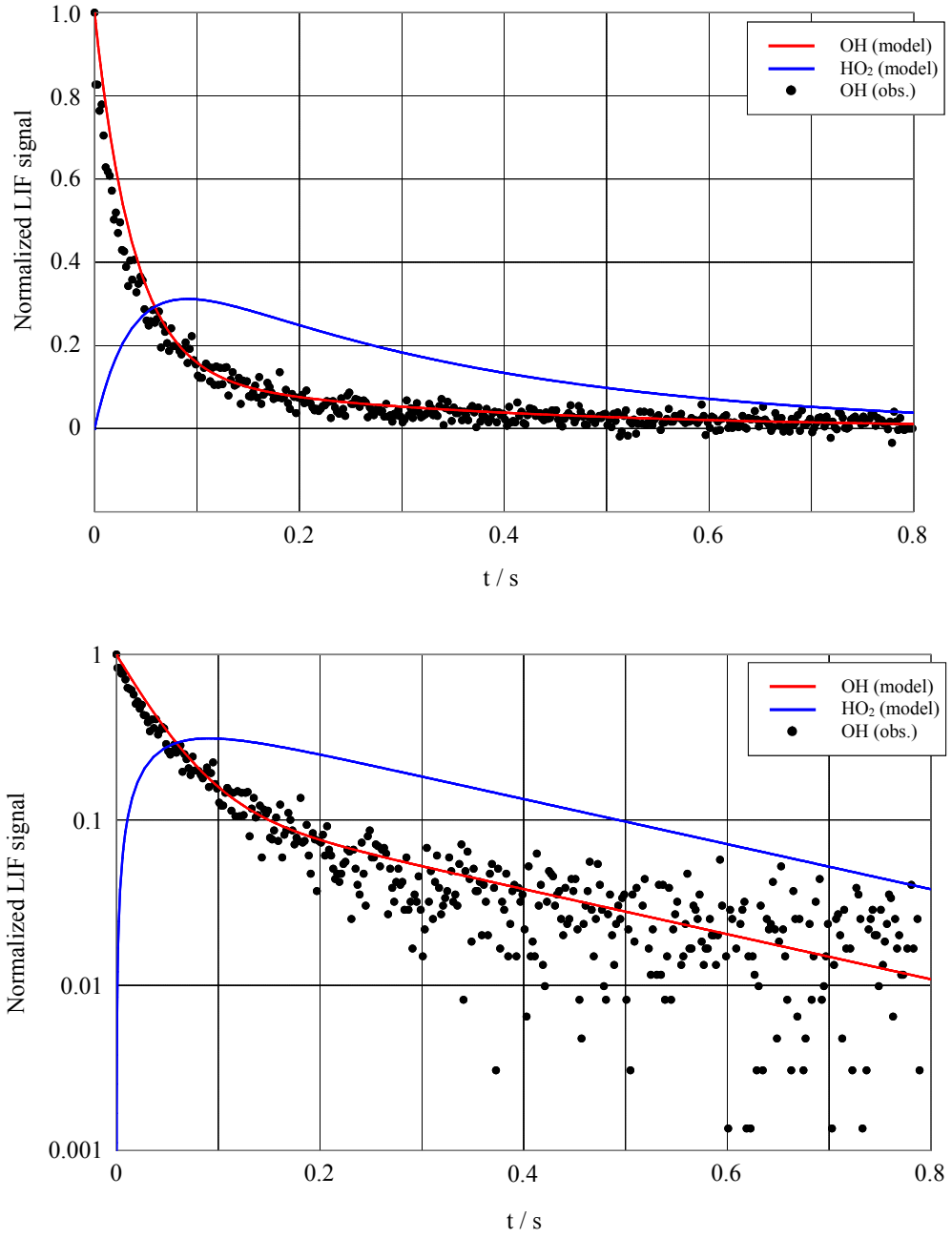

Figure.2-18 An example of the OH decay profiles and simulated OH and HO_2 profiles under CO and NO rich condition. Dot indicate measured OH decay profiles and solid lines indicate simulated OH and HO_2 profiles. [CO] = 2.94×10^{13} molecules cm^{-3}, [NO] = 7.16×10^{11} molecules cm^{-3}. Upper shows linear scale plot and lower shows log scale plot.

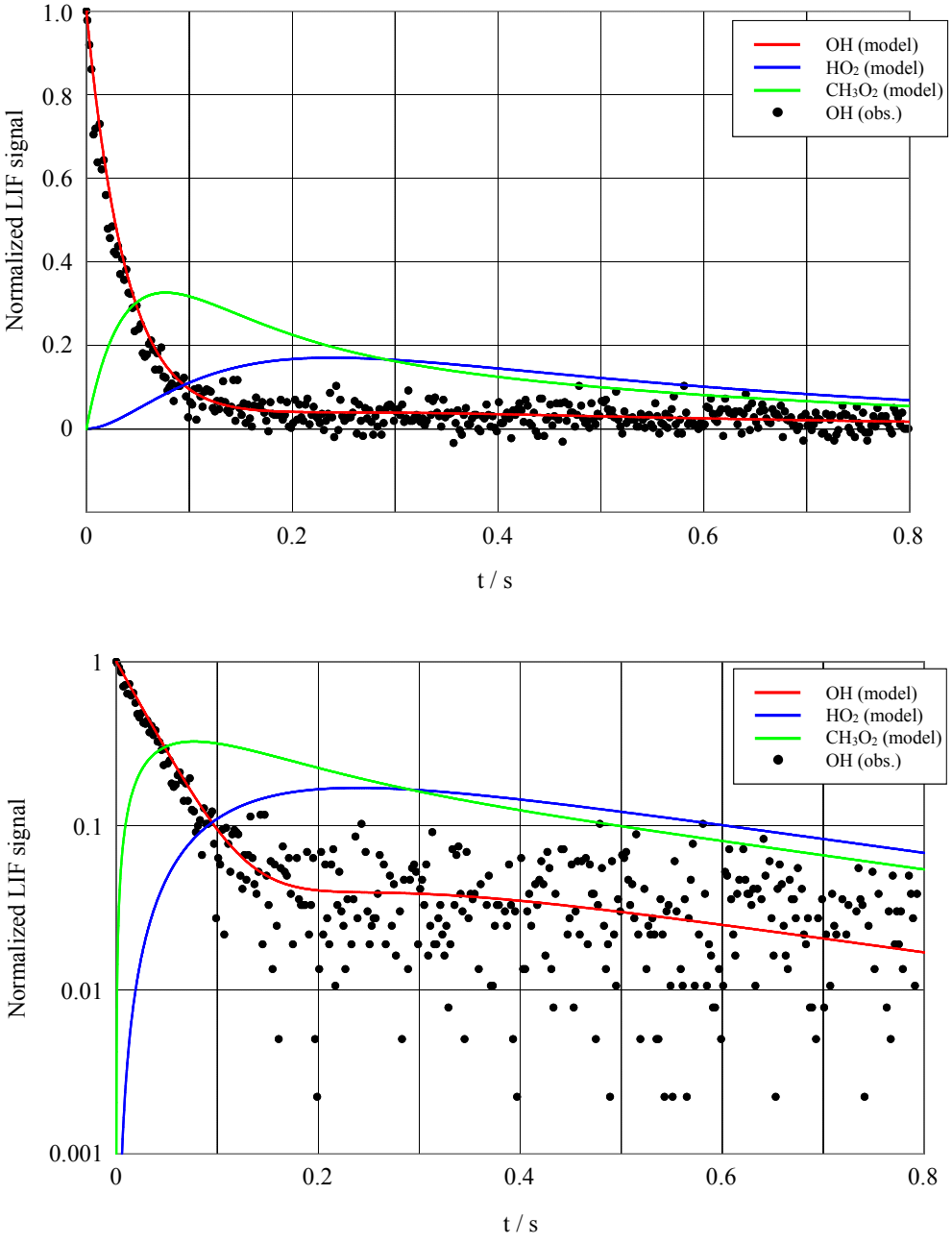

Figure.2-19 An example of the OH decay profiles and simulated OH, HO_2 and CH_3O_2 profiles under CH_4 and NO rich condition. Dot indicate measured OH decay profiles and solid lines indicate simulated OH, HO_2 and CH_3O_2 profiles. $[CH_4] = 1.37\times10^{15}$ molecules cm^{-3}, $[NO] = 7.16\times10^{11}$ molecules cm^{-3}. Upper shows linear scale plot and lower shows log scale plot.

In order to evaluate how influential these effects are to routine data analysis, they are analyzed by Equation (2-3) with analysis range of 0.01 to 0.8 sec as resulted in Figure.2-20 (in case of CO) and 2-21 (in case of CH_4). Ratios of OH decay rate in Figure.2-20 and 2-21 indicate the analyzed OH decay rate divided by the calculated OH decay rate using CH_4, CO and NO concentration and rate coefficient for OH reaction with CH_4, CO and NO. Figure.2-20 shows ratios of OH decay rate are decreasing with increasing NO concentration in each CO concentrations. On the other hand, Figure.2-21 shows ratios of OH decay rate are increasing with increasing NO concentration in each CH_4 concentrations. These differences can be mainly caused by following reasons. In case of CH_4, because long time remaining OH signal after 0.2 sec due to HO_2 reaction with NO as shown in Figure.2-19 is counted as background signal in routine analysis, the analyzed OH decay rate can be higher than ideal OH reactivity. On the other hand in case of CO, because HO_2 decreases faster than that of CH_4 after 0.1 sec (Figure.2-18), the analyzed OH decay rate can be lower than ideal OH reactivity. It is also confirmed that the routine analysis was applied to modeled OH decays to be the same behavior as the experimental OH decays. Measurement deviations caused by these effects can be within ±10 % under NO concentration of $< 2\times10^{11}$ molecules cm^{-3} in this study. Ambient NO concentration can be over 2×10^{11} molecules cm^{-3} during commuting time such as in urban area. Some countermeasure should be taken under these conditions.

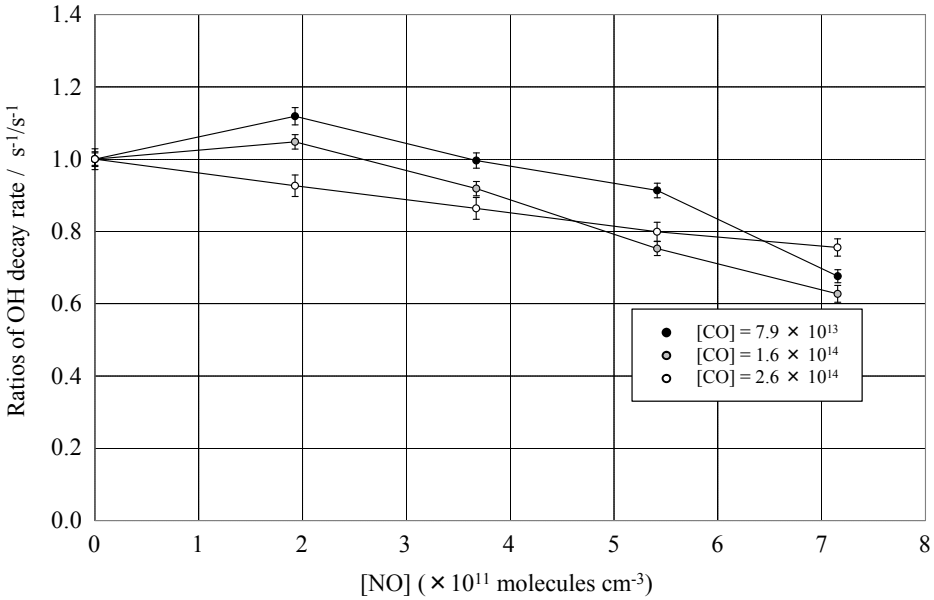

Figure.2-20 Plot of ratios of OH decay rate as a function of NO concentrations obtained under several CO concentrations.

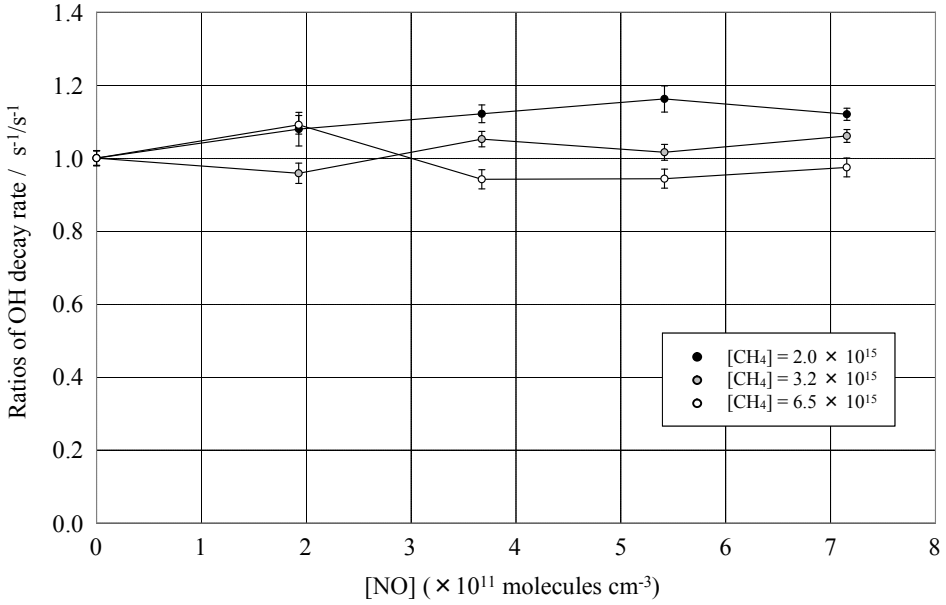

Figure.2-21 Plot of ratios of OH decay rate as a function of NO concentrations obtained under several CH_4 concentrations.

Under higher NO concentration than discussed above, two methods to reduce these effects are suggested here. One is to dilute the sample by zero air [Nakashima et al., 2010]. NO concentration can be reduced and these effects can be also reduced. The other one is to measure HO_2 profile simultaneously. The differential equation for OH can be described assuming the HO_2 reaction including with NO is the only pathway to produce OH in the photolysis cell as follow,

$$\frac{d[OH]}{dt} = k_{loss\,(OH\ prod)}[HO_2] - k_{loss} \times [OH] \qquad (2\text{-}4)$$

Both sides of Equation.(2-4) are divided by $[HO_2]$ as

$$\frac{d[OH]}{dt} \cdot \frac{1}{[HO_2]} = k_{loss\,(OH\ prod)} - k_{loss} \times \frac{[OH]}{[HO_2]} \qquad (2\text{-}5)$$

The real OH loss rate can be derived from its slope by plotting $\frac{d[OH]}{dt} \cdot \frac{1}{[HO_2]}$ against $\frac{[OH]}{[HO_2]}$.

2-4. Summary

An instrument for measuring total OH reactivity by a laser-induced pump and probe technique in University of Lille 1 was characterized in several ways. OH decay rate in zero air consist of two decay components; the fast decay component and the slow decay component. The occurrence factor for the fast decay components was investigated by changing some physical factors. Experiments show that the fast decay component is reflected mainly by the pinhole size (i.e. flow rate introduced to LIF cell), flow rate inside the photolysis cell and photolysis laser beam size, indicating that the fast decay component seemed to be caused by generated OH diffusion and turbulence at around the LIF inlet. To minimize that effect, configuration 1 which is achieved by smaller pinhole, higher flow rate in the photolysis cell and/or larger beam size is preferred, but the analysis range should be considered carefully in each instrumental configuration.

OH recycle effects caused by HO_2 reaction with NO in the photolysis cell were investigated. CO and CH_4 are tested both which can re-produce OH radicals under NO-rich condition. These effects can be the interference to OH reactivity measurement. Results show that measurement deviations caused by these effects can be within ±10 % under NO concentration of $< 2\times10^{11}$ molecules cm^{-3} in this study.

Chapter 3.

Development of a technique for total HO_2 reactivity measurement

An instrument for measuring total HO_2 reactivity by a laser-induced pump and probe technique was developed, and the developed one is specified in this chapter. First, the methodology for HO_2 reactivity measurement using laser-induced pump and probe technique is described as in Section.3-1. Second, the developed instrument for measuring total HO_2 reactivity by a laser-induced pump and probe technique is specified in Section.3-2. Third, the validation and testing are conducted through the kinetic measurement of HO_2 reaction with NO_2 as in Section.3-3. The last, a test observation of ambient air was conducted at Hachioji campus of Tokyo Metropolitan University to test the practical use as described in Section.3-4.

3-1. Methodology

A laser-induced pump and probe OH reactivity measurement technique was applied to total HO_2 reactivity measurement. A laser-induced pump and probe OH reactivity measurement technique incorporates laser flash photolysis technique and laser-induced fluorescence (LIF) OH detection technique. Ambient air is introduced into a photolysis reaction tube where OH reactions with ambient species take place. OH radicals are generated artificially from the photolysis of O_3 by a pump laser beam passing through the reaction tube and subsequent reaction with water vapor described as below.

$$O_3 + h\nu \rightarrow O_2 + O(^1D) \quad \text{(R2-1)}$$
$$O(^1D) + H_2O \rightarrow 2OH \quad \text{(R2-2)}$$

High excess of CO (0.1 %, corresponding to ~3500 s^{-1} as OH loss rate) is added to the reaction tube to convert all of the OH radicals to HO_2 radicals as

$$CO + OH \rightarrow CO_2 + H \quad \text{(R1-1)}$$
$$H + O_2 + M \rightarrow HO_2 + M \quad \text{(R1-2)}$$

Since the produced HO_2 radicals are diffused and react with trace species in the reaction tube, HO_2 concentrations decrease after irradiation of the pump laser beam. Concentration change of HO_2 radicals after photolysis laser shot is monitored by using a time-resolved laser-induced fluorescence OH detection coupled with chemical conversion method by the HO_2 reaction with NO. LIF HO_2 detection method has its interference of RO_2 radical in ambient measurement described in Section.1-3. But in this technique, almost only the HO_2 radicals can exist in the reaction tube due to high excess of CO.

Some part of HO_2 radicals (or predominantly) can react with NO to produce OH radicals. But, generated OH radicals can be converted to HO_2 radicals immediately due to high excess of CO. That is why the loss rate for HO_2 reaction with NO does not contribute to the observed HO_2 loss rate principally. NO is known to have another reaction pathway to produce HNO_3 [Butkovskaya et al., 2009] although the branching ratio to this pathway is reported to be very low (~0.5 %) [Butkovskaya et al., 2009]. This loss rate for this reaction can contribute to the observed HO_2 loss rate. Much the same is true on HO_2 loss reaction with O_3, where HO_2 react with O_3 to produce OH radicals although the rate coefficient for this reaction is slow enough to be negligible in ambient condition. From these instrumental character, this technique enable to measure total HO_2 loss rate exclusively for the termination reaction which does not re-produce radicals such as OH, HO_2 and RO_2 detectable to LIF OH detection coupled with chemical conversion by the reaction with NO.

HO_2 and RO_2 reactions with HO_2 can be the predominant HO_2 loss process in remote area. This technique is supposed to be used in urban area where the loss rate contribution of the HO_2 reaction with HO_2 and RO_2 is relatively small and that with NO_X is dominant.

The advantage of high sensitive OH detection by using LIF technique is that low initial concentrations of HO_2 radicals can be used so that the self-reaction of HO_2 radicals in the reaction tube can be negligible. Also, as the reacting species are in large excess over HO_2 radicals, pseudo-first-order conditions are achieved and the HO_2 loss rate in the reaction tube is given by Eq. (3-1):

$$\frac{d[HO_2]}{dt} = -\left(k[NO_2] + k[NO] + k[Others] + k_{wall}\right) \times [HO_2] \qquad (3\text{-}1)$$

with k representing the rate coefficient of the HO_2 reaction with respective reacting

species and k_{wall} representing losses due to diffusion and wall losses. It should be noted that the term of k[NO] in Equation.(3-1) is contributed by HO_2 reaction with NO to produce HNO_3. Hence under general understanding of ambient reactions in urban area, total ambient HO_2 loss rate is described as below,

$$L(HO_2)_{amb.} = L(HO_2)_{obs.} + L(HO_2)_{prod.} \quad (3\text{-}2)$$

with $L(HO_2)_{amb.}$ representing total HO_2 loss rate in ambient air, $L(HO_2)_{obs.}$ representing observed HO_2 loss rate in the reaction tube and $L(HO_2)_{prod.}$ representing HO_2 loss rate for HO_2 reaction with NO and O_3 to produce OH radicals.

3-2. Experimental

3-2-1. Instrumental description of HO_2 reactivity measurement

A recently developed OH reactivity measurement system at Tokyo Metropolitan University (Sadanaga et al., 2004) was used for the experiments described in this chapter, which comprised three main components, (1) a photolysis laser, (2) a reaction cell, and (3) the LIF OH detection combined with chemical conversion part of HO_2 to OH. A schematic diagram of the instrument is shown in Figure.3-1.

The photolysis laser is a YAG laser (Tempest 300, New Wave Research) operating at 0.25 Hz with a pulse energy of ~ 10 mJ and top-hat beam shape at 266 nm after frequency quadrupling. The beam is directly entering the reaction cell, and in this work normally had a diameter of 10 mm.

The reaction cell is an aluminum cylinder 114 cm long with an internal diameter of 4 cm. Both ends are closed by a quartz window allowing the photolysis laser beam to enter. The sampling cone of LIF detection cell is amounted at 74 cm after from the inlet, sealed with an o-ring. Gas is introduced via a Swagelok (2 inch tube connectable) fitting at the quartz window end, at the other end the same Swagelok fitting is mounted. The flow within the reaction tube in front of LIF cell was 15 SLPM controlled by using a mass flow controller (Model 3660, Kofloc) pumped by diaphragm pump (DA-30D,

ULVAC), of which 3 SLPM is drawn into the LIF cell with 0.5 mm pinhole. Pure CO (Nippon Sanso) passing through a charcoal trap to remove reactive hydrocarbons in its cylinder is added in front of the reaction tube and its flow rate is controlled at 20 sccm (standard cc per minute) by using a mass flow controller (model 3660, Kofloc). CO concentration is calculated to be 0.1 % inside the reaction tube. The air inside the photolysis reaction tube is calculated to be replaced every 3.7 sec ideally.

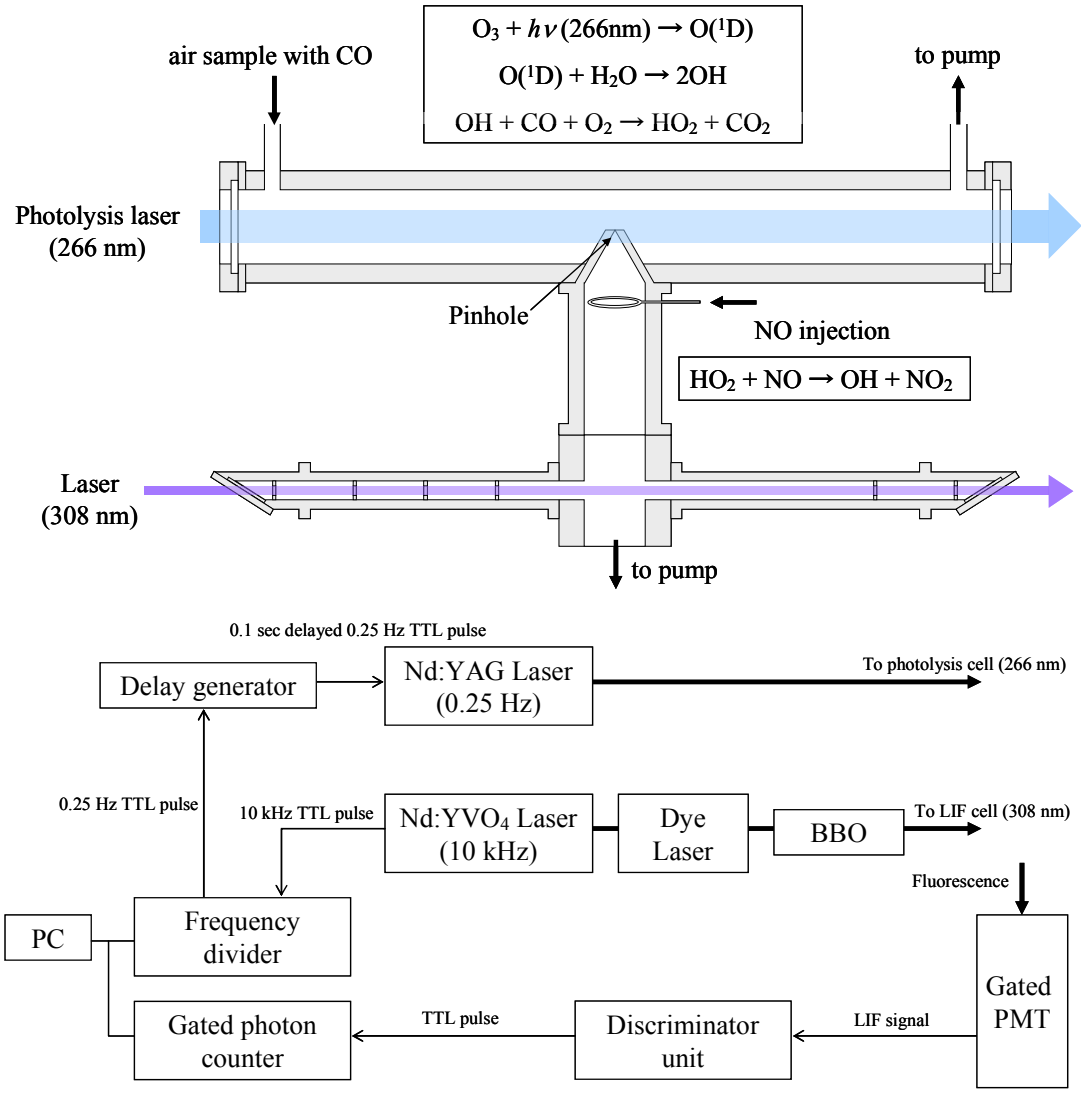

Figure.3-1 Schematic diagram of HO_2 reactivity instrument. Upper figure shows the cross-sectional view of the developed instrument. Lower firure shows the electrical lines and laser lines. Electrical lines: thin line, Laser lines: thick line.

The HO_2 radicals are detected with chemical conversion and laser-induced fluorescence HO_2 detection technique, which is similar to the method reported by Kanaya et al.[2001] as can be seen in Figure.3-1 (Upper figure). Single laser alignment was employed in this study. The central part of the fluorescence detection cell is made of a 100 mm cubic block made of aluminum. Two baffled arms, a gas flow tube and a fluorescence collection system are attached to this central part. The inner and outer walls of the cell are coated with black anodic oxidized alumina to reduce stray light which causes background signal. Probe laser is passed through both baffled arm with quarts windows. Each baffled arm is also coated with black anodic oxidized alumina. The length of each arm is 350 mm and inner diameter is 27 mm. Four baffle disks are mounted in the entrance arm with its interval of 73 mm. On the other hand, only two baffles are mounted in the exiting arm. Every baffle disks have an aperture of 10 mm. Partial sample air in the reaction tube is introduced into the fluorescence detection cell through a pinhole which is located 216 mm upstream from the fluorescence detection region. The pinhole is located at the center of an aluminum flange (120 mm dia.) which is mounted on the top of an aluminum cylindrical tube (inner 60 mm dia.). The flange is a flat 6 mm thick disk with a cone whose angle is 60°. In order to minimize a possible heterogeneous loss of OH and/or HO_2 radicals, the inner wall of the flange, the cylindrical tube and the outer surface of the cone were coated with Halocarbon wax (1500, Halocarbon Products). Pure NO gas (Sumitomoseika), which convert HO_2 into OH through the reaction of HO_2+NO, is injected through a handmade Teflon loop injector mounted just below the pinhole. The flow rate for NO is optimized and controlled at 2 sccm by a mass flow controller (model 3660, Kofloc) (Figure.3-2). Pure NO is passed in advance through a Drierite/Ascarite/Drierite trap to remove HONO and NO_2 in its cylinder. The pressure inside the fluorescence detection cells is reduced to ca. 2.0 Torr using a pinhole (0.5 mm id.) and an oil rotary pump (D-950, ULVAC) in order to minimize the collisional quenching of the excited OH molecules by air (FAGE technique).

The A-X(0,0) $Q_1(2)$ line of OH (corresponding to λ = 307.9951 nm [Dorn et al., 1995]) was excited by use of a tunable frequency-doubled dye laser (Credo, Sirah) pumped by the frequency doubled output of a Nd:YVO_4 laser (YHP40-532Q, Spectra Physics) with a repetition rate of 10 kHz and the typical laser energy of 3 mW. The fluorescence is collected and focused through four optical lenses and passes through interference filter (Barr Associates) onto a gated PMT (Photomultiplier tube, Hamamatsu, R2256P) achieved by coupling with a normally-off dynode gating system (C1392SMOD, Hamamatsu). The output signal from the PMT is led to a discriminator

unit (C3866, Hamamatsu) and is converted to positive TTL (transistor-transistor logic) pulse, which is counted between 1.00 and 3.00 μs after the laser excitation using a photon counting board (PCI-6259, National Instruments). The probe laser power was monitored in each shot by a calibrated photodiode (R1226-5BQ, Hamamatsu) to normalize the LIF signal.

The synchronization of both pump and probe laser is achieved with a homemade delay generator and the PC counting card via LabVIEW (v8.5, National Instruments) as can be seen in Figure. 3-1 (Lower figure). Data are normally accumulated for 4 minutes (i.e. 60 times photolysis shots).

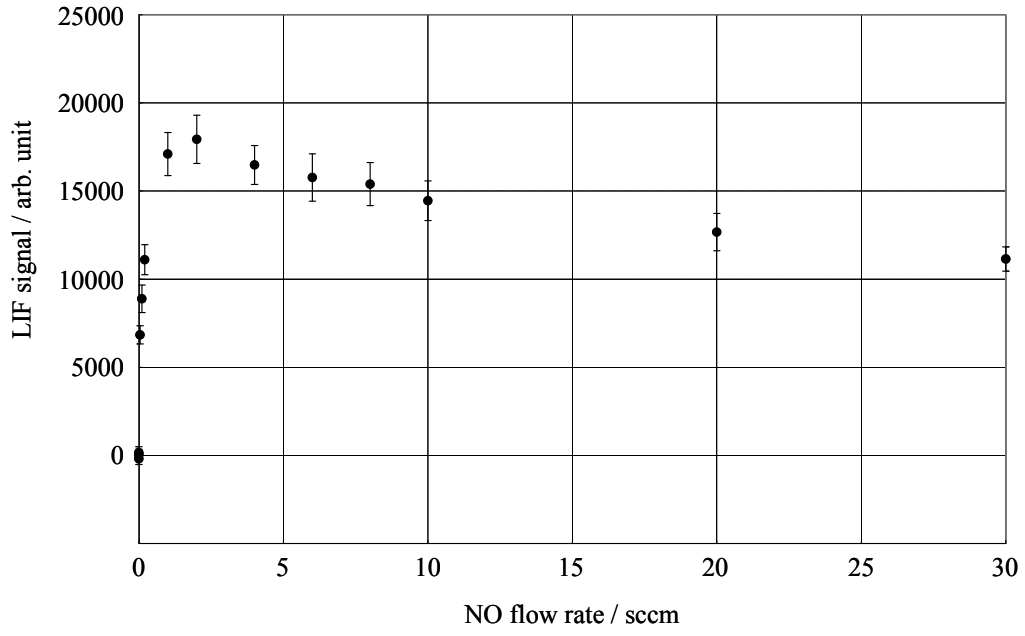

Figure.3-2 The signal dependence on NO flow rate.

3-2-2. Gas preparation and data analysis

O_3 was produced by the photolysis of oxygen molecule in zero air using a low-pressure mercury lamp (SP5-2H, Sen lights Co.) and mixed with variable flows of humid air (generated by passing a fraction of the bath gas through a water bubbler) and NO_2 (or NO) (both Nippon Sanso, both 5 ppm in N_2). In the kinetic experiment of HO_2 reaction with NO_2 as described in Section.3-3-1, NO_2 (Nippon Sanso, 5 ppm in N_2) was added to the sample and measured its concentration by a laser-induced fluorescence NO_2 analyzer developed in Tokyo Metropolitan University [Miyazaki et al., 2008]. In the NO interference test as described in Section.3-3-2, NO (Nippon Sanso, 5 ppm in N_2) was added to the sample and measured its concentration by a commercial NO_X analyzer (42i TL, Thermo). All experiments were carried out at 295 K and at pressures of 750 Torr of air. The different gases were introduced to the reactor using calibrated mass flow controllers (model 3660, Kofloc). Pressure within the photolysis cell was kept constant and monitored with a pressure transmitter (626A, MKS). Typical concentrations of O_3 and water vapor inside the photolysis cell are 30 ppbv, 3000 ppmv which are monitored by an O_3 analyzer (model1150, Dylec) and a hygrometer (TR-72S, T&D Co.), respectively. A large excess of NO_2 over the HO_2 radical concentration (~10^9 molecules cm^{-3}, typically) has been used, allowing pseudo-first order conditions. As a consequence, radical decay kinetics follows Equation. (3-3):

$$\frac{d[HO_2]}{dt} = -\left(k[NO_2] + k_{wall}\right) \times [HO_2] \qquad (3\text{-}3)$$

with k being the second-order rate coefficient for HO_2 reaction with corresponding species and k_{wall} the wall losses. The decay rate was analyzed by the following fitting equation.

$$S = a + b \cdot \exp(-k' t) \qquad (3\text{-}4)$$

where S is the LIF signal normalized by energy of each 308 nm shot, a and b are parameters according to the background signal and the initial HO_2 concentrations, respectively.

3-3. Validation and testing

3-3-1. Kinetics of HO_2 reaction with NO_2

NO_2 concentrations were changed from 0 to 9.7×10^{11} molecules cm^{-3}. The observed HO_2 decay profiles with and without NO_2 are shown in Figure.3-3. As similar to be discussed in Chapter.2, HO_2 signals show two distinct decay components in both with and without NO_2. So, the observed HO_2 decay was analyzed using Equation.(3-3) with the analysis range from 0.1 – 3.5 sec where the fast decay component does not affect to the slow decay component. Analyzed HO_2 decay rate were plotted as the function of NO_2 concentration indicating the second order rate coefficient of HO_2 reaction with NO_2 from its slope obtained by regression analysis as $1.25\pm0.07\times10^{-12}$ cm^3 $molecule^{-1}$ s^{-1} (Figure.3-4, open circle).

In order to evaluate the effect of its back reaction, unimolecular decomposition of HO_2NO_2, the differential equation considering the reactions as followings

$$HO_2 + NO_2 + M \rightarrow HO_2NO_2 + M \quad \text{(R3-1)}$$
$$HO_2NO_2 + M \rightarrow HO_2 + NO_2 + M \quad \text{(R3-2)}$$
$$HO_2 \rightarrow \text{wall} \quad \text{(R3-3)}$$

are solved for HO_2 concentration allowing pseudo-first order conditions described as

$$[HO_2]_t = \frac{1}{\lambda_1 - \lambda_2}\left\{\left(k_1[NO_2] + k_3 - \lambda_2[HO_2]_0\right)\exp(\lambda_1 t) - \left(k_1[NO_2] + k_3 - \lambda_1[HO_2]_0\right)\exp(\lambda_2 t)\right\} \quad \text{(3-4)}$$

where k_1, k_2 and k_3 representing the rate coefficient for the reaction (R3-1), (R3-2) and (R3-3), respectively and λ_1 and λ_2 representing

$$\lambda_1 = \frac{-(k_1[NO_2] + k_2 + k_3) + \sqrt{(k_1[NO_2] + k_2 + k_3)^2 - 4k_2k_3}}{2}$$
$$\lambda_2 = \frac{-(k_1[NO_2] + k_2 + k_3) - \sqrt{(k_1[NO_2] + k_2 + k_3)^2 - 4k_2k_3}}{2}.$$

The observed HO_2 decay was analyzed again using fitting Equation.(2-4) with k_2 value of 0.12 s^{-1} [Sander et al., 2006］. The analyzed HO_2 decay rates are plotted as the function of NO_2 concentration indicating the second order rate coefficient of HO_2 reaction with NO_2 from its slope obtained by regression analysis as $1.23\pm0.06\times10^{-12}$ cm^3 $molecule^{-1}$ s^{-1} (Figure.3-4, closed circle). These results show the unimolecular decomposition reaction of HO_2NO_2 does not affect so much HO_2 decay under our experimental condition. The current JPL-06 recommendation value for the rate coefficient of HO_2 reaction with NO_2 at 298 K and 760 Torr is 1.18×10^{-12} cm^3 $molecule^{-1}$ s^{-1} [Sander et al., 2006] indicating the good agreement with the obtained value within < 5 %.

To the best of my knowledge, this is the first time to obtain the rate coefficient of HO_2 reaction with NO_2 under almost standard condition (750 torr, 295 K) with buffer gas of air and nearly close to the ambient concentration range for HO_2 and NO_2.

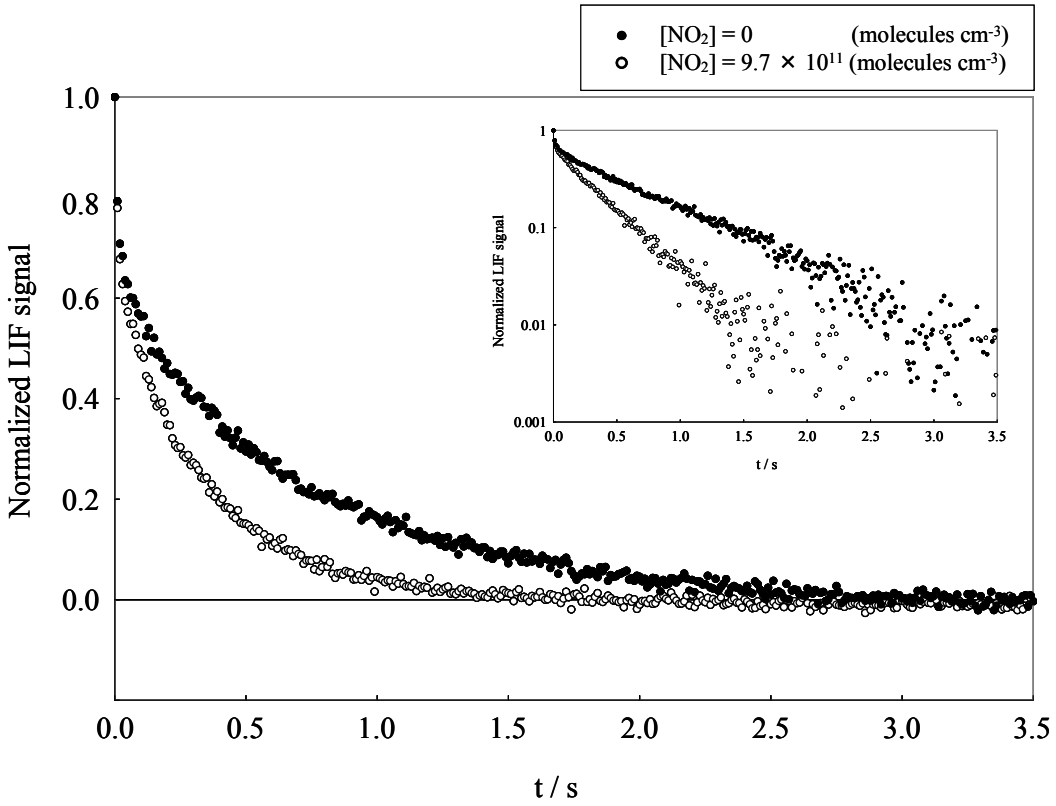

Figure.3-3 The measured HO_2 decay profiles in zero air (closed circle) and with NO_2 (open circle). Inserted figure shows its log scale plot.

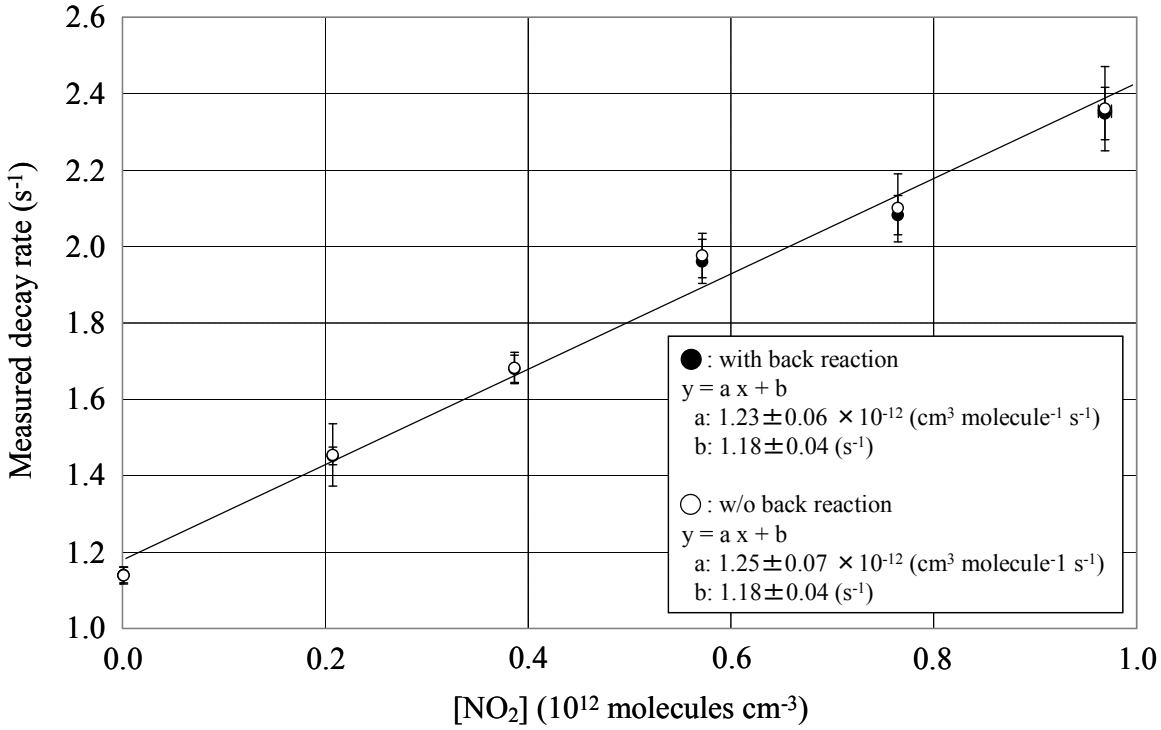

Figure.3-4 The measured HO_2 decay rate as a function of NO_2 concentration. Closed circle show HO_2 decay rates analyzed considering back reaction. Open circle show HO_2 decay rates analyzed by Equation.(3-4).

3-3-2. The HO_2 decay profile dependence on NO concentrations

NO concentrations were changed from 0 to 6.1×10^{11} molecules cm^{-3}. The observed HO_2 decay profiles with and without NO are shown in Figure.3-5. The observed HO_2 decay was analyzed using Equation.(2-3) with the analysis range from 0.1 – 3.5 sec. Analyzed HO_2 decay rate were plotted as the function of NO concentration as shown in Figure.3-6. Results show that no dependency exist on NO concentration, indicating that generated OH radicals are converted to HO_2 radicals and generated NO_2 through the HO_2 reaction with NO is small enough to neglect the contribution to HO_2 loss rate.

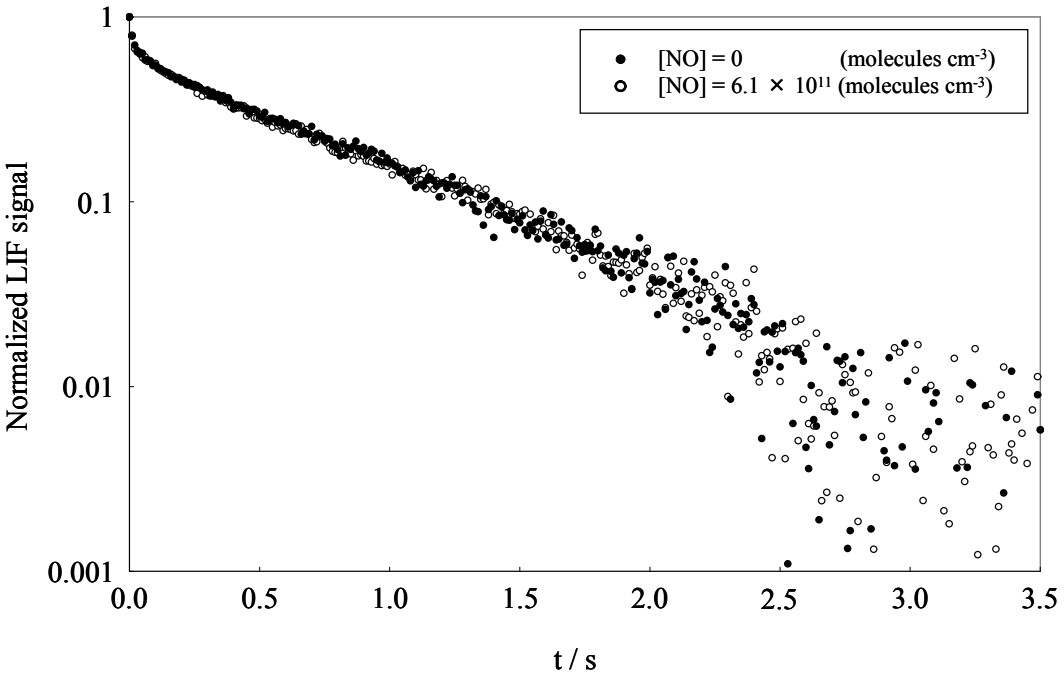

Figure.3-5 The measured HO_2 decay profiles in zero air (closed circle) and wih NO (open circle).

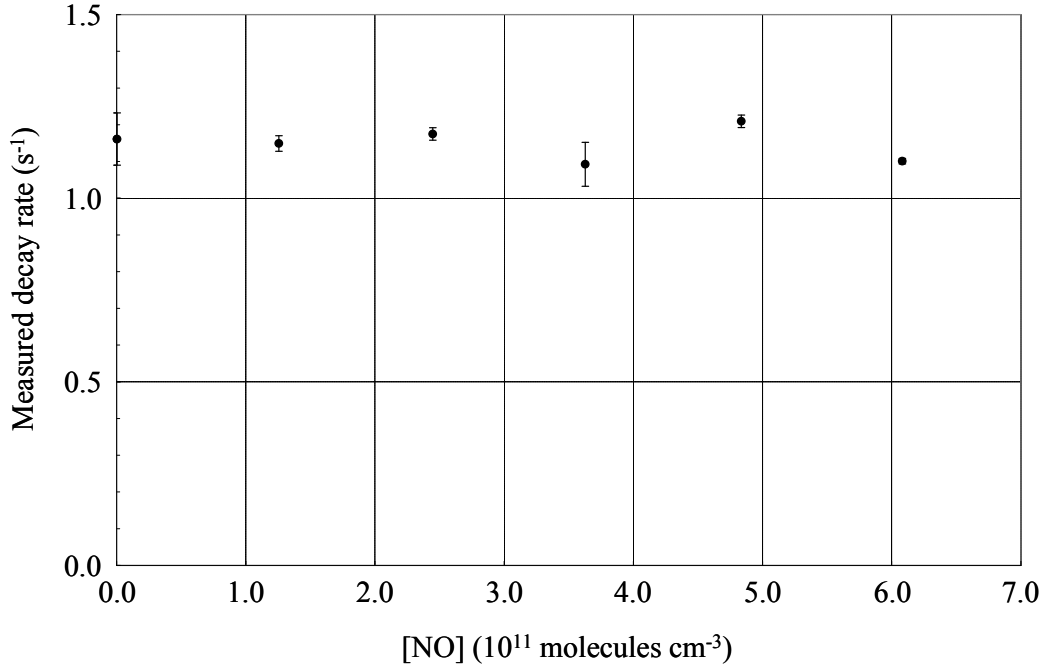

Figure.3-6 The measured HO_2 decay rate as a function of NO concentration.

3-4. Ambient observation

Measurement of total HO_2 reactivity was conducted in Hachioji, Tokyo, by using the developed instruments described as above. Other chemical species were monitored simultaneously with each instrument. The measured and calculated HO_2 reactivity are compared to evaluate HO_2 loss process in urban atmosphere.

3-4-1. Overview of the observation

3-4-1-1. Site description

Measurements were conducted at Tokyo Metropolitan University (35°37'03"N, 139°23'29"E), located about 30 km west of the central city of Tokyo as shown in Figure.3-7. This site is affected by local anthropogenic emissions of VOCs and NO_X from central city of Tokyo and TMU is surrounded by Hachioji town. The frequented roads, Tama New-town Street and Yaen Street are passing through near TMU. Local biogenic emissions from forests around TMU also affect the atmosphere. The instruments were mounted on the 3rd floor of Bld.9 which is "Faculty of Urban Environmental Sciences" of TMU.

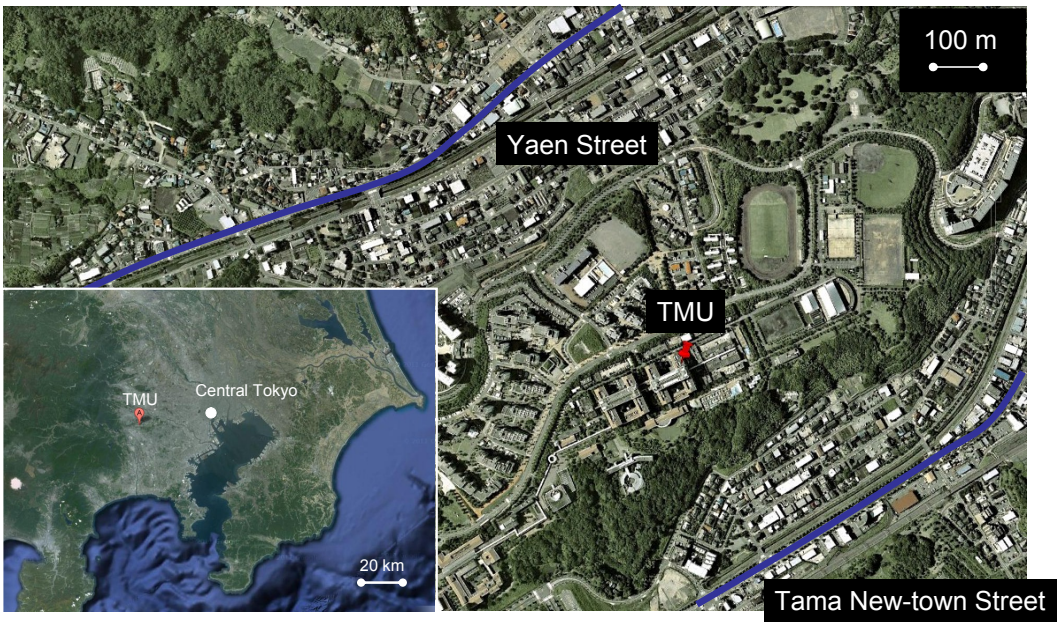

Figure.3-7. The site of Tokyo Metropolitan University, Hachioji, Tokyo, Japan

3-4-1-2. HO_2 reactivity measurement

HO_2 reactivity measurement was carried out using the developed instrument as described in Chapter 3 above. The instruments were mounted near the window in the laboratory of the 3rd floor. The ambient air is introduced into the photolysis reaction tube through a 1/2 inch Teflon tube of 3 m length. The resident time in the Teflon tube was calculated to be 0.9 sec. After the observation for each day, zero air decays were measured for several times. To test the stability of the decay rate in zero air through the observation, HO_2 decays were measured several times everyday. The zero air was synthesized by the same method as described in Section.3-2-2. The obtained data were analyzed by the same manner as described in Section.3-2-2 using the fitting Equation.(3-4). All of data was checked whether the HO_2 decay profile meets the pseudo-first order conditions as Equation.(3-3). An example of HO_2 decay profile for both in zero air and ambient air is shown in Figure.3-8.

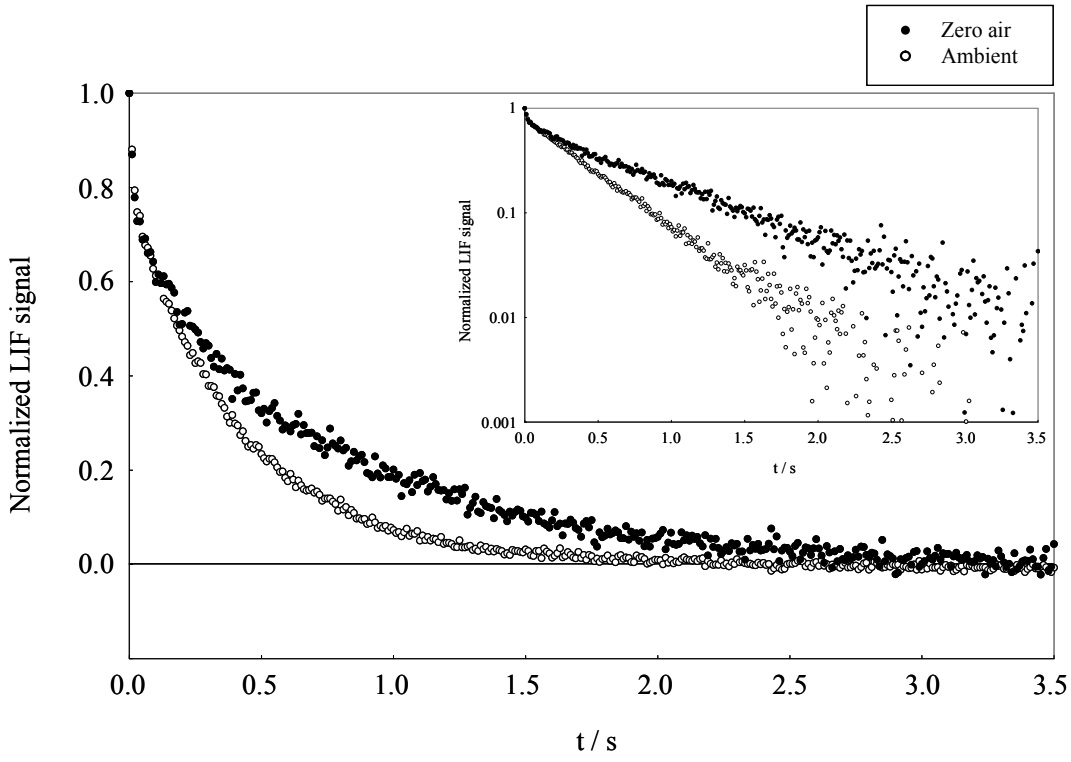

Figure.3-8. An example of HO_2 decay profile for both in zero air (closed circle) and ambient air (open circle). Inserted figure shows its log scale plot.

3-4-1-3. Trace species measurement

The concentrations of some kinds of trace species were measured simultaneously in order to calculate HO_2 loss rate and to consider the possible candidate species for missing sink. O_3 was measured by UV absorption (Model 49C, Thermo), CO by non dispersive infrared spectroscopy (Model 48C, Thermo), SO_2 by pulsed fluorescence (Model 43C, Thermo) and NO by O_3 chemiluminescence (42i TL, Thermo). NO_2 was measured by LIF technique [Miyazaki et al., 2008]. PTR/MS (Proton Transfer reaction mass spectrometry) [Kato et al., 2004] was used for some kinds of VOCs measurement. OVOCs were also measured by PTR/MS. The zero air was introduced to all instruments every 1 hour to measure zero level of the instrument. HCHO was measured by Hantzsch reaction fluorescence technique (AL4021, AERO-LASER). Particles size and its distribution were measured by a particle counter (0.25~32 μm; Model 1.109, GRIMM), which was used for the surface area estimation assuming all of particles are in a spherical shape. Measured species and their methods are summarized in Table.3-1.

Table.3-1 List of observed trace species during the observation.

Species		Method
CO		Non Dispersive IR
O_3		UV abs.
NO		Chemiluminescence
NO_2		Laser Induced Fluorescence
Particle		Optical Particle Counter
HCHO		Hantzsch Reaction Fluorescence
NMHC		PTR-MS
Aromatics	benzene	
Biogenic	isoprene	
Oxygenates	formaldehyde, acetaldehyde, acetone, methanol	
Others	acetonitrile	

3-4-2. Results and discussion

Figure.3-9 shows the diurnal variation of each observed species. Data averaged over 4 min are plotted. O_3 concentration varies from 0 to 60 ppb. The NO_2 concentration varies in the range between 5 and 40 ppb and shows a trend similar to the CO concentration, indicating the occurrence of fossil fuel combustion. However, the trend of the NO concentration is somewhat different from the trends of the concentrations of both NO_2 and CO. Entire O_3 titration by NO was observed at the noon time of Sep. 6 indicating the effect of local vehicular emission near around TMU. The diurnal variations of NMHCs observed by PTR/MS are shown in Figure.3-10. As shown in Figure.3-10, benzene and acetonitrile have a similar trend to NO_X and CO, indicating the occurrence of fossil fuel combustion. But, acetone, methanol and acetaldehyde had a somewhat different trend as fossil fuel combustion. Acetone, methanol and acetaldehyde have its direct emission process and secondary production process in the atmosphere. The same behavior of isoprene concentration and temperature has been observed as shown in Figure.3-11. This is mainly caused by the temperature dependent emission of biogenic VOCs and short time transportation around TMU. The averaged concentration of each species is summarized in Table.3-2. The concentrations of each species obtained in this study are a similar to before works observed in summer time in suburban areas [e.g. Yoshino et al., 2006].

Table.3-2 Averaged concentrations of trace species during the observation.

Species	Concentration / ppbv
CO	235 ± 54.2
O_3	25.9 ± 20.0
NO	5.22 ± 5.42
NO_2	15.96 ± 5.96
Particle	3.97 ± 2.21 × 10^{-7} cm^2/cm^3
HCHO	5.94 ± 0.83
Benzene	0.17 ± 0.10
Isoprene	0.71 ± 0.37
Formaldehyde	5.94 ± 0.83
Acetaldehyde	1.53 ± 0.71
Acetone	4.15 ± 2.01
Methanol	14.87 ± 14.83
Acetonitrile	0.19 ± 0.07

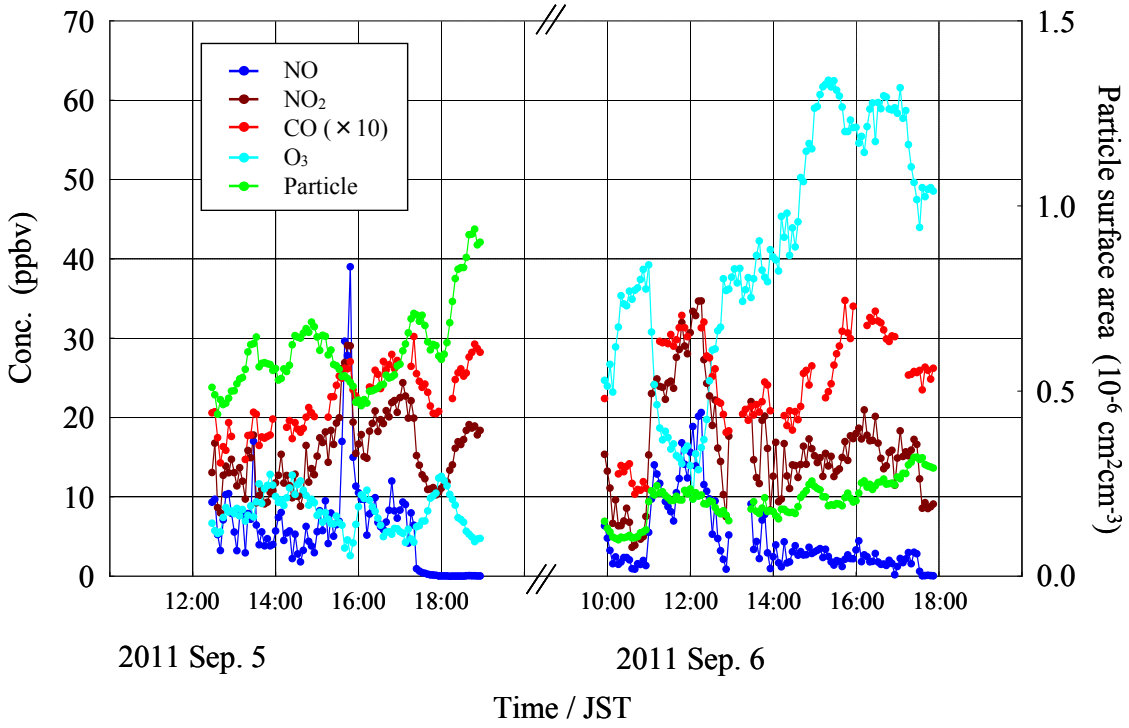

Figure.3-9. The diurnal variation of each observed species. Data averaged over 4 min are plotted.

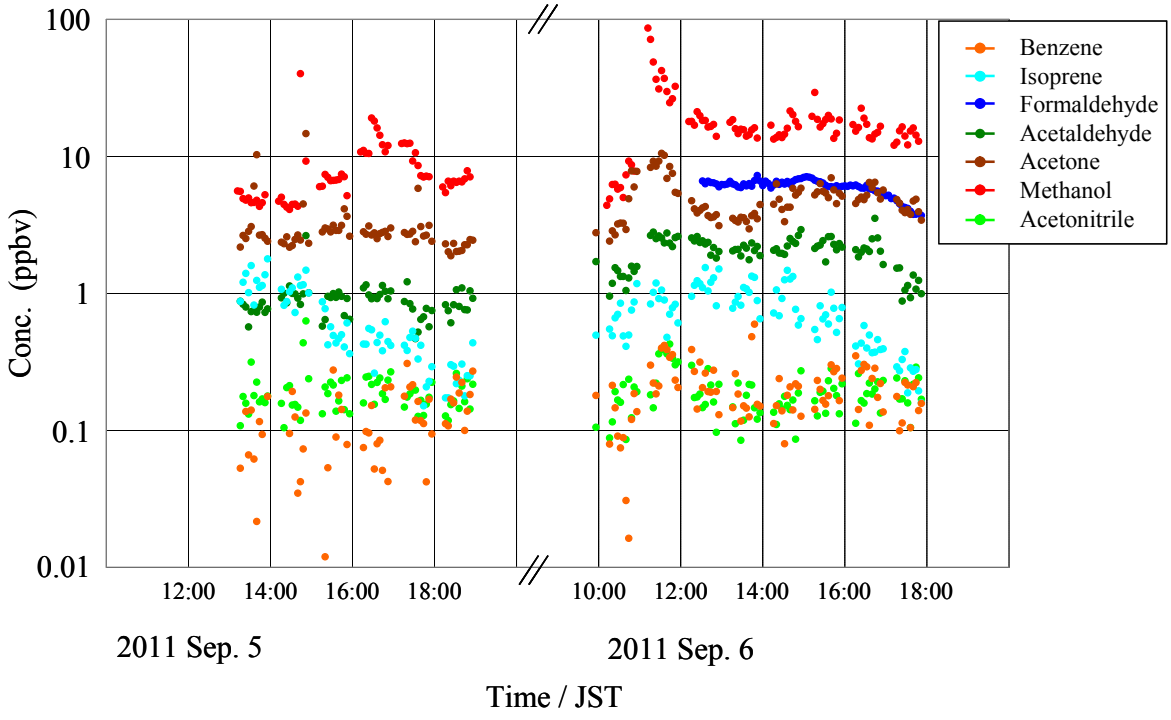

Figure.3-10. The diurnal variation of each observed NMHCs. Data averaged over 4 min are plotted.

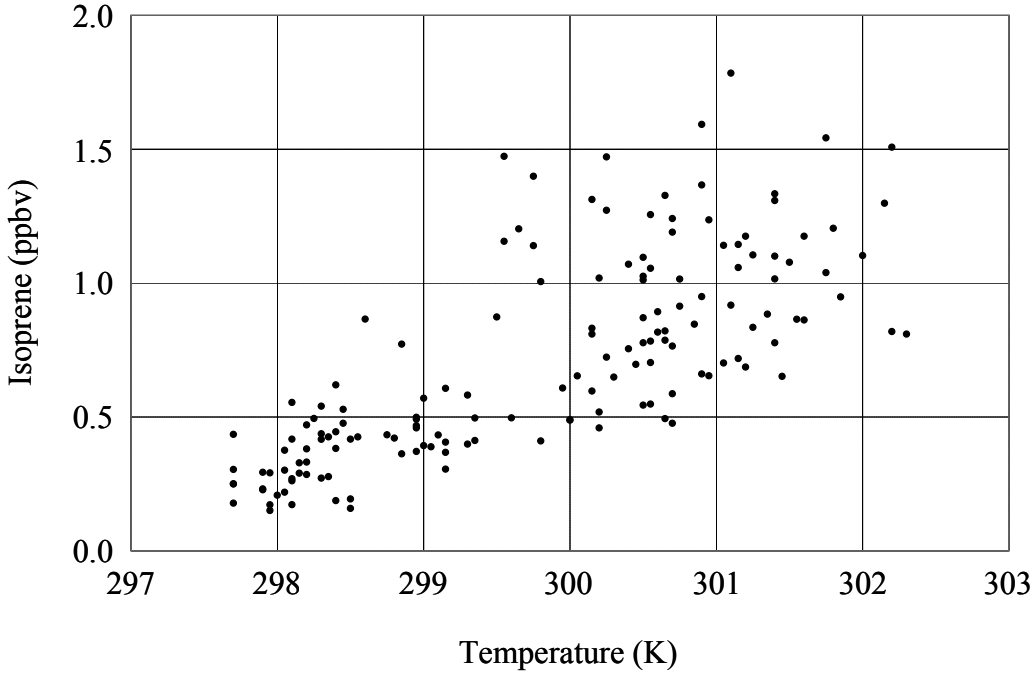

Figure.3-11. Isoprene concentration dependency on temperature.

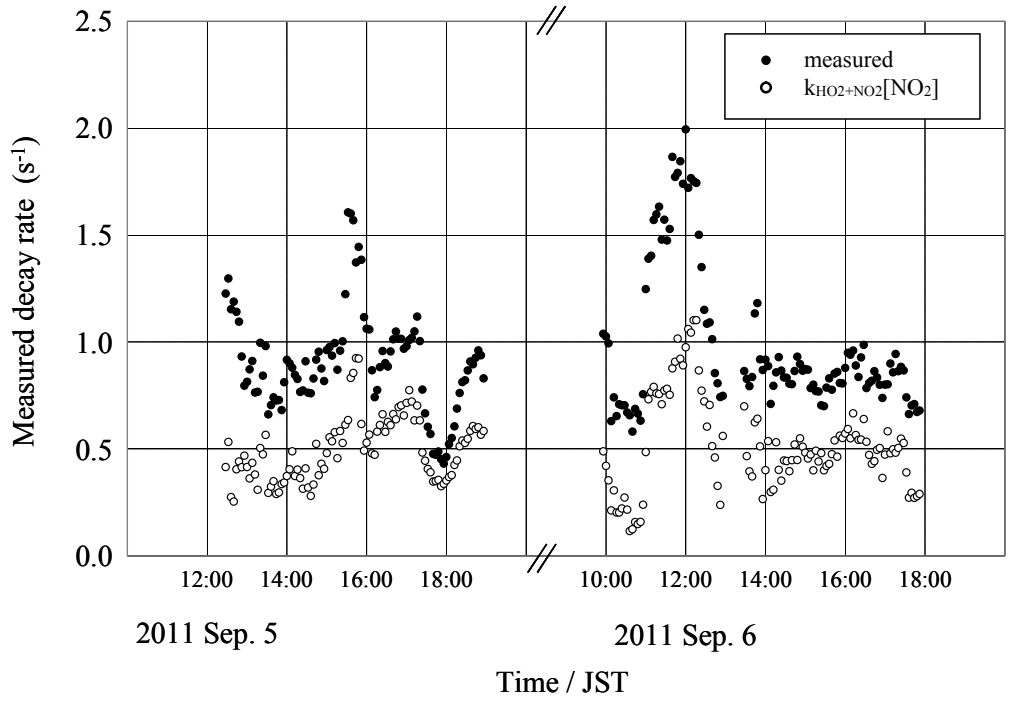

Figure.3-12. The observed HO_2 reactivity and NO_2 contribution to HO_2 reactivity calculated from observed NO_2 concentration and its rate coefficient obtained in Section 3-3-1

Figure.3-12 shows the observed HO_2 reactivity and NO_2 contribution to HO_2 reactivity calculated from observed NO_2 concentration and its rate coefficient obtained in Section.3-3-1. Temperature inside the photolysis cell was monitored by thermometer (TR-72S, T&D Co.) and the rate coefficient in each observation is calculated by its temperature.

The other loss process was estimated. HO_2 loss rate k of HO_2 uptake on the aerosol surfaces can be calculated by following equation,

$$k = \gamma \times \frac{\bar{c}}{4} \times \frac{A}{V} \qquad (3\text{-}5)$$

where γ is uptake coefficient onto aerosol, $\bar{c}$ is mean molecular velocity, and A/V is aerosol surface area per unit volume of air. The uptake coefficient onto aerosol is assumed to be 0.1. The surface area averaged through the observation is 3.97×10^{-7} cm^2 cm^{-3}. The HO_2 reactivity for uptake is calculated to be 0.0004 s^{-1}, contributing only 0.05 % to observed HO_2 reactivity. Even if the real surface area is ten times larger than observed one because particles counter can not observe below the particles size of 0.25 μm, HO_2 reactivity is calculated to be 0.004 s^{-1} , contributing only 0.5 % to observed HO_2 reactivity. This value comes from the comparison of ambient particle measurement conducted in this area between the particle counter used in this study and SMPS (Scanning Mobility Particle Sizer, TSI Inc. model 3936) which can measure the particle size of 14 – 673 nm. From these results, the surface area can be nearly ten times larger than that obtained with two instruments. The factor of ten is the maximum reasonable value to consider. The aerosol removal can be considered in the inlet tube of HO_2 reactivity measurement instrument. Even though it happened, calculated HO_2 loss rate onto particle is very low (0.0004 s^{-1}) relative to observed HO_2 loss rate and this interference of aerosol removal can not be a significant error.

OVOCs such as HCHO, CH_3CHO and CH_3COCH_3 can be photolyzed to produce peroxy radicals in the photolysis cell by photolysis laser at 266 nm, which can react with HO_2 and contribute to observed HO_2 loss rate. However the generated peroxy radical concentration is calculated to be 1.7×10^{7} molecules cm^{-3} considering the photolysis of HCHO, CH_3CHO and CH_3COCH_3, and this value is enough small to neglect the contribution to observed HO_2 loss rate ($< 10^{-4}$ s^{-1}).

As for NO reaction producing HNO_3, branching ratio was assumed to be 0.5 % contributing only 0.6 % to observed HO_2 reactivity.

It should be noted that ambient observation employed the same instrument as that

used in HO_2+NO_2 kinetic measurement as described in Section.3-3-1. This procedure is a kind of calibration for each instrument. And even though the derived rate coefficient is different from the real one, the contribution to observed HO_2 reactivity for NO_2 is not affected by the systematical error. Also, some tests shows that no dependency of HO_2 loss rate on humidity have been found in this instrument.

The contribution of each species to (a) $L(HO_2)_{obs.}$ and (b) $L(HO_2)_{amb.}$ is summarized in Figure.3-13. Almost half of observed HO_2 reactivity can be the missing sink. The ambient HO_2 reactivity was calculated using Equation.(3-2) with the rate coefficient for HO_2 reaction with NO and O_3 of 8.5×10^{-12} cm^3 $molecule^{-1}$ s^{-1} and 2.0×10^{-15} cm^3 $molecule^{-1}$ s^{-1}, respectively as shown in Figure.3-13 (b). Results show that 22.1 % of ambient HO_2 reactivity can be missing sink, resulting in that recent chemical model overestimate the ambient HO_2 concentrations. Figure.3-14 shows the diurnal variation of the observed missing HO_2 sink. The missing HO_2 reactivity represents existence of unknown HO_2 loss process. The averaged missing HO_2 reactivity during the observation is 0.46 s^{-1}. This difference corresponds with a several or several tens of ppbv of chemicals (Assuming k_{HO2} = 1.0×10^{-11} cm^3 $molecule^{-1}$ s^{-1} or 1.0×10^{-12} cm^3 $molecule^{-1}$ s^{-1}). This is almost impossible to describe certain chemical species in the atmosphere.

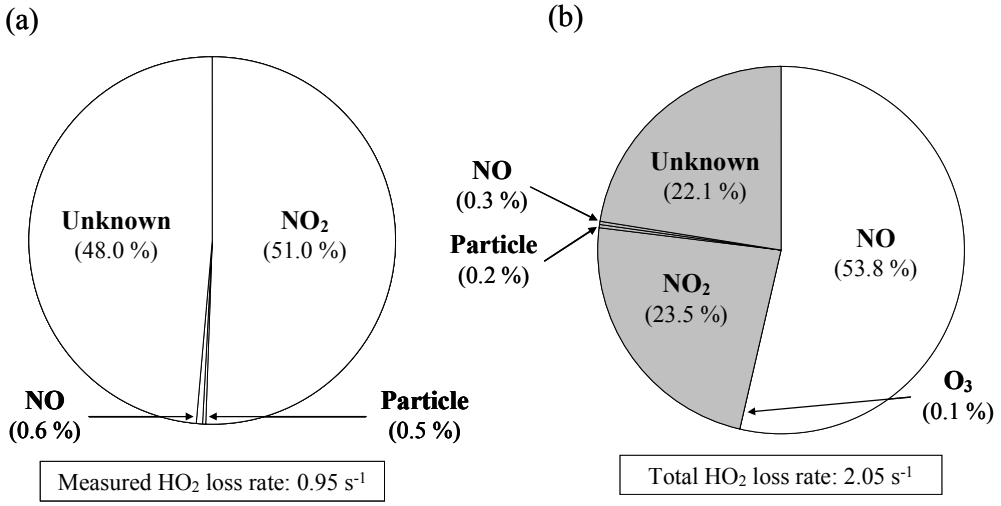

Figure.3-13. The contribution of each species to (a) $L(HO_2)_{obs}$ and (b) $L(HO_2)_{amb}$.

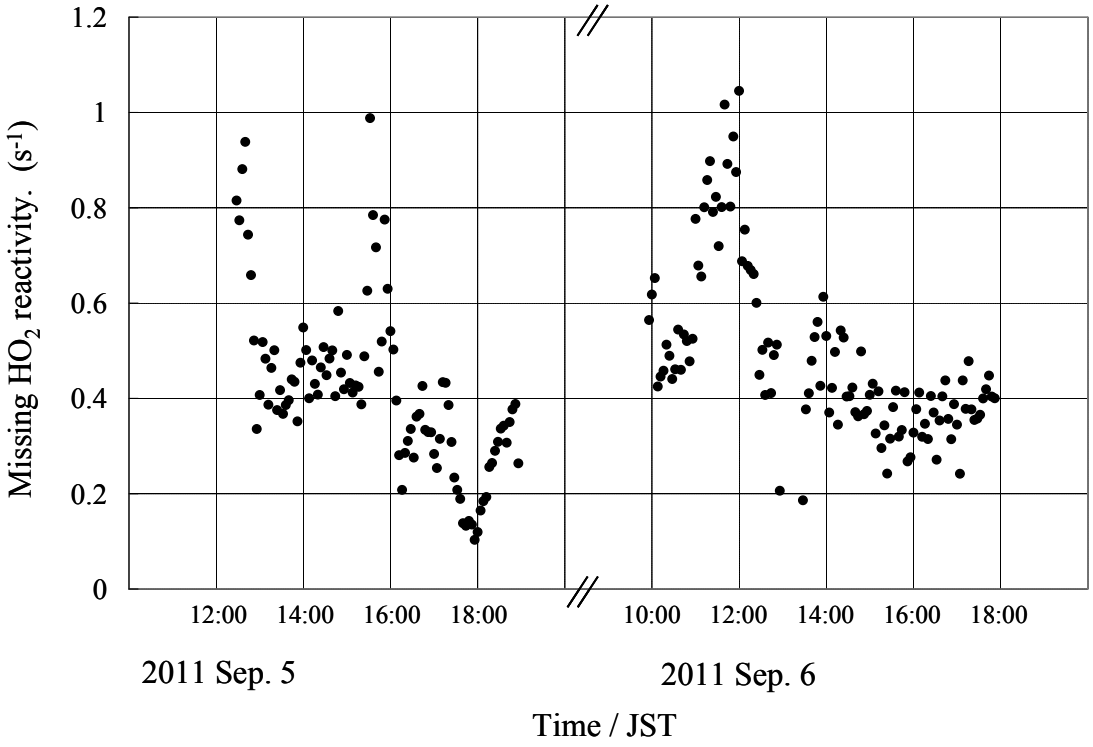

Figure.3-14. The diurnal variation of the observed missing HO_2 sink.

One of the possible candidate species for these missing sink is thought to be VOCs. HO_2 is considered to be less reactive to almost all of VOCs. But, recent reports show the HO_2 can react with some kinds of VOCs, especially oxygenated VOCs (e.g. acetone [Grieman et al., 2011] and HCHO [Finlayson-Pitts and Pitts, 2000]). During the observation, 7 kinds of VOCs were monitored by using PTR-MS as shown in Figure.3-10 including acetone and HCHO. Even though considering acetone and HCHO concentration and representative rate coefficient, these are not contributed to the missing HO_2 reactivity so much (< 0.1 % for total HO_2 reactivity). But, relatively strong correlations between the missing HO_2 reactivity and NOx, isoprene and CH_3CHO are observed as shown in Figure.3-15 and 3-16, respectively. And also, strong correlation can be found between the missing HO_2 reactivity and ambient temperature as shown in Figure.3-17. At the noon time of September 6th, strong fossil fuel combustion enough to titrate O_3 entirely has observed. At this time, almost maximum missing HO_2 reactivity has observed. From these results, some part of the missing HO_2 reactivity can be contributed by the VOCs directly emitted from fossil fuel combustion. Other species can contribute to the missing sink such as the semi-volatile organic compounds

(SVOCs) emitted from biogenic and/or anthropogenic emission source which are emitted depending on the temperature. Secondary produced VOCs in the photochemistry can be also the missing sinks. But, further investigations are necessary to explore these missing sink.

Figure.3-13 shows the contribution of each species to (a) $L(HO_2)_{obs.}$ and (b) $L(HO_2)_{amb.}$. And in this Figure.3-13(b), NO is the only specie to recycle OH in the atmosphere and its contribution is 53.8 %. The other reaction path ways do not recycle OH and produce non radical products. This means, in urban areas, tropospheric ozone could not be produced so much efficiently than the past understandings of atmospheric chemistry, because 22.1 % of HO_2 radicals can react to produce non-radical products.

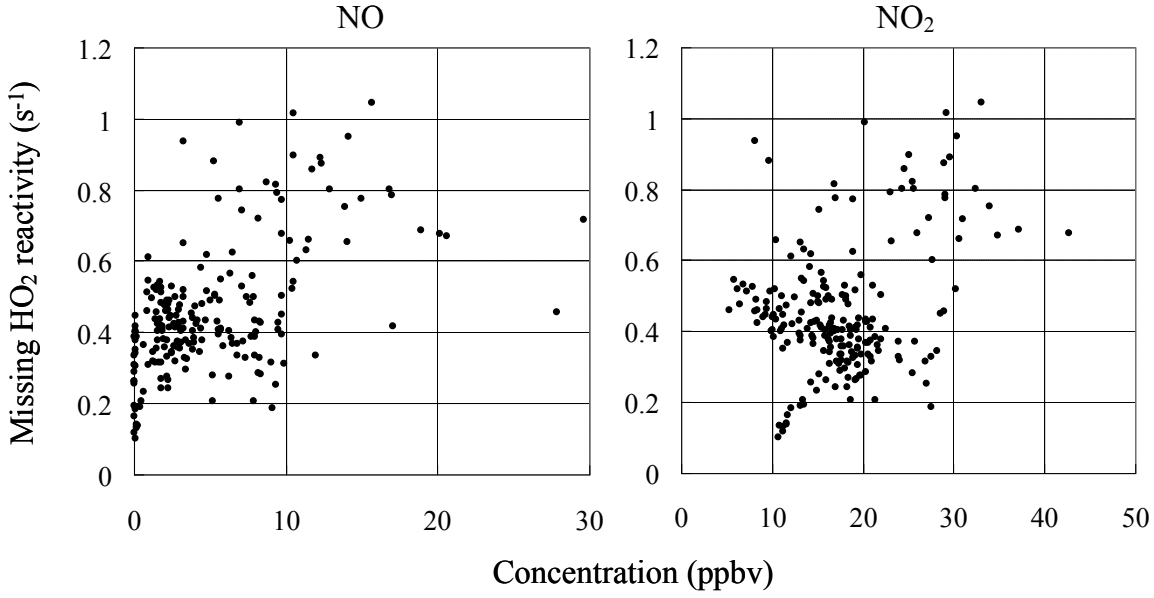

Figure.3-15. The correlation between NO_X and missing HO_2 reactivity.

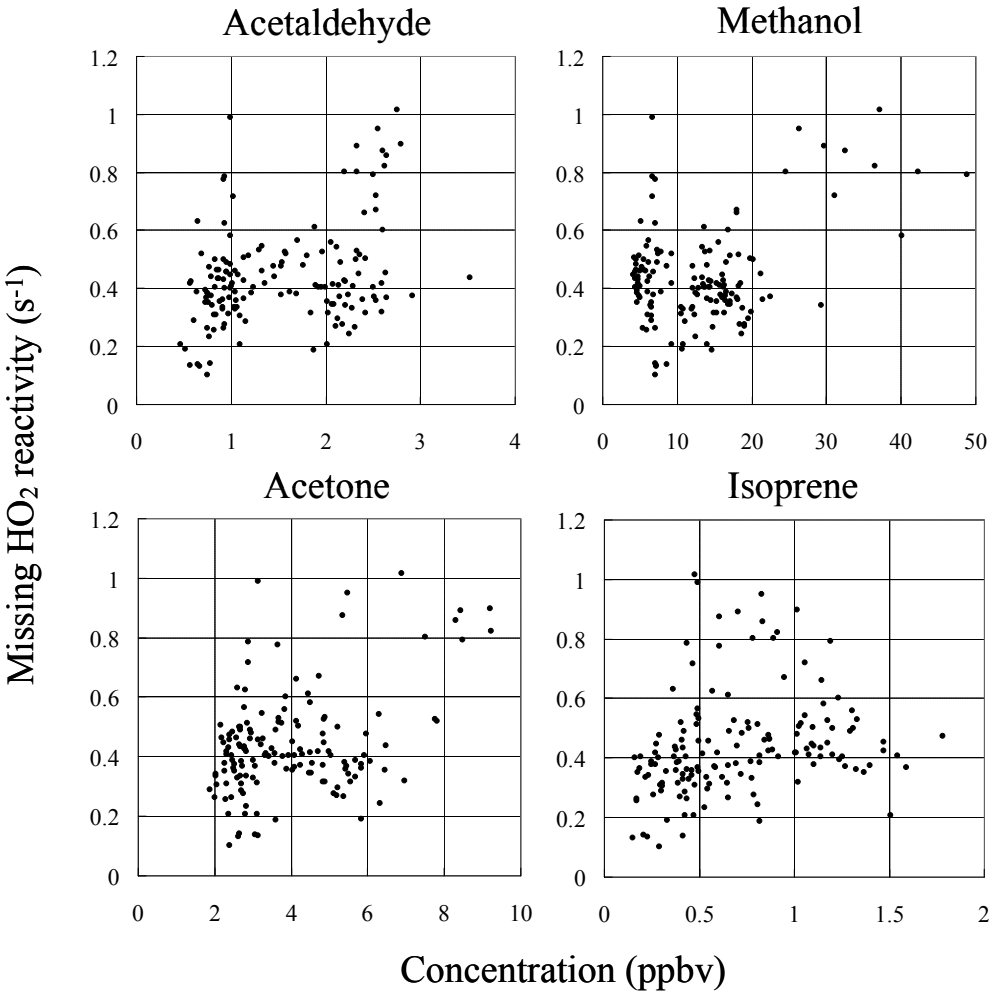

Figure.3-16. The correlation between VOCs and missing HO_2 reactivity.

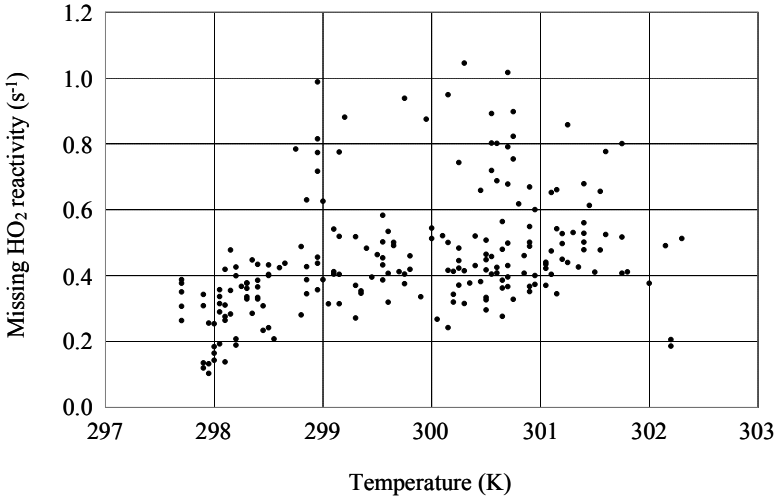

Figure.3-17. The correlation between temperature and missing HO_2 reactivity.

3-5. Summary

An instrument for measuring total HO_2 reactivity by a laser-induced pump and probe technique was developed. The practical utility has evaluated through the kinetic measurement of HO_2 reaction with NO_2, the interference test on NO and ambient observation. Consequently, this technique was confirmed to be sufficiently sensitive to measure ambient HO_2 loss rate. Measurement of total HO_2 reactivity was conducted in Hachioji, Tokyo, by using the developed instruments. Other chemical species were monitored simultaneously with each instrument. The measured and calculated HO_2 reactivity are compared to evaluate HO_2 loss process in urban atmosphere. Results show that 22.1 % of ambient HO_2 reactivity can be missing sink, resulting in that recent chemical model overestimate the ambient HO_2 concentrations. The possible candidate species for these missing sink is thought to be VOCs, especially SVOCs. But, further investigations are necessary to explore these missing sinks.

Chapter 4.

Development of a technique for the selective measurement of atmospheric peroxy radical concentrations of HO_2 and RO_2 using a denuding method

A technique for the selective measurement of atmospheric HO_2 and RO_2 using peroxy radical chemical amplification coupled to laser-induced fluorescence NO_2 detection (PERCA-LIF) technique is demonstrated.

Recent studies of PERCA have reported a greater wall loss rate of HO_2 relative to RO_2. For example, Mihele et al. [1999] reported a wall loss rate on a ¼'' Teflon tube of 2.8 ± 0.2 s^{-1} for HO_2 and 0.8 ± 0.1 s^{-1} for both CH_3O_2 and $C_2H_5O_2$ radicals in dry conditions. In this report, the HO_2 loss rate increased markedly with the relative humidity while the organic radicals showed no dependence.

The greater wall loss rate of HO_2 relative to RO_2 can be actively used to separate HO_2 and RO_2 during atmospheric measurements by predominantly denuding HO_2 prior to the PERCA inlet. Pre-inlet conditions have been found where ca. 90 % of HO_2 was removed whereas the comparable CH_3O_2 loss was 5%. The dependence of loss rate on humidity and peroxy radical concentration has been investigated. When using glass beads as the surface for peroxy radical remove, the influence of the relative humidity on the removal efficiency becomes negligible. Therefore, it may be possible to apply this technique to the measurement of absolute concentrations of solely RO_2 as well as the sum of HO_2 and RO_2. The practical utility of the PERCA-LIF coupled to a denuder has been demonstrated with atmospheric measurements.

4-1. Experimental

The experimental system used in this work is similar to the PERCA system described and validated in detail by Sadanaga et al. [2004] (see also Figure.4-1). The system consists of (1) a peroxy radical generator, (2) a removal cell which is original invention

of this work (3) chemical amplification reaction tube and (4) LIF NO_2 detector.

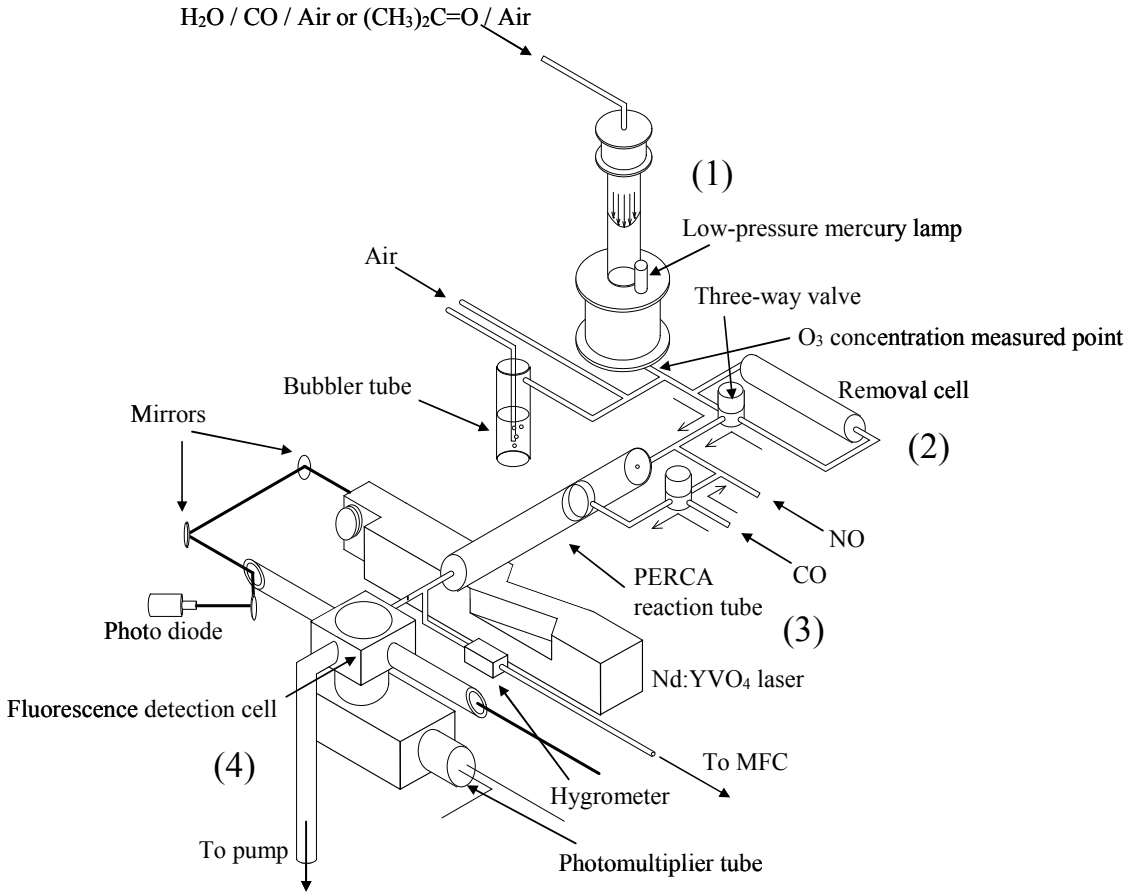

Figure.4-1 Schematic diagram of the experiment. The system can be divided into 4 parts, (1) peroxy radical generator, (2) removal cell, (3) chemical amplification reaction tube and (4) LIF NO_2 detector. MFC indicates mass flow controller.

The peroxy radical generation system is similar to the HO_X generator described by Kanaya et al. [2001]. HO_2 radicals are generated by the photolysis of H_2O at 185 nm using a low-pressure mercury lamp (Sen light, SP-5-2H). By addition of CO, generated OH is converted to HO_2:

$$H_2O + h\nu \rightarrow H + OH, \quad \text{(R4-1)}$$
$$H + O_2 + M \rightarrow HO_2 + M. \quad \text{(R1-2)}$$
$$OH + CO + O_2 \rightarrow HO_2 + CO_2 \quad \text{(R4-2)}$$

As proxy for RO_2, CH_3O_2 and $CH_3C(O)O_2$ radicals were generated in the same radical generator by photolysis of acetone (Kanto Chemical, 99.0 %):

$$(CH_3)_2CO + h\nu \rightarrow CH_3CO + CH_3 \quad (\lambda < 338\ nm) \quad \text{(R1-24)}$$
$$\rightarrow 2CH_3 + CO \quad (\lambda < 299\ nm)$$
$$CH_3 + O_2 + M \rightarrow CH_3O_2 + M. \quad \text{(R4-3)}$$
$$CH_3CO + O_2 + M \rightarrow CH_3C(O)O_2 + M \quad \text{(R4-4)}$$

The low-pressure mercury lamp was not filtered and the photolysis of acetone will occur mainly at 254 nm from its absorption cross section [Gierczak et al., 1998]. The principal products are thought to be CH_3O_2 and $CH_3C(O)O_2$ at nearly equal concentrations ($[CH_3O_2] : [CH_3C(O)O_2] \approx 1.1 : 0.9$) [Rajakumar et al., 2008]. Peroxy radicals can be diverted either through the removal cell or through a blank cell, easy switching between both pathways is enabled by use of a Teflon solenoid three-way valve (Flon Industry, FSS-0306YN). Hereafter, we refer to these pathways as removal and blank mode respectively. In order to investigate the water dependence of the peroxy radical removal efficiency, varying quantities of dry air and humidified air (the air is humidified by passing it through a water bubbler) were mixed allowing air of varying relative humidity to be added to the flow at the exit of the radical generator as shown in Figure.4-1. The relative humidity is measured at the exit of the PERCA instrument using a humidity sensor (VAISALA, HMT 330). Air used in these experiments was synthesized from N_2 and O_2 (Nippon Sanso, 99.99%>) by using mass flow controllers (KOFLOC, Model3660). After passing through either the removal or blank cell the gas flow is introduced to the PERCA reaction tube.

The removal cell consists of a tube and beads of the same material. Two different types of Teflon (PFA and PTFE) as well as glass have been tested. Cylindrical Teflon (PFA and PTFE) beads (Flon Industry, 2 dia. × 5 mm high) were packed into a 30 cm long 1.27 cm diameter Teflon tube. For testing glass, spherical glass beads (GL Science, 1 mm dia.) were packed into a 5cm long 1.27 cm glass tube. For easy comparison, the length of the removal cell was adjusted to obtain a removal efficiency of approximately 90% for HO_2 radicals. Additionally, the length of the blank cell was set so as to have the same residence time as in the removal cell.

Concentrations of HO_2 and RO_2 radicals were measured by a chemical amplification and laser-induced fluorescence (PERCA/LIF) instrument, based on Sadanaga et al. [2004]. The inlet consists of a 300 mm long glass tube of 20 mm diameter. When used in chemical amplification mode (PERCA mode), the flow from the radical generator

was mixed with a NO / N_2 mixture (Nippon Sanso, 100 ppmv NO) and pure CO gas (Nippon Sanso) at the entrance of the reaction tube; flows were adjusted to obtain concentrations of NO and CO of 5 ppmV and 10 % respectively. In order to measure the background NO_2 concentration (BG mode), CO was added approximately 75 mm downstream from the inlet, leading to a distance of 225 mm between second addition point and radical detection point. OH generated from the reaction of HO_2 with NO will thus have no CO with which to react and the chain cycle is terminated. By switching the CO addition and not just stopping it, the decrease of the fluorescence signal owing to CO addition (dilution of the gas mixture and fluorescence quenching) is kept constant. A Teflon solenoid valve (Flon Industry, FSS-0306YN) is used to switch between the two modes once per minute. The total flow rate in the reaction tube was set to 2 SLPM (Standard Litres per Minute). A part of the total flow was introduced into the LIF detector. The excess air flow from the reaction tube was evacuated by a diaphragm pump (ULVAC, MD-4) through a mass flow controller (KOFLOC, Model3660) and its humidity and temperature were monitored with a humidity sensor (VAISALA, HMT330).

The NO_2 fluorescence detection system was essentially the same as the instrument described in an earlier work by Miyazaki et al. [2008]. The pressure inside the fluorescence detection cell is reduced to ca. 2 Torr using a critical orifice (0.3 mm id) and an oil rotary pump (Ulvac, GVD-200A; 200 litre min^{-1}) in order to minimize the collisional quenching of the excited NO_2 molecules by air [Matsumoto et al., 2001]. The second harmonic of a diode-laser-pumped solid-state pulsed Nd:YVO_4 laser (Spectra-Physics, YHP70-106Q; 5 W, 10 kHz, 532 nm) is used for NO_2 excitation. The laser power is monitored outside the detection cell by using a calibrated photodiode (Hamamatsu, S1226-5BQ) in order to correct for possible drifts of the laser power. The fluorescence is collected and focused through optical lenses and passes through a sharp cut-off glass filter (Asahi Technoglass Corp., R62) onto a photomultiplier tube (PMT; Hamamatsu, R928P). The output signal from the PMT is counted between 1.10 and 3.02 μs after the laser excitation using a photon counter (Stanford, SR400). The limit of detection (LOD) for HO_2 is estimated by the following equation when governed by a background-limited case:

$$\mathrm{LOD}_{HO2} \approx \frac{(S/N)}{S_{HO2}} \left(\frac{1}{m}+\frac{1}{n}\right)^{1/2} \left(\frac{S_{BG}}{I \cdot \Delta t}\right)^{1/2}, \qquad (4\text{-}1)$$

where (S/N) is the signal-to-noise ratio for defining the LOD, S_{HO2} is the sensitivity of the HO_2 radical measurement, m and n are the number of measurements of the background and sample, respectively, S_{BG} is the signal of the background measurement (cps W^{-1}: count per second per Watt), I is the laser energy (W), and Δt is the averaging interval (s) [Sadanaga et al., 2004]. Under typical conditions, the LOD in dry conditions is determined to be 0.41 pptv when (S/N) = 2, S_{HO2} = 26 cps $pptv^{-1}$ W^{-1}, m = n = 1, S_{BG} = 2064 cps W^{-1}, I = 2.3 W, and Δt = 60 s. Calibration of S_{HO2} was conducted by the method of simultaneous photolysis of O_2 and H_2O using peroxy radical generator as described above [Sadanaga et al., 2004]. O_3 concentration was measured by an ozone monitor (Dylec, Model 1100) at the exit of the peroxy radical generator by changing the inlet tube. Typically, HO_2 and RO_2 radicals were generated at concentrations between 150 – 200 pptv.

4-2. Results and discussion

Figure.4-2 shows an example of the removal efficiency measurement: the upper part (a) of the figure illustrates the measurement of HO_2 radicals, while the lower part (b) is a typical example for CH_3O_2 + $CH_3C(O)O_2$ radicals. In both cases, the signal differences between PERCA and BG modes arise from the HO_2 or CH_3O_2 + $CH_3C(O)O_2$ concentration. The left part of each figure shows the HO_2 or CH_3O_2 + $CH_3C(O)O_2$ concentration after passing through the blank cell, while the right part of the graph shows the signal obtained after passing the gas mixture through the removal cell prior to entering the PERCA inlet, also in PERCA and BG mode. The connecting tubing in the blank cell path and in the removal cell path are made of the same material. The HO_2 concentrations for each blank or removal mode can be described as follows

$$[HO_2]_{removal} \text{ or } [HO_2]_{blank} = \frac{I_{HO2\_removal} \text{ or } I_{HO2\_blank}}{S_{HO2} \times C_{humid}}, \qquad (4\text{-}2)$$

where $[HO_2]_{removal}$ and $[HO_2]_{blank}$ indicates the concentration of HO_2 radicals in the removal and blank mode respectively and C_{humid} indicate the correction coefficient of S_{HO2} for humidity. It has been shown by several authors [Mihele and Hastie, 1998; Reichert et al., 2003; Salisbury et al., 2002] that the chain length of the chemical amplification decreases with increasing humidity: this correction factor accounts for this

characteristic. Our PERCA-LIF instrument also experiences chain length variations with changing humidity as reported by Sadanaga et al. [2004], in which the method of determining the correction factor is also described. However, for the experiments described in this work, the humidity dependence of the chain length is of no importance as only the ratio of signals from the blank and removal cells is measured: both blank and removal path exhibit the same relative humidity and chain length and therefore the correction factor cancels.

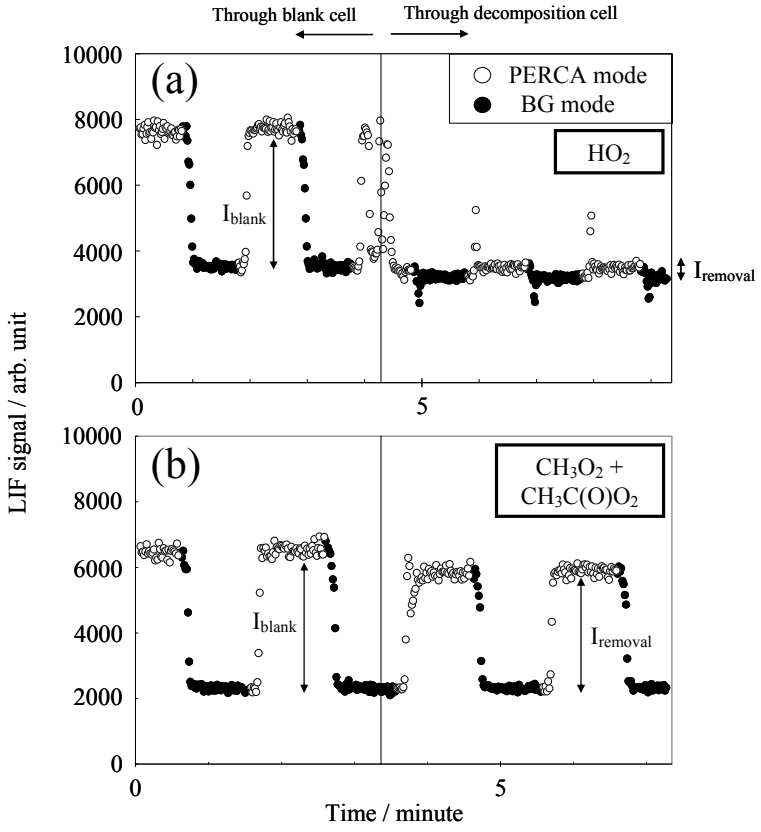

Figure.4-2 An example of removal efficiency measurements showing PERCA / BG mode for both blank (left side) and removal (right side) mode. PERCA / BG mode are switched every minute. Upper figure (a) shows HO_2, lower figure (b) is $CH_3O_2 + CH_3C(O)O_2$.

Variation in the removal of HO_2 was evaluated by defining a removal efficiency factor α as follows,

$$\alpha = 1 - \frac{[HO_2]_{removal}}{[HO_2]_{blank}} \quad . \tag{4-3}$$

$[HO_2]_{removal}$ and $[HO_2]_{blank}$ can be substituted by Eq.(4-2) and finally the removal efficiency α of HO_2 radicals is determined as follows:

$$\alpha = 1 - \frac{I_{HO2\_removal}}{I_{HO2\_blank}} \tag{4-4}$$

The removal efficiency of CH_3O_2 + $CH_3C(O)O_2$ radicals can be expressed the same way:

$$\beta = 1 - \frac{I_{CH3O2+CH3C(O)O2\_removal}}{I_{CH3O2+CH3C(O)O2\_blank}} \tag{4-5}$$

Figures.4-3 summarizes the results of the removal efficiency measurements by plotting α and β as a function of relative humidity for the three different materials tested in this study: for all experiments, the initial radical concentration was kept constant at around 150 pptv. Figure.4-3(a), (b) and (c) show the results for PFA, PTFE and glass. Error bars indicate the 95 % confidence interval. As mentioned above, the lengths of the removal cells have been adjusted as to obtain around 90 % removal efficiency for HO_2 at a relative humidity between 20-60 %.

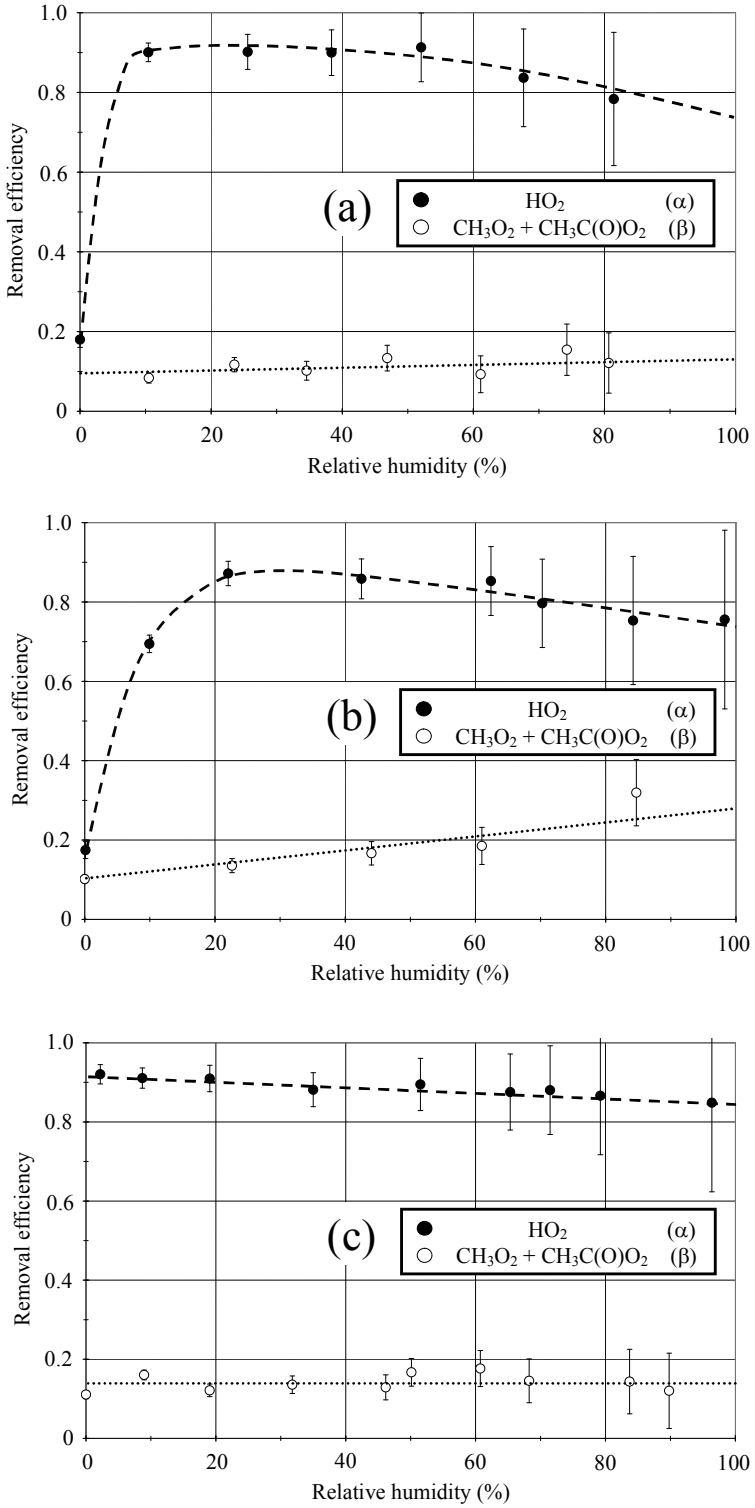

Figure.4-3 Results of the removal efficiency α (HO_2) and β(CH_3O_2 + $CH_3C(O)O_2$) as a function of relative humidity using (a) PFA, (b) PTFE and (c) glass as the material in the removal cell.

As can be seen from Figure.4-3, the removal efficiency β for CH_3O_2 + $CH_3C(O)O_2$ is approximately 15 % for all three materials and only slightly depends on the relative humidity. However, the removal efficiency of HO_2 is more sensitive to the relative humidity and shows different behaviours for the three materials tested in this work. When using Teflon (PFA, PTFE), the removal efficiency of HO_2 radicals decreases rapidly with decreasing humidity and is only around 10 % in dry conditions. With increasing humidity, α increases for both materials and approaches the maximum of 90 % at humidities of around 20 %. Further, increasing the humidity leads to a slow decrease of α for both materials, showing a slightly more rapid decrease in the case of PFA compared to PTFE. In the case of CH_3O_2 + $CH_3C(O)O_2$, this behaviour is not observed: for both materials the removal efficiency β increases slightly and steadily with relative humidity. Though the removal efficiency of RO_2 might depend on the structure of R, the average removal efficiency for both CH_3O_2 and $CH_3C(O)O_2$ radicals is 0.15 as shown in Figure.4-3. These result consistent with the observation already reported by Mihele et al. [1999] in the point of humidity dependent peroxy radical loss on the wall.

Results change markedly when using glass as material in the removal cell: even in dry conditions a removal efficiency of about 90 % for HO_2 is observed. With increasing relative humidity, α decreases slightly and steadily approaching 85 % at approximately 100% humidity. The removal efficiency of CH_3O_2 + $CH_3C(O)O_2$ radicals was found to be almost constant at around 15 % across the entire range of relative humidity.

These results indicate clearly that the removal efficiency variation is affected by the surface structure of the material within the removal cell. The removal efficiency has almost been constant for several days of experiment, i.e. no saturation effect has been observed. Therefore, HO_2 and RO_2 radicals seem to be removed from the gas phase not by a simple absorption process, but probably react at the surface to generate non-radical products. Furthermore, HO_2 radicals seem to interact with hydrophilic surface sites since the removal efficiency of HO_2 radicals is high when using glass, even under dry conditions.

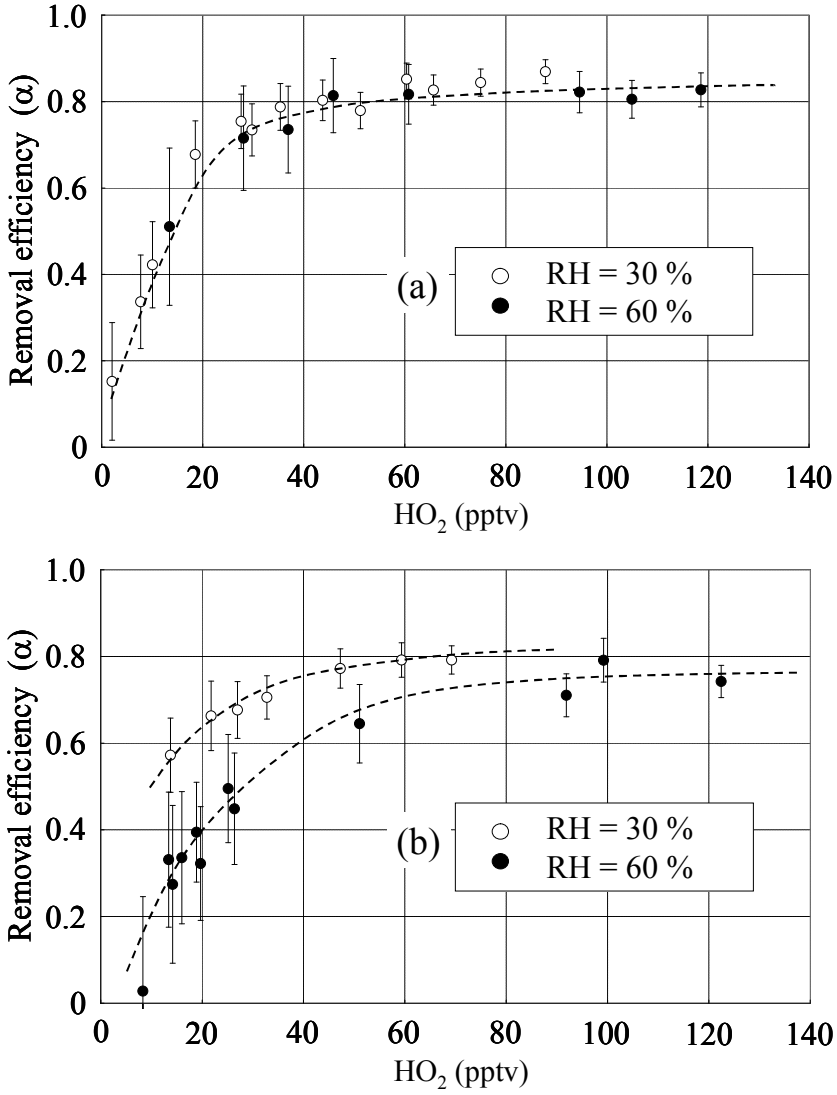

Figure.4-4 Removal efficiency α for two different relative humidities as a function of initial HO_2 radical concentration: figure (a) shows the results with glass as filling material, figure (b) is for PFA.

We have further investigated the removal efficiency of HO_2 radicals as a function of initial radical concentration: the results are summarized in Figure.4-4 for glass (Figure.4-4a) and PFA (Figure.4-4b). As can be seen, the efficiency depends strongly on the initial concentration over ambient HO_2 concentration range. For glass as filling material, the removal efficiencies do not depend on the relative humidity, while for PFA the efficiency is somewhat higher at lower relative humidity. The concentration dependence of the removal is probably connected to the removal mechanism, for example a bimolecular reaction on the surface between two absorbed radicals. On the

other hand, the constant removal efficiency for CH_3O_2 + $CH_3C(O)O_2$ was obtained at a concentration range of ~150 pptv. Further work is needed to understand the removal mechanism. The concentration dependence of α has of course an impact on the applicability of this experimental technique to atmospheric measurements and needs to be taken into account when developing a field instrument. In this experiment, the geometry of the removal cell was designed to achieve a removal efficiency of approximately 90 % for HO_2 radicals at HO_2 concentrations of ~150 pptv, allowing for an easy comparison. However, some improvement on the removal cell is necessary for observations under ambient HO_2 concentrations because the removal efficiency for HO_2 decreases steeply over the typical ambient HO_2 concentration range. If the HO_2 loss reaction occurs through bimolecular reaction on the surface, relatively high removal efficiency for HO_2 even under the ambient concentration range can be obtained by increasing the residence time and/or controlling the surface temperature. As for controlling the surface temperature, HO_2 loss in the removal cell is considered to be initiated by chemical adsorption on the surface. Generally in chemical adsorption, adsorbed amount can be larger with decreasing the surface temperature. Some optimization is necessary for ambient measurements to be made with high precision.

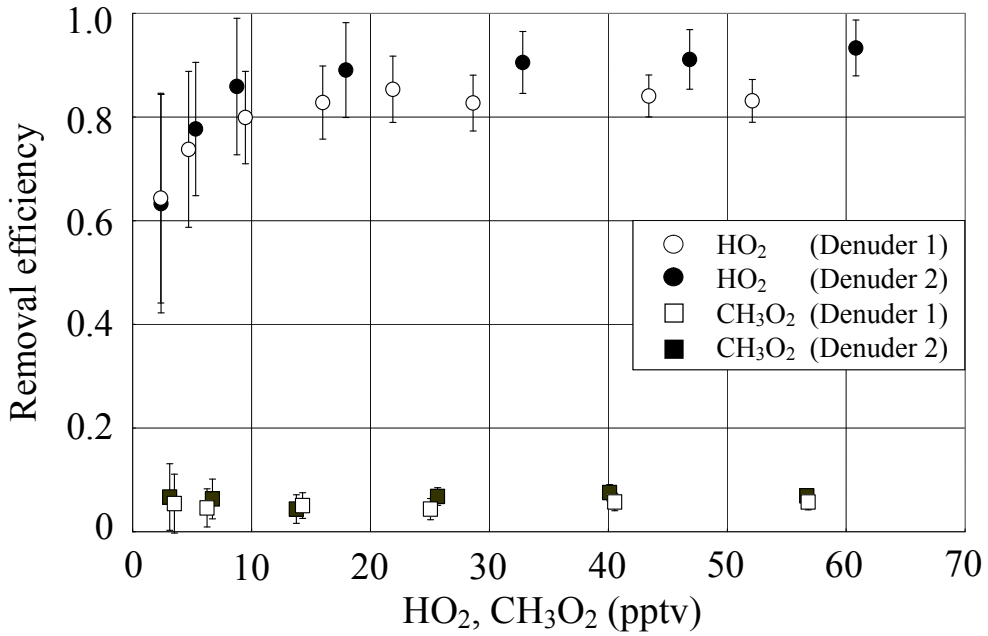

Figure.4-5 Removal efficiency α for two different long denuders as a function of initial HO_2 radical concentration: Denuder 2 is the twice as long as Denuder 1.

In order to improve the removal efficiency for HO_2 radicals under typical ambient concentrations, a longer removal cell with an increased surface was applied to the measurement. The results are summarized in Figure.4-5. The removal efficiency α for two different long removal cells was plotted as a function of initial HO_2 radical concentration. Unlike the previous removal cells that were used for earlier experiments, these cells have a honeycomb structure in that many narrow pyrex glass tubes are packed in the cylindrical cell. The length of Denuder 1 was adjusted to obtain a removal efficiency of approximately 90% for HO_2 radicals. Denuder 2 is twice as long as Denuder 1. As can be seen, the removal efficiency still depends on initial HO_2 concentrations as in Figure.4-5. However, as can be seen in Figure.4-5, high removal efficiencies can be obtained even in the lower range of typical ambient HO_2 radical concentration range. Compared with denuder 1 results, denuder 2 shows higher removal efficiency for the same radical concentrations. This result suggests that a high removal efficiency for HO_2 can be obtained even under the ambient concentration range by increasing the residence time. As for the removal efficiency for CH_3O_2 by using these denuder 1 and 2, the constant lower removal efficiency of 0.05 - 0.06 can be obtained for both denuders. In this experiment, CH_3O_2 radicals were generated by the photolysis of CH_3I by using the radical generator described above. The low-pressure mercury lamp was not filtered and the photolysis of CH_3I will occur mainly at 254 nm to generate mainly CH_3O_2 radical [Clemitshaw et al., 1997]. This results shows that the removal efficiency for $CH_3C(O)O_2$ is relatively higher than that for CH_3O_2. Considering the result of the acetone photolysis experiment, a removal efficiency of at least 0.27 for the $CH_3C(O)O_2$ radical can be obtained. This result indicates that the removal mechanism might be affected by the peroxy radical structure. The other kinds of RO_2 radicals are generated through the OH reaction with some kinds of hydrocarbons (RH). The different structure of RO_2 radicals can be obtained by changing the RH added to radical generator. The reaction schemes are shown as.

$$RH + OH + O_2 \rightarrow RO_2 \qquad \text{(R4-5)}$$

Simultaneously, HO_2 can be generated as described above. Approximately 100 pptv of HO_2 and RO_2 in approximately 1:1 ratio have been generated during the experiments. Figure.4-6 shows the removal efficiency for each kind of RO_2 radicals. Removal efficiency of HO_2 radicals and hydrophilic RO_2 radicals are higher than non-hydrophilic RO_2. Especially, RO_2 radicals with OH group are found to be high removal efficiency.

Further tests show that the removal efficiency for HO_2 does not depend on the

presence of RO_2 radicals. In some experiments, C_2H_6 was added to photolysis gas instead of CO: now OH radicals will be converted to $C_2H_5O_2$ and equal amounts of HO_2 and $C_2H_5O_2$ radicals will be generated. The LIF signal obtained through these experiments was consistent with an LIF signal calculated using separately pre-measured removal efficiencies for HO_2 and RO_2.

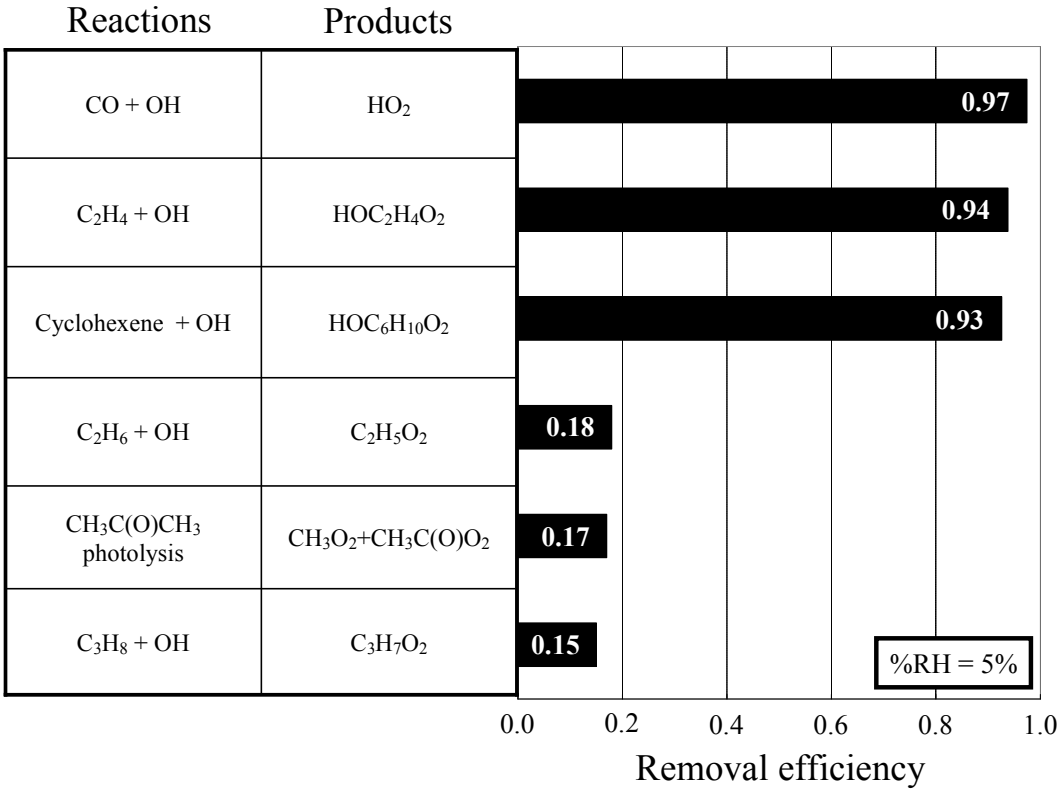

Figure.4-6 Results for the HO_2 and RO_2 removal efficiency as a function of the structure of each peroxy radicals.

As discussed above, the LOD for total peroxy radicals can be calculated by Eqs.(4-1). And, here the LOD for each measurement of HO_2 and RO_2 was calculated to be 1 pptv in dry conditions considering the removal efficiencies for HO_2 and RO_2 under experimental conditions.

Since the effect of humidity on removal efficiency can be minimized by using glass, this material seems to be a good choice as material for the removal cell. By using the removal efficiency factors, the concentrations of HO_2 and RO_2 can then be described using LIF signal S as follow:

$$S_{HO2}[HO_2]_{blank} + S_{RO2}[RO_2]_{blank} = \frac{I_{blank}}{C_{humid}}, \quad (4\text{-}6)$$

$$S_{HO2}[HO_2]_{removal} + S_{RO2}[RO_2]_{removal} = \frac{I_{removal}}{C_{humid}}, \quad (4\text{-}7)$$

where S_{HO2} and S_{RO2} indicate the sensitivity for HO_2 and RO_2 respectively. I_{blank} and $I_{removal}$ indicate the LIF signal in the blank and removal mode, respectively. Here, $[HO_2]_{removal}$ is described by $[HO_2]_{blank}$ in consideration of the combination of first and second order reactions for HO_2 as below:

$$[HO_2]_{removal} = \frac{[HO_2]_{blank}}{F_1 \times [HO_2]_{blank} + F_2}, \quad (4\text{-}8)$$

where F_1 and F_2 are correction factors obtained by fitting the data in Figure. 4-5 using Eq (4-8).

In the same way, $[RO_2]_{removal}$ can be described by $[RO_2]_{blank}$ because the constant removal efficiency for RO_2 can be obtained:

$$[RO_2]_{removal} = (1-\beta)[RO_2]_{blank}, \quad (4\text{-}9)$$

Eqs.(4-6), (4-7), (4-8) and (4-9) were solved for $[HO_2]$ and $[RO_2]$ to give HO_2 and RO_2 concentrations. This methodology allows the concentrations of HO_2 and RO_2 to be

described separately by the LIF signals obtained in the two measurement modes and the calibration factors, if the factor C_{humid}, i.e. the variation of the chain length only with relative humidity, independent of the radical concentration, has been determined in separate experiments. Furthermore, using this method it is not necessary to correct for the sensitivity of HO_2 and RO_2 based on the hypothesis of an abundance ratio of HO_2 and RO_2, because now the concentrations of HO_2 and RO_2 can be corrected by separate sensitivity factors of S_{HO2} and S_{RO2}. More selective and precise measurements of HO_2 and RO_2 concentrations can therefore be possible using this technique.

4-3. Ambient measurement

Ambient measurements were performed using the newly developed PERCA-LIF set-up coupled with denuder instrument during July 2010 at our campus located in Hachioji, Tokyo, Japan. Denuder 1 in Figure.4-5 was used during the observation. The instruments were set up on the roof container of the ninth building of Tokyo Metropolitan University. The site is located in the suburban of Tokyo as shown in Firure.3-8.

Figure.4-7 shows an example of the measured diurnal profiles of HO_2 and RO_2 radical concentrations. Data averaged over 2 min are plotted in Figure.4-7 and the error bars represent 1σ precisions of the data points. Each solid line in Figure.4-7 indicates a 10 points moving average data.

A typical diurnal variation was observed for each HO_2 and RO_2 radicals, and a maximum concentration value of 50 pptv for RO_2 ($R = C_xH_y$) and 25 pptv for HO_2 was observed at noon time. The removal efficiency for CH_3O_2 of 0.05 was used for the analysis. The variations in RO_2 and HO_2 are highly correlated, and the concentrations of the HO_2 radical were half the magnitude of that of RO_2 radical. The ratio HO_2 / (HO_2 + RO_2) was observed to be 0.33 at noon time. In October 2006, the separation experiment between HO_2 and RO_2 was carried out using PERCA-LIF instrument and LIF-HO_2 instrument at TMU. PERCA-LIF instrument measured total HO_2 + RO_2 concentration and LIF-HO_2 instrument measured HO_2 concentration. In this experiment, the ratio HO_2 / (HO_2 + RO_2) was observed to be 0.37 at noon time. Although the seasons are different, nearly the same values of HO_2 / (HO_2 + RO_2) ratio were observed. In general, the modelled HO_2 / (HO_2 + RO_2) ratio is calculated to be almost 0.5 through the day time [e.g. Ren et al., 2005]. But in this study, observed HO_2 / (HO_2 + RO_2) ratio was 0.33 at noon time, indicating the recent chemical model overestimates HO_2 concentration. This

means that the recent model needs more HO_2 loss and/or less HO_2 production process. This suggestion has been confirmed to be true in the point of more HO_2 loss needed by measuring total HO_2 loss rate described in Chapter 3.

It should be noted that the observed HO_2 concentration can have it's highly contribution of hydrophilic RO_2 radicals if there exist high amount of such peroxy radicals in the atmosphere during the observation. Further works are needed in order to generalise these observations to other types of RO_2, but the concentrations of HO_2 obtained in this study are similar to concentrations observations before [Kanaya et al., 2007]. The practical utility of our PERCA-LIF coupled with denuder instrument has been demonstrated under atmospheric measurement.

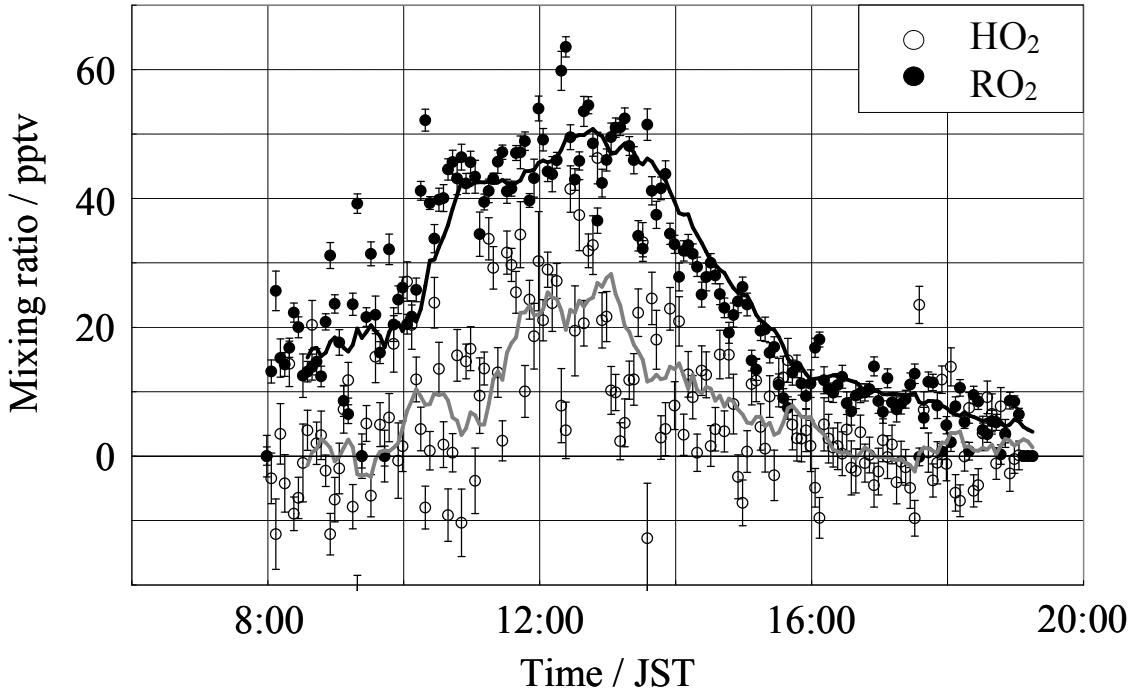

Figure.4-7 In situ measurements of HO_2 and RO_2 radical concentrations with 1σ precision error bars. Each solid line indicates the 10 points moving average data. The measurements were obtained on 23 July 2010 in Hachioji, Tokyo.

4-4. Summary

An improvement to the well-established PERCA technique allowing the selective measurement of HO_2 and RO_2 radical concentrations has been described in this paper. Advantage is taken of different heterogeneous removal efficiencies for HO_2 and RO_2 radicals prior to the inlet of the PERCA reaction cell. Three different materials have been tested to investigate the variation of the removal efficiency as a function of relative humidity. From these results, glass has been found to be best suited as the material for the removal cell as it shows very low dependence on relative humidity, the difference of removal efficiency seems to be linked to the surface structure. The removal cell filled with glass showed about 90 % removal efficiency of HO_2 over the entire relative humidity range, compared to only 15 % removal efficiency of CH_3O_2. The investigation of the dependence of the removal efficiency on the concentration at a given relative humidity has been tested for HO_2 radicals on glass and PFA as filling material. Both materials show a pronounced dependence on the concentration, i.e. the removal efficiency decreases steeply at low initial radical concentrations, probably due to the removal mechanism. On the other hand, the constant removal efficiency for CH_3O_2 and $CH_3C(O)O_2$ was obtained at a concentration of ~150 pptv. In order to improve the removal efficiency for HO_2 under ambient concentrations range, a longer removal cell with increased surface to volume ratio was applied to the instrument. Using a longer removal cell a higher removal efficiency can be obtained at lower radical concentrations demonstrating a high removal efficiency for HO_2. LOD for each HO_2 and RO_2 measurement was calculated to be 1 pptv in dry condition considering the removal efficiency for HO_2 and RO_2 under experimental condition. This performance could be applicable for the field measurement. First ambient measurements were performed by the newly developed PERCA-LIF coupled with denuder instrument in summertime of Tokyo, Japan. Typical diurnal variation was observed for each HO_2 and RO_2 radicals, and the maximum concentration value of 50 pptv for RO_2 and 25 pptv for HO_2 was observed at noon time. The ratio HO_2 / (HO_2 + RO_2) was observed to be 0.37 at noon time, indicating that the recent model needs more HO_2 loss process. This suggestion is consistent with the results in Chapter 3 in the point of HO_2 missing sinks have been observed. The practical utility of our PERCA-LIF coupled with denuder instrument has been demonstrated under atmospheric measurement.

The results presented in this work are promising and indicate the possibility of selective measurement of peroxy radicals. It has been shown that the concentrations of

HO_2 and RO_2 can be independently corrected by separate sensitivities of S_{HO2} and S_{RO2}. Clearly, there is more work needed in order to generalise these observations to other types of RO_2, but we think that this technique has the potential of increasing the precision of atmospheric peroxy radical measurements in the future.

Chapter 5.
Conclusions

In order to get better understanding the nature and roles of peroxy radicals, two kind of instrument have been developed and ambient observation have been conducted.

An instrument for measuring total HO_2 reactivity by a laser-induced pump and probe technique was developed. The practical utility has evaluated through the kinetic measurement of HO_2 reaction with NO_2, the interference test on NO and ambient observation. Consequently, this technique was confirmed to be enough sensitive to measure ambient HO_2 loss rate. Measurement of total HO_2 reactivity was conducted in Hachioji, Tokyo, by using the developed instruments. Other chemical species were monitored simultaneously with each instrument. The measured and calculated HO_2 reactivity are compared to evaluate HO_2 loss process in urban atmosphere. Results show that 22.1 % of ambient HO_2 reactivity can be missing sink, resulting in that recent chemical model overestimate the ambient HO_2 concentrations. The possible candidate species for these missing sink is thought to be VOCs, especially SVOCs. But, further investigations are necessary to explore these missing sinks and its products. In future work, it will become imperative to find the missing HO_2 reaction pathway. To do this, ambient observation should be carried out through the year to confirm the seasonal behavior of HO_2 reactivity. Not only in urban area, but also in any areas this technique should be used widely to assess the air quality.

An improvement to the well-established PERCA technique allowing the selective measurement of HO_2 and RO_2 radical concentrations has been described. Advantage is taken of different heterogeneous removal efficiencies for HO_2 and RO_2 radicals prior to the inlet of the PERCA reaction cell. Three different materials have been tested to investigate the variation of the removal efficiency as a function of relative humidity. From these results, glass has been found to be best suited as the material for the removal cell as it shows very low dependence on relative humidity, the difference of removal efficiency seems to be linked to the surface structure. The removal cell filled with glass showed about 90 % removal efficiency of HO_2 over the entire relative humidity range, compared to only 15 % removal efficiency of CH_3O_2. The investigation of the dependence of the removal efficiency on the concentration at a given relative humidity has been tested for HO_2 radicals on glass and PFA as filling material. Both materials show a pronounced dependence on the concentration, i.e. the removal efficiency

decreases steeply at low initial radical concentrations, probably due to the removal mechanism. On the other hand, the constant removal efficiency for CH_3O_2 and $CH_3C(O)O_2$ was obtained at a concentration of ~150 ppt. And it is also confirmed removal efficiency of HO_2 radicals and hydrophilic RO_2 radicals are higher than non-hydrophilic RO_2. Especially, RO_2 radicals with OH group are found to be high removal efficiency. First ambient measurements were performed by the newly developed PERCA-LIF coupled with denuder instrument in summertime of Tokyo, Japan. Typical diurnal variation was observed for each HO_2 and RO_2 radicals, and the maximum concentration value of 50pptv for RO_2 and 25 pptv for HO_2 was observed at noon time. The ratio HO_2 / (HO_2 + RO_2) was observed to be 0.37 at noon time, indicating that the recent model needs more HO_2 loss process. This suggestion is consistent with the results in Chapter 3 in the point of HO_2 missing sinks have been observed. The practical utility of our PERCA-LIF coupled with denuder instrument has been demonstrated under atmospheric measurement. The results presented in this work are promising and indicate the possibility of selective measurement of peroxy radicals. It has been shown that the concentrations of HO_2 and RO_2 can be independently corrected by separate sensitivities of S_{HO2} and S_{RO2}. Clearly, there is more work needed in order to generalise these observations to other types of RO_2, but this technique has the potential of increasing the precision of atmospheric peroxy radical measurements in the future.

Chapter 6.

References

Akimoto, H., “Global Air Quality and Pollution”, *Science.*, 302(5651), 1716 (2003).

Aloisio, S. and Francisco, J. S., "Existence of a Hydroperoxy and Water ($HO_2 \cdot H_2O$) Radical Complex", *J. Phys. Chem. A.*, 102(11), 1899 (1998).

Amedro, D., K. Miyazaki, A. Parker, C. Schoemaecker, and C. Fittschen, “Atmospheric and kinetic studies of OH and HO_2 by the FAGE technique”, *J. Environ. Sci.*, 24, 78 (2012).

Atkinson, R., D. L. Baulch, R. A. Cox, J. N. Crowley, R. F. Hampson, R. G. Hynes, M. E. Jenkin, M. J. Rossi, and J. Troe, “Evaluated kinetic and photochemical data for atmospheric chemistry: Volume I - gas phase reactions of Ox, HOx, NOx and SOx species”, *Atmos. Chem. Phys.*, 4, 1461 (2004).

Atkinson, R., D. L. Baulch, R. A. Cox, J. N. Crowley, R. F. Hampson, R. G. Hynes, M. E. Jenkin, M. J. Rossi, J. Troe, and IUPAC Subcommittee, “Evaluated kinetic and photochemical data for atmospheric chemistry: Volume II – gas phase reactions of organic species”, *Atmos. Chem. Phys.*, 6, 3625 (2006).

Butkovskaya, N., M.-T. Rayez, J.-C. Rayez, A. Kukui, and G. Le Bras, “Water Vapor Effect on the HNO_3 Yield in the HO_2 + NO Reaction: Experimental and Theoretical Evidence”, *J. Phys. Chem. A.*, 113, 42, 11327 (2009).

Cantrell, C. A. and D. H. Stedman, “A possible technique for the measurement of atmospheric peroxy radicals”, *Geophys. Res. Lett.*, 9, 846 (1982).

Carter, W. P. L., and R. Atkinson, ”Alkyl nitrate formation from the atmospheric photooxidation of alkanes: a revised estimation method”, *J. Atmos. Chem.*, 8, 165 (1989).

Clemitshaw, K. C., L. J. Carpenter, S. A. Penkett, and M. E. Jenkin, “A calibrated peroxy radical chemical amplifier for ground-based tropospheric measurements”, *J. Geophys. Res.*, 102, 25405 (1997).

Dillon, T. J. and Crowley, J. N., "Direct detection of OH formation in the reactions of HO_2 with $CH_3C(O)O_2$ and other substituted peroxy radicals", *Atmos. Chem. Phys.*, 8, 4877 (2008).

Dorn, H.-P., R. Neuroth, and A. Hofzumahaus, “Investigation of OH absorption cross sections of rotational transitions in the A $^2\Sigma^+$, $\upsilon'=0 \leftarrow$ X $^2\Pi$, $\upsilon''=0$ band under atmospheric conditions: Implications for tropospheric long-path absorption measurements”, *J. Geophys. Res.*, vol. 100, no. 4, 7397 (1995).

Edwards, G. D., C. A. Cantrell, S. Stephens, B. Hill, O. Goyea, R. E. Shetter, R. L. Mauldin, E. Kosciuch, D. J. Tanner, and F. L. Eisele, “Chemical Ionization Mass Spectrometer Instrument for the Measurement of Tropospheric HO_2 and RO_2”, *Anal. Chem.*, 75, 5317 (2003).

Faloona, I. C., Tan, D., Lesher, R. L., Hazen, N. L., Frame, C. L., Simpas, J. B., Harder, H., Martinez, M., Di Carlo, P., Ren, X., and Brune, W. H., "A laser induced fluorescence instrument for detecting tropospheric OH and HO_2: Characteristics and calibration", *J. Atmos. Chem.*, 47, 139 (2004).

Farmer, D. K., Perring, A. E., Wooldridge, P. J., Blake, D. R., Baker, A., Meinardi, S., Huey, L. G., Tanner, D., Vargas, O., and Cohen, R. C., "Impact of organic nitrates on urban ozone production", *Atmos. Chem. Phys.*, 11, 9, 4085 (2011).

Finlayson-Pitts, B.J., and J. N. Pitts, Jr., “Chemistry of the Upper and Lower Atmosphere”, *Academic Press*, pp. 216-217, (1999).

Fuchs, H., F. Holland, and A. Hofzumahaus, “Measurement of tropospheric RO_2 and HO_2 radicals by a laser-induced fluorescence instrument”, *Rev. Sci. Instrum.*, 79(8), 084104 (2008).

Fuchs, H., Bohn, B., Hofzumahaus, A., Holland, F., Lu, K. D., Nehr, S., Rohrer, F., and Wahner, A., "Detection of HO_2 by laser-induced fluorescence: calibration and interferences from RO_2 radicals", *Atmos. Meas. Tech.*, 4, 6, 1209 (2011).

Gierczak, T., J. B. Burkholder, S. Bauerle, and A. R. Ravishankara, “Photochemistry of acetone under tropospheric conditions”, *Chem. Phys. 231*, 229 (1998).

Dillon, T. J., A. Pozzer, L. Vereecken, J. N. Crowley, and J. Lelieveld, "Does acetone react with HO_2 in the upper-troposphere?", *Atmos. Chem. Phys.*, 12, 3, 1339 (2012).

Hanke, M., J. Uecker, T. Reiner, and F. Arnold, "Atmospheric peroxy radicals: ROXMAS, a new mass-spectrometric methodology for speciated measurements of HO_2 and ΣRO_2 and first results", *Int. J. Mass Spectrom.*, 213, 2-3, 91 (2002).

Hard, T. M. and L. George, “FAGE Determination of Tropospheric OH and HO_2”, *J. Atmos. Sci.*, 52, 3354 (1995).

Hasson, A. S., G. S. Tyndall, and J. J. Orlando, "A Product Yield Study of the Reaction of HO_2 Radicals with Ethyl Peroxy ($C_2H_5O_2$), Acetyl Peroxy ($CH_3C(O)O_2$), and Acetonyl Peroxy ($CH_3C(O)CH_2O_2$) Radicals", *J. Phys. Chem. A.*, 108, 28, 5979 (2004).

Hornbrook, R. S., Crawford, J. H., Edwards, G. D., Goyea, O., Mauldin III, R. L., Olson, J. S., and Cantrell, C. A., "Measurements of tropospheric HO_2 and RO_2 by oxygen dilution modulation and chemical ionization mass spectrometry", *Atmos. Meas. Tech.*, 4, 4, 735 (2011).

Johnson, D., and G. Marston, "The gas-phase ozonolysis of unsaturated volatile organic compounds in the troposphere", *Chem. Soc. Rev.*, 37, 4, 699 (2008).

Kanaya, Y., Y. Sadanaga, J. Hirokawa, Y. Kajii and H. Akimoto, "Development of a Ground-Based LIF Instrument for Measuring HOx Radicals: Instrumentation and Calibrations", *J. Atmos. Chem.*, 38, 73 (2001).

Kanaya, Y., R. Cao, H. Akimoto, M. Fukuda, Y. Komazaki, Y. Yokouchi, M. Koike, H. Tanimoto, N. Takegawa and Y. Kondo, "Urban photochemistry in central Tokyo:1. Observed and modeled OH and HO_2 radical concentrations during the winter and summer of 2004", *J. Geophys. Res.*, *112,* D21312 (2007).

Kanno, N., K. Tonokura, A. Tezaki and M. Koshi, "Water Dependence of the HO_2 self Reaction: Kinetics of the HO_2-H_2O Complex", *J. Phys. Chem. A.*, 109, 3153 (2005).

Kato, S., Y. Miyakawa, T. Kaneko, and Y. Kajii, "Urban air measurements using PTR-MS in Tokyo area and comparison with GC-FID measurements", *Int. J. Mass Spectrom.*, 235, 2, 103 (2004).

Kovacs, T. A. and W. H. Brune, "Total OH loss rate measurement", *J. Atmos. Chem.*, 39, 2, 105 (2001).

Kovacs, T. A., Brune, W. H., Harder, H., Martinez, M., Simpas, J. B., Frost, G. J., Williams, E., Jobson, T., Stroud, C., Young, V., Fried, A., and Wert, B., "Direct measurements of urban OH reactivity during Nashville SOS in summer 1999", *J. Environ. Monit.*, 5, 1, 68 (2003).

Lewis, A. C., N. Carslaw, P. J. Marriott, R. M. Kinghorn, P. Morrison, A. L. Lee, K. D. Bartle, and M. J. Pilling, "A larger pool of ozone-forming carbon compounds in urban atmospheres", *Nature*, 405, 778 (2000).

Liu, Y., R. Morales-Cueto, J. Hargrove, D. Medina and J. Zhang, "Measurements of Peroxy Radicals Using Chemical Amplification−Cavity Ringdown Spectroscopy", *Environ. Sci. Technol.*, 43, 7791 (2009).

Malkin, T. L., A. Goddard, D. E. Heard, and P. W. Seakins, "Measurements of OH and HO_2 yields from the gas phase ozonolysis of isoprene", *Atmos. Chem. Phys.*, 10, 3, 1441 (2010).

Mather, J. H., P. S. Stevens, and W. H. Brune, "OH and HO_2 measurements using laser-induced fluorescence", *J. Geophys. Res.*, 102, 5, 6427 (1997).

Matsumoto, J., J. Hirokawa, H. Akimoto, Y. Kajii, “Direct Measurement of NO_2 in the Marine Atmosphere by Laser Induced Fluoresecence Technique”, *Atmos. Environ.*, 35, 2803 (2001).

Mihelcic, D., Ehhalt, D. H., Kulessa, G. F., Klomfass, J., Trainer, M., Schmidt, U., Röhrs, H., "Measurements of free radicals in the atmosphere by matrix isolation and electron paramagnetic resonance", *Pure appl. Geophys.*, 116, 2-3, 530 (1978).

Mihelcic, D., P. Müsgen, and D. H. Ehhalt, “An Improved Method of Measuring Tropospheric NO_2 and RO_2 by Matrix Isolation and Electron Spin Resonance”, *J. Atmos. Chem.*, 3, 341 (1985).

Mihelcic, D., A. Volz-Thomas, H. Pätz, D. Kley, and M. Mihelcic, "Numerical analysis of ESR spectra from atmospheric samples", *J. Atmos. Chem.*, 11, 3, 271 (1990).

Mihelcic, D., D. Klemp, P. Müsgen, H. W. Pätz, and A. Volz-Thomas,, “Simultaneous Measurements of Peroxy and Nitrate radicals at Schauinsland”, *J. Atmos. Chem.*, 16, 313 (1993).

Mihele, C.M. and D.R. Hastie, “The sensitivity of the radical amplifier to ambient water vapour”, *Geophys. Res. Lett.*, 25(11), 1911 (1998).

Mihele, C.M., M. Mozurkewich, D. R. Hastie, “Radical loss in a chain reaction of CO and NO in the presence of water: implications for the radical amplifier and atmospheric chemistry”, *Int. J. Chem. Kinet*, 31, 145 (1999).

Miyazaki, K., J. Matsumoto, S. Kato, and Y. Kajii, “Development of Atmospheric NO Analyzer by Using a Laser-induced Fluorescence NO_2 Detector”, *Atmos. Environ.*, 42(33), 7812 (2008).

Monks, P. S., Gas-phase radical chemistry in the troposphere, *Chem. Soc. Rev.*, *34*, 376 (2005).

Parker, A. E., D. Amédro, C. Schoemaecker, and C. Fittschen, "OH RADICAL REACTIVITY MEASUREMENTS BY FAGE", *Environ. Eng. Manage. J.*, 10, 1, 107 (2011).

Rajakumar, B., Tomasz Gierczak, Jonathan E. Flada, A.R. Ravishankara, James B. Burkholder, “The CH_3CO quantum yield in the 248 nm photolysis of acetone, methyl ethylketone, and biacetyl”, *J. Photochem. Photobio. A.,* 199, 336 (2008).

Reichert, L., M.D.A. Hernandez, D. Stobener, J. Burkert and J.P. Burrows, “Investigation of the effect of water complexes in the determination of peroxy radical ambient concentrations: Implications for the atmosphere”, *J. Geophys. Res.*, *108*(D1), 4017 (2003).

Reiner, T., Hanke, M., Arnold, F., “Atmospheric peroxy radical measurement by ion molecule reaction-mass spectrometry: A novel analytical method using amplifying chemical conversion to sulfuric acid”, *J. Geophys. Res.*, 102, 1311 (1997).

Ren, X., Harder, H., Martinez, M., Faloona, I.C., Tan, D., Lesher, R.L., Di Carlo, P., Simpas, J.B., Brune, W.H., "Interference testing for atmospheric HOx measurements by laser-induced fluorescence", *J. Atmos. Chem.*, 47, 2, 169 (2004).

Ren, X., Brune, W. H., Cantrell, C. A., Edwards, G. D., Shirley, T., Metcalf, A. R., and Lesher, R. L., "Hydroxyl and Peroxy Radical Chemistry in a Rural Area of Central Pennsylvania: Observations and Model Comparisons", *J. Atmos. Chem.*, 52, 3, 231 (2005).

Sadanaga, Y., J. Matsumoto, and Y. Kajii, "Photochemical reactions in the urban air: Recent understandings of radical chemistry", *J. Photochem. Photobio. C: Photochem. Rev.*, 4, 1, 85 (2003).

Sadanaga, Y., Yoshino, A., Watanabe, K., Yoshioka, A., Wakazono, Y., Kanaya, Y., Kajii, Y., "Development of a measurement system of OH reactivity in the atmosphere by using a laser-induced pump and probe technique", *Rev. Sci. Instrum.*, 75, 8, 2648 (2004).

Sadanaga, Y., Matsumoto, J., Sakurai, K., Isozaki, R., Kato, S., Nomaguchi, T., Bandow, H., Kajii, Y., “Development of a measurement system of peroxy radicals using a chemical amplification/laser-induced fluorescence technique”, *Rev. Sci. Instrum.*, 75, 864 (2004).

Salisbury, G., P.S. Monks, S. Bauguitte, B.J. Bandy and S.A. Penkett, “A seasonal comparison of the ozone photochemistry in clean and polluted air masses at Mace Head, Ireland”, *J. Atmos. Chem.*, *41*(2), 163 (2002).

Sander, S. P.,Golden, D. M.,Kurylo, M. J.,Moortgat, G. K.,Wine, P. H.,Ravishankara, A. R.,Kolb, C. E.,Molina, M. J.,Finlayson-Pitts, B. J.,Huie, R. E.,Orkin, V. L.,Friedl, R. R.,Keller-Rudek, H., “Chemical Kinetics and Photochemical for Use in Atmospheric Studies: Evaluation Number 15”, *Jet Propulsion Laboratory Publication* (2006).

Skov, H., Benter, T., Schindler, R.N., Hjorth, J., Restelli, G.,, “Epoxide formation in the reactions of the nitrate radical with 2,3-dimethyl-2-butene, cis- and trans-2-butene and isoprene”, *Atmos. Environ.*, 28, 1583 (1994).

Taketani, F., Kanaya, Y., Akimoto, H.,, “Kinetics of Heterogeneous Reactions of HO_2 Radical at Ambient Concentration Levels with $(NH_4)SO_4$ and NaCl Aerosol Particles”, *J. Phys. Chem. A.*, 112, 2370 (2008).

Thornton, J. A., Wooldridge, P. J., Cohen, R. C., Martinez, M., Harder, H., Brune, W. H., Williams, E. J., Roberts, J. M., Fehsenfeld, F. C., Hall, S. R., Shetter, R. E., Wert, B. P., Fried, A., "Ozone production rates as a function of NOx abundances and HOx production rates in the Nashville urban plume", *J. Geophys. Res.*, 107, 12, 1 (2002).

Thornton, J. A., L. Jaeglé, and V. F. McNeill, "Assessing known pathways for HO_2 loss in aqueous atmospheric aerosols: Regional and global impacts on tropospheric oxidants", *J. Geophys. Res.*, 113, 5, (2008).

Wegener, R., Brauers, T., Koppmann, R., Rodríguez Bares, S., Tillmann, R., Wahner, A., Hansel, A., Wisthaler, A., "Simulation chamber investigation of the reactions of ozone with short-chained alkenes", *J. Geophys. Res.*, 112, 13, 1 (2007).

Yoshino, A., Sadanaga, Y., Watanabe, K., Kato, S., Miyakawa, Y., Matsumoto, J., Kajii, Y., "Measurement of total OH reactivity by laser-induced pump and probe technique—comprehensive observations in the urban atmosphere of Tokyo", *Atmos. Environ.*, 40, 40, 7869 (2006).

Acknowledgement

This research has been carried out as doctoral courses of Graduate school of Urban Environmental Sciences, Tokyo Metropolitan University and PhysicoChimie des Processus de Combustion et de l'Atmosphère, Université Lille1.

At first, I would like to express my sincere gratitude to my academic supervisors, Prof. Yoshizumi Kajii (Tokyo Metro. Univ.) and Dr. Christa Fittschen (Univ. Lille1) for their guides and helpful advices to the research of this doctoral thesis.

I am deeply grateful to Associate Prof. Shungo Kato (Tokyo Metro. Univ.), Associate Prof. Jun Matsumoto (Tokyo Metro. Univ.), Prof. Keitaro Yoshihara (Tokyo Metro. Univ.), and Prof. Jean-Francois Pauwels (Univ. Lille1) for accepting jury member and for giving specific comments and advices on my thesis.

I am also deeply grateful to Dr. John C. Wenger (University College Cork) and Dr. Yugo Kanaya (JAMSTEC) for accepting jury reporter and for giving specific comments and advices on my thesis.

I am also grateful to Prof. Paul S. Monks (University of Leiceter) for giving specific comments and advices on PERCA experiments in Chapter 4.

I am grateful to Research Associate Yoshihiro Nakashima, Dr. Akira Ida, Dr. Jeeranut Suthawaree, and Dr. Charlotte Jones for their helps and encouragements on the research and my student life in Tokyo. I am also grateful to the secretary at Kajii Lab., Ms. Mariko Hiraoka for her helps and efforts. I would also like to express appreciation to all the members of Kajii Lab. at Tokyo Metropolitan University.

I am grateful to Dr. Coralie Schoemaecker and Dr. Alexander E. Parker for their helps and encouragements on the research and my student life in Lille. I would also like to express appreciation to all the members of Fittschen Lab. at University of Lille1.

I also thank Dr. Koichiro Ishii of Tokyo Metropolitan Research Institute for his cooperation on field experiments.

I would like to acknowledge JSPS (The Japan Society for the Promotion of Science) and Égide for scholarship.

At last I show my great thankfulness to my family for their encouragements and supports.

March, 2012
Koji MIYAZAKI

Publication list:

1. Yoshino, A., Nakashima, Y., **Miyazaki, K.**, Kato, S., Suthawaree, J., Shimo, N., Matsunaga, S., Chatani, S., Apel, E., Greenberg, J., Guenther, A., Ueno, H., Sasaki, H., Hoshi, J., Yokota, H., Ishii, K., Kajii, Y., "Air quality diagnosis from comprehensive observations of total OH reactivity and reactive trace species in urban central Tokyo", *Atmos. Environ.*, 49, 51 (2012).
2. Amedro, D., **K. Miyazaki,** A. Parker, C. Schoemaecker, and C. Fittschen, "Atmospheric and kinetic studies of OH and HO_2 by the FAGE technique", *J. Environ. Sci.*, 24, 78 (2012).
3. **Miyazaki, K.**, A. E. Parker, C. Fittschen, P. S. Monks, and Y. Kajii, "A new technique for the selective measurement of atmospheric peroxy radical concentrations of HO_2 and RO_2 using a denuding method", *Atmos. Meas. Tech.*, 3, 6, 1547 (2010).
4. Kamei, N., Y. Nakashima, K. Yamazaki, T. Osada, **K. Miyazaki**, S. Kato, K. Ishii, H. Konno, S. Kobayashi, and Y. Kajii, "Measurements of OH reactivity and analysis of trace species in gasoline vehicular exhaust", J. Jpn. Soc. Atmos. Environ., Vol.45, No.1, 21 (2010) (in Japanese).
5. Chatani, S., Shimo, N., Matsunaga, S., Kajii, Y., Kato, S., Nakashima, Y., **Miyazaki, K.**, Ishii, K., Ueno, H., "Sensitivity analyses of OH missing sinks over Tokyo metropolitan area in the summer of 2007", *Atmos. Chem. Phys.*, 9, 22, 8975 (2009).
6. Nakashima, Y., H. Matsuda, S. Ide, **K. Miyazaki**, K. Yamazaki, H. Okazaki, T. Osada, Y. Tajima, J. Suthawaree, S. Kato, N. Shimo, S. Matsunaga, E. Apel, J. Greenberg, A. Guenther, H. Ueno, H. Sasaki, J. Hoshi, A. Yoshino, H. Yokota, K. Ishii, and Y. Kajii, "Diagnosis of urban air quality by measurement of total OH reactivity II -Comprehensive observations in the urban of Tokyo-", J. Jpn. Soc. Atmos. Environ., Vol.44, No.1, 33 (2009) (in Japanese).
7. Okazaki, H., S. Kato, T. Osada, **K. Miyazaki**, Y. Tajima, Y. Nakashima, Y. Kajii, "Total OH Reactivity Measurement in Ambient Air by a Comparative Method using PTR-MS", J. Jpn. Soc. Atmos. Environ., Vol.44, No.5, 236 (2009) (in Japanese).
8. **Miyazaki, K.**, J. Matsumoto, S. Kato, and Y. Kajii, "Development of Atmospheric NO Analyzer by Using a Laser-induced Fluorescence NO_2 Detector", *Atmos. Environ.*, 42(33), 7812 (2008).

9. **Miyazaki, K.**, J. Matsumoto, S. Kato, and Y. Kajii, "Development of a Measurement System for NO using a NO_2 Detector", J. Jpn. Soc. Atmos. Environ., Vol.43, No.2, 112 (2008) (in Japanese).
10. Yoshihara, K., Y. Takatori, **K. Miyazaki** and Y. Kajii, "Ultraviolet light-induced water-droplet formation from wet ambient air", Proc. Jpn. Acad., Ser. B, Vol. 83, 320-325 (2007).